

AD-A133 509

HEAT TRANSFER RETARDATION AT ELEVATED TEMPERATURES

1/2

PHASE I ANALYSIS OF HE. (U) UNITED TECHNOLOGIES

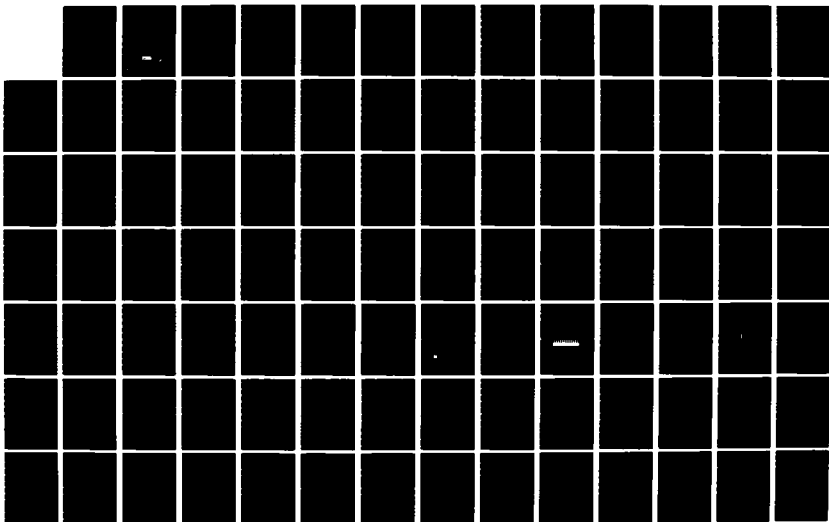
RESEARCH CENTER EAST HARTFORD CT C W DEANE SEP 83

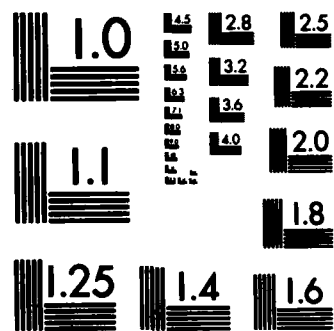
UNCLASSIFIED

UTRC/R83-956216-1 N00014-82-C-0671

F/G 20/13

NL





MICROCOPY RESOLUTION TEST CHART  
NATIONAL BUREAU OF STANDARDS-1963-A

12

AD-A133509

# HEAT TRANSFER RETARDATION AT ELEVATED TEMPERATURES

## Phase I — Analysis of Heat Transfer Retardation Configurations and Materials

### Annual Technical Report September 1983

Charles W. Deane

Prepared for  
The Office of Naval Research, Arlington, Virginia  
Under Contract No. N00014-82-C-0671



DTIC  
ELECTE  
OCT 13 1983  
S A

This document has been approved for public release and sale; its distribution is unlimited.

83 09 29 020.

DTIC FILE COPY

REPORT DOCUMENTATION PAGE		READ INSTRUCTIONS BEFORE COMPLETING FORM
1. REPORT NUMBER R83-956216-1	2. GOVT ACCESSION NO. AD-A133509	3. RECIPIENT'S CATALOG NUMBER
4. TITLE (and Subtitle) Heat Transfer Retardation at Elevated Temperatures (Phase I - Analysis of Heat Transfer Retardation Configurations and Materials)		5. TYPE OF REPORT & PERIOD COVERED Annual Technical Report Aug. 15, 1982 - Aug. 14, 1983
		6. PERFORMING ORG. REPORT NUMBER UTRC/R83-956216-1
7. AUTHOR(s) Charles W. Deane, Principal Investigator		8. CONTRACT OR GRANT NUMBER(s) N00014-82-C-0671
9. PERFORMING ORGANIZATION NAME AND ADDRESS United Technologies Research Center Silver Lane East Hartford, CT 06108		10. PROGRAM ELEMENT, PROJECT, TASK AREA & WORK UNIT NUMBERS Program Element: 61153N Project: RRO 24-03 Task Area: RRO 24-03-02 Work Unit: NR 097-457
11. CONTROLLING OFFICE NAME AND ADDRESS Office of Naval Research 800 North Quincy Street Arlington, VA 22217		12. REPORT DATE September 1983
		13. NUMBER OF PAGES
14. MONITORING AGENCY NAME & ADDRESS (if different from Controlling Office)		15. SECURITY CLASS. (of this report)  Unclassified
		15a. DECLASSIFICATION DOWNGRADING SCHEDULE
16. DISTRIBUTION STATEMENT (of this Report) Approved for public release; distribution unlimited		
17. DISTRIBUTION STATEMENT (of the abstract entered in Block 20, if different from Report) Same as block 16		
18. SUPPLEMENTARY NOTES		
19. KEY WORDS (Continue on reverse side if necessary and identify by block number) Heat Transfer Retardation High-Temperature Insulation Hot-Gas Ducting		
20. ABSTRACT (Continue on reverse side if necessary and identify by block number) The heat transfer retardation characteristics at high temperatures of selected combinations of configurations and their materials of construction were analyzed, and lightweight retardation configurations have been identified for hot-gas applications with hot-side temperatures of 3000 F. The scope of the investigation was to use available materials and passive retardation techniques. Candidate structural configurations with promising heat transfer (Cont'd)		

Cont'd

Unclassified

SECURITY CLASSIFICATION OF THIS PAGE (When Data Entered)

retardation characteristics were defined, candidate materials were identified, and combinations of these configuration types and their materials of construction were selected for analysis.

A heat transfer model was formulated for the analyses of the retardation configurations selected for hot-gas applications and was used to estimate the retardation characteristics in terms of an overall thermal resistance and unit weight. Multi-layer configurations were selected with the thin outer layer of ceramic foam providing a hard and relatively smooth surface for flow path and structure, and the inner fibrous layer(s) providing the bulk of the thermal resistance. The overall lightweight combination consists of All-Alumina foam and Dynaquartz (silica) fibrous insulation, because each material has the lowest value of the insulation performance factor in its category of materials.

Unclassified

SECURITY CLASSIFICATION OF THIS PAGE (When Data Entered)

R83-956216-1

Heat Transfer Retardation at Elevated Temperatures  
Phase I - Analysis of Heat Transfer Retardation  
Configurations and Materials

Annual Technical Report

*CW Deane*

Charles W. Deane  
Principal Investigator  
(203) 727-7245

Prepared for:

The Office of Naval Research  
Arlington, Virginia  
Under Contract No. N00014-8-2-C-0671

Mr. M. Keith Ellingsworth, Scientific Officer

September 1983



Application For

SEARCHED	INDEXED
SERIALIZED	FILED

SEP 1983

A

Heat Transfer Retardation at Elevated Temperatures  
Phase I - Analysis of Heat Transfer Retardation Configurations  
and Materials

TABLE OF CONTENTS

	<u>Page</u>
FOREWORD . . . . .	1
SUMMARY . . . . .	2
RESULTS AND CONCLUSIONS . . . . .	4
INTRODUCTION . . . . .	6
INTRODUCTION REFERENCES . . . . .	9
PHASE I - ANALYSIS OF HEAT TRANSFER RETARDATION CONFIGURATIONS AND MATERIALS . . . . .	10
I.1 Crucial Problems and Technology Status . . . . .	10
I.2 Definition of Candidate Structural Configurations . . . . .	23
I.3 Physical Properties of Candidate Materials . . . . .	27
I.4 Selection of Configuration and Materials Combinations . . . . .	33
I.5 Analysis of Retardation Characteristics . . . . .	39
I.6 Lightweight Retardation Configurations . . . . .	50
REFERENCES . . . . .	53
TABLES	
FIGURES	

FOREWORD

The work described in this Annual Technical Report was performed at the United Technologies Research Center (UTRC) under Contract N00014-82-C-0671 entitled "Study of Heat Transfer Retardation at Elevated Temperatures", for the Office of Naval Research (ONR). This report summarizes the results obtained for the Phase I - Analysis of Heat Transfer Retardation Configurations and Materials study program. Prior to his departure from UTRC on July 15, 1983, Dr. Simion C. Kuo was the Principal Investigator for this program, and his contributions to this program are gratefully appreciated.

The contract program was initiated with ONR on August 15, 1982, and the ONR Scientific Officer for this contract program is Mr. M. Keith Ellingsworth, Mechanics Division, ONR, Arlington, Virginia. Valuable guidance and comments received from Mr. Ellingsworth are gratefully acknowledged.

Heat Transfer Retardation at Elevated Temperatures  
Phase I - Analysis of Heat Transfer Retardation Configurations  
and Materials

SUMMARY

The objectives of the work presented in this report were to analyze the retardation characteristics of selected combinations of configurations and their materials of construction, and then to identify lightweight retardation configurations. As a basis for the analysis, the crucial problems and technology status of heat transfer retardation at high temperatures were assessed. Candidate structural configurations with promising heat transfer retardation characteristics were defined, candidate materials for retardation applications were identified, and combinations of these configuration types and their materials of construction were selected for analysis. A model of heat transfer was formulated for the analyses of the retardation configurations selected for hot-gas applications and was used to estimate the retardation characteristics and to identify lightweight retardation configurations.

The technology status of heat transfer retardation at high temperatures was assessed by reviewing previous investigations, both analytical and experimental, and the physical geometries used and their materials of construction were summarized in order to identify the crucial problems encountered by previous investigations. Candidate structural configurations with promising heat transfer retardation characteristics and relatively low weight were defined for detailed analysis. The physical properties of materials of construction for these configurations were examined for application to heat transfer retardation in hot-gas applications and also passive laser countermeasures applications. Then combinations of configuration types and their materials of construction were selected for analysis of their overall retardation characteristics relative to their weight characteristics, and possible operating limits of these combinations were identified for selected applications.

Finally, a model of heat transfer for the configurations and materials selected for hot-gas applications was formulated and has been used to estimate

the heat transfer retardation characteristics in terms of an overall thermal resistance through the configuration. The unit weight of the overall configuration was also analyzed for use in identifying lightweight combinations of configuration types and their materials of construction. The limitations in the model caused by the simplifying assumptions were described. Based on performance analyses of the selected configurations using this model, lightweight retardation configurations have been identified for hot-gas applications, and the effects of the geometric parameters of each configuration upon heat transfer retardation have been estimated.

This study program was conducted by the Thermal Engineering Group at UTRC under Contract N00014-82-C-0671 from the Office of Naval Research, Mechanics Division, Arlington, Virginia.

## RESULTS AND CONCLUSIONS

1. The crucial problems of heat transfer retardation at high temperatures can generally be grouped into three areas: the temperature capability of available materials, the heat transfer and weight characteristics, and stress and attachment problems.
2. Candidate structural configurations of retardation materials for hot-gas applications can be grouped into five categories: fibrous, ceramic foam, ceramic composite, radiation/layered, and powder materials.
3. Few insulating materials are available for applications at 3000 F and higher, as problems with shrinkage, chemical reactions, and/or melting drastically reduce the field of candidate materials as the expected temperature level increases.
4. The available candidate materials with the advantageously lowest values of the insulating performance factor ( $\rho k$ ) are: All-Alumina ceramic foam which has a maximum operating temperature that approaches 3000 F; and Dynaquartz (silica) fibrous insulation which has a maximum operating temperature of 2700 F. Ceramic composites offer excellent mechanical properties at high temperatures but are currently limited to 1800 F because of oxidation problems.
5. The rationale of using multi-layer configurations to provide heat transfer retardation for hot-gas applications is that: (1) a thin outer layer of ceramic foam provides a hard and relatively smooth surface for flow path and structure, and (2) the inner fibrous layer(s) provide the bulk of the heat transfer resistance because of the lower effective thermal conductivity.
6. A multi-layer approach is also preferred for passive laser countermeasures applications. The outer layer is reflective, to reflect the electromagnetic energy of the beam before it is converted to thermal energy; the middle layer is an ablative material (possibly incorporating capsules of gas that would absorb the beam's energy, to provide protection during attack); while the inner layer(s) of thermal insulation would protect the underlying structure and/or electronics against the thermal wave induced by the high-intensity beam of short duration.

7. The analyses of heat transfer retardation characteristics for hot-gas applications show that, at equal values of the overall thermal resistance (R-factor), the overall lightweight combination consists of All-Alumina foam and Dynaquartz fibrous insulation because each material has the lowest value of the insulation performance factor in its category of materials.
  
8. If the total thickness of insulation is limited to one inch, with a 3000 F hot-side and a 1200 F cold-side temperature, the expected heat loss is approximately 2900 BTU/hr-ft<sup>2</sup> and the weight per unit face area is approximately 0.6 lbm/ft<sup>2</sup> for the lightweight combination of All-Alumina foam with Dynaquartz fibrous material.

## INTRODUCTION

Advances in high-temperature heat transfer retardation have been made in recent years in response to the development trends of various propulsion devices and heat transfer equipment towards higher temperatures in order to obtain improved performance with minimum size and weight. For example, one method of increasing the efficiency of a gas turbine engine is to increase the combustion gas temperature to the maximum temperature limits of the turbine and nozzle structure. Projections for growth versions of current commercial aircraft engines indicate that the turbine inlet temperature will approach 2800 F, while future engine generations for the later 1980's will require turbine inlet temperatures of 3200 F. Gas temperatures in gas turbine engines are already higher than the maximum temperature capabilities of conventional superalloys because of heat-resistant coatings and because compressor bleed air is used to cool the hot components, but the loss of this high-pressure air from the cycle results in an engine performance penalty. Further, the components that do require this cooling are more complex than similar but uncooled parts and are therefore more expensive to fabricate and maintain than parts that do not require cooling.

When protected from rapid oxidation by an attrition-resistant coating, carbon-carbon composites have excellent mechanical properties at temperatures of up to 5000 F. Otherwise, without the coating, carbon rapidly oxidizes and erodes at temperatures above 700 F. Carbon-carbon composites are being considered (Ref. 1) for high-temperature components such as augmentor liners, nozzles, and tailcones in advanced engine technologies. Carbon-carbon composites have also been assessed (Ref. 2) for limited-life gas turbine engines, with the conclusion that the use of these composites is not a question of payoff but rather a question of achieving the necessary levels of material properties and oxidation protection. The design philosophy of using carbon-carbon composites with their relatively high thermal conductivity is to allow the components to see the high temperatures of the environment.

In contrast, the design philosophy of using a heat transfer retardation configuration made, in part, of ceramic is to minimize the heat being transferred to the component being protected. Ceramic materials have the advantage over carbon-carbon composites of offering insulation capabilities. Ceramics have been explored (Ref. 3) with increasing interest during the last decade for use in turbine engines to provide both insulating qualities and high-temperature capabilities. Reusable heat shields using ceramic materials instead of ablating techniques have been under investigation (Refs. 4 and 5) for space shuttle orbiters. Some of these concepts use fibrous ceramic materials for insulation (Refs. 6 and 7), and a closed-pore insulation (Ref. 8) made from low-cost fly ash (which is a product of coal combustion) has also received attention. The use of thermal coatings - a thin layer of ceramic, typically 0.015 in. thick - as

applied to gas turbine airfoils (Ref. 9) has the potential for protecting the gas turbine components from the erosive and corrosive environment of hot combustion gases, thereby permitting the use of less refined and cheaper fuels in a gas turbine/steam turbine combined cycle. Plasma-sprayed ceramic coatings, typically 0.12 in. thick, are also being developed (Refs. 10, 11 and 12) by United Technologies/Pratt and Whitney Aircraft under NASA contract for use as abradable blade-tip seals in high-pressure turbine applications.

The previous work on heat transfer retardation at high temperatures (over 2000 F) has made important advances, but problems still exist and require additional analytical and experimental research. First, the thin thermal barrier coatings that are being developed for use in gas turbines do not provide the high levels of heat transfer retardation that are necessary for other applications.

A second problem occurs with the thicker configurations that weigh too much for the level of heat transfer retardation that is provided. Promising configurations must be identified and then analyzed to select lightweight configurations, which must then be tested to confirm the thermal analyses.

The third shortcoming of the previous work is that only a limited amount of analytical work has been done to sort out the various options available in terms of configurations and the materials of construction for each of the possible layers in a multi-layer heat transfer retardation configuration. The overall heat transfer retardation characteristics of a multi-layer construction can be described in terms of a thermal resistance per unit thickness for comparison with other retardation configurations.

The objectives of the Phase I - Analysis of Heat Transfer Configurations and Materials study program described herein were to analyze the heat transfer retardation characteristics of selected combinations of configurations and their materials of construction, and then to identify preferred lightweight combinations. The scope of the investigation is to employ available materials in the selected combinations, to examine the heat transfer and weight characteristics of selected combinations, and to utilize passive retardation techniques. The main application of interest here is for hot-gas flows, such as hot sections in gas turbines or hot-gas ducting. These are relatively steady-state applications, with the hot-side temperature of interest above 3000 F, and the cold-side temperature in the range of 1200 F to 1800 F. A brief look was also taken at heat transfer retardation for passive laser countermeasures applications, which involve rapid heat transients caused by high-intensity beams of short duration. Sacrificial material loss (ablation) is the approach to absorb this energy, with an insulating layer to protect the underlying structure and/or electronics from the subsequent thermal wave.

The results of this Phase I study program are presented in this report. The crucial problems and technology status of heat transfer retardation at high temperatures were assessed and summarized in Task I.1. Candidate structural configurations with promising heat transfer retardation characteristics were defined in Task I.2, candidate materials for retardation applications were identified in Task I.3, and combinations of these configuration types and their materials of construction were selected in Task I.4 for analysis. A model of heat transfer was formulated in Task I.5 for the analyses of the retardation configurations selected for hot-gas applications and was used to estimate the heat transfer retardation characteristics in terms of an overall thermal resistance, and lightweight retardation configurations were identified in Task I.6 based on these analyses.

## INTRODUCTION REFERENCES

1. Parkola, S.: Advanced Technology Engine Studies (ATES) - Task II Final Report. United Technologies/Pratt & Whitney Aircraft Report No. FR-14592 on Department of the Navy Contract No. N00019-80-C-0025, December 1981.
2. Cruzen, G. S., L. J. Davis, and J. B. Carlton: Advanced Gas Turbine Carbon/Carbon Components Feasibility Assessment. Report No. AFWAL-TR-80-4036, April 1980.
3. Burte, H. M., ed.: Ceramics for Turbine Engine Applications. AGARD Conference Proceedings, No. 276 1979.
4. Giezma, C. J., W. B. Hunter, et al.: Final Report on Structural Heat Shield for Reentry and Hypersonic Lift Vehicles - High Temperature Composite Structure. Report No. ML-TDR-64-267, Part I, Vols. 1 and 2, 1965.
5. Chapman, A. J.: Evaluation of Reusable Surface Insulation for Space Shuttle Over a Range of Heat-Transfer Rate and Surface Temperature. NASA TM X-2823, 1973.
6. Rolinski, E. J., et al: Development of High-Temperature Insulation Systems. AIAA Paper No. 66-43, 1966.
7. Kummer, D. L. and G. B. Bilow: Refractory Materials and Insulation. AIAA Paper No. 68-1128, 1968.
8. Tobin, A., et al.: Development of a Closed Pore Insulation Material. NASA Report CR-2254, 1973.
9. Nainiger, J. J.: Effect of Thermal Barrier Coatings on The Performance of Steam- and Water-Cooled Gas Turbine-Steam Turbine Combined Cycle Systems. NASA Report TM-79057, 1968.
10. Shiembob, L. T.: Development of a Plasma Sprayed Ceramic Gas Path Seal for High Pressure Turbine Applications. NASA Report CR-135387, 1977.
11. Shiembob, L. T.: Development of a Plasma Sprayed Ceramic Gas Path Seal for High-Pressure Turbine Application. NASA Report CR-135387, 1978.
12. Shiembob L. T.: Development of Improved High Pressure Turbine Outer Gas Path Seal Components. NASA Report CR-1519801, 1980.

## PHASE I - ANALYSIS OF HEAT TRANSFER RETARDATION CONFIGURATIONS AND MATERIALS

The object of this study program is to analyze the retardation characteristics of selected combinations of configurations and their materials of construction and then to identify lightweight retardation configurations. This study consists of six tasks: I.1) Crucial Problems and Technology Status; I.2) Definition of Candidate Structural Configurations; I.3) Physical Properties of Candidate Materials; I.4) Selection of Configuration and Materials Combinations; I.5) Analysis of Retardation Characteristics; and I.6) Lightweight Retardation Configurations. The results obtained in each of these six tasks are presented in the following sections.

### I.1 Crucial Problems and Technology Status

Progress in the fields of space exploration and reentry applications has sparked interest in the development of high-temperature thermal retardation systems. Many aerospace applications involve exposure to a hyperthermal environment where severe heating and stress loading conditions occur. Hence, a high-temperature thermal retardation system may be required to protect the load carrying structure. Figure I.1 shows a typical example of a multi-layer retardation device that was designed as the heat shield for a reentry vehicle.

Thermal protection systems can generally be categorized as either absorptive or radiative, depending upon the primary method by which the incident energy is dissipated. Included among the absorptive types of thermal retardation systems are systems that involve ablation, heat sinks, convection cooling, and film and transpiration cooling. There are several forms in which the energy can arrive at the retardation surface from its source: forced convection, thermal radiation, and electromagnetic radiation (laser). The design of a thermal retardation system involves the interaction of environmental, material, and application factors, which must all be considered in the evolution of the design of a thermal retardation system. The form in which the energy arrives can affect the surface design of the retardation device. To minimize forced convection heat transfer, a smooth surface to minimize the heat transfer coefficient and area will be preferred. Electromagnetic energy can be reflected by the surface before being converted into thermal energy. To lose heat by radiation from the surface, a colder heat sink elsewhere would be necessary.

Because of the many possible applications and the vast array of design requirements which are specific to each application, many different approaches have received attention. Hence, to lay the groundwork for the analyses of heat transfer retardation characteristics to be done in this study program, crucial

problems and the technology status of heat transfer retardation were examined to identify the physical geometries and the materials of construction used in previous investigations and their limitations. Previous analyses of retardation characteristics were identified, and previous experimental work was summarized in terms of data, experimental conditions, and intended applications.

### I.1.1 Physical Geometries and Materials of Construction

Combinations of physical geometries and materials of construction that previous investigators have examined are discussed in this section. The physical geometries include honeycomb structures, fibrous blanket configurations, molded block construction, flakes, and various combinations of these geometries to form the overall thermal retardation device. In fact, most thermal retardation systems consist of a combination of geometries and materials tailored to be compatible with the temperature gradient.

Honeycomb structures have been examined by several investigators. Giemza et al. (Ref. 1) developed a high-temperature composite heat shield using foamed ceramics for reentry and hypersonic lift vehicles. The thermantic structure that they developed combines the refractoriness of oxides, the insulation qualities of ceramic foam, and the honeycomb reinforcement of the ceramic foam to assure the integrity of the heat shield with the back-up structure. The risk of catastrophic failure, which can occur in monolithic structures under thermal stress, is substantially minimized by the individual ceramic cell arrangement. For the high surface temperatures associated with reentry vehicles, most of the incident heat is rejected by radiation. Control of the ceramic porosity is an important factor, because an increase in porosity will result in a reduction of density and thermal conductivity but correspondingly lower strength characteristics. The main limitation appears to be that the metallic honeycomb core would substantially reduce the thermal resistance of its layer, because the heat would be preferentially conducted through the metal core and in that manner bypass the thermal resistance of the ceramic foam.

Scanlon (Ref. 2) proposed folded metal inserts to increase the thermal resistance of an otherwise empty honeycomb panel. The thin cell walls of a metallic honeycomb structure provide quite high thermal resistance to conduction, but when the temperature of the hot side of the panel is above 1000 F, then radiation from the hot side of the panel to the cold side can become the principal mode of heat transfer. Thin folded metallic inserts are attached by means such as brazing, welding, or diffusion bonding to the inside of each honeycomb cell and shield the cold side from the thermal radiation from the hot side. The main limitation with this configuration would appear to be the problem of insuring that the numerous small inserts are properly placed and attached to the wall of each of the honeycomb cells.

Fibrous-type heat transfer retardation devices have also been examined. Rolinski et al. (Ref. 3) evaluated fibrous insulations for use in thermal retardation systems for reusable reentry and hypersonic cruise vehicles. Thermal conductivities of promising fibrous insulations were measured. Based on test results for low-density fibrous insulations above 2000 F, gas conduction and radiation through the insulation may account for up to 30 percent and 90 percent, respectively, of the total heat transfer through the insulation, while solid conduction heat transfer is of limited importance. In other words, if several modes of heat transfer are operating in series, the heat will be transferred through the low-resistance paths and will bypass the high-resistance path (of pure conduction through the fibers, in this instance). But the principal shortcoming of fibrous materials is their mechanical instability. Although shrinkage may be reduced by controlled fabrication procedures and pretreatment at high temperatures, compressive strength and resistance to sonic fatigue are only marginal. Sintering at temperatures above the pretreatment temperature may also limit the use of fibrous insulations. Very-low-density compacts of ceramic fibers (Ref. 4) are competitive with low-density ablators and are potentially reusable. Many conventional ceramic fiber insulations are not dimensionally stable at temperatures above 2200 F, or will not withstand noise and vibration to be reusable for multiple flights of reentry vehicles if heated above this temperature. But fibers such as zirconia and sapphire do show promise for applications above 2500 F.

An investigation was conducted by Chapman (Ref. 5) to evaluate reusable surface insulation materials for use as heat shields for the space shuttle orbiter. These materials are formed by rigidizing low-density ceramic fibers and applying a dense high-emittance coating. A silica-base material experienced only minimal degradation during repeated tests which included conditions twice as severe as predicted shuttle entry and withstood cumulative exposures three times longer than the best mullite material. Mullite-base materials cracked and experienced incipient melting at conditions within the range predicted for shuttle entry but neither silica nor mullite materials consistently survived the test series with unbroken waterproof surfaces.

Martynenko et al (Ref. 6) used high-alumina wool for insulation tubes (with inside diameters of 4.3 in. and 5.7 in.) to be used as ducts for molten non-ferrous metals at temperatures of up to 2000 F. The tubes were manufactured from the ceramic fibers by in-vacuo forming and by the layer-wise deposition of ceramic-fiber paper with a bonding substance.

Molded block configurations have been studied by many investigators and offer the feature of modularity. Generally, molded blocks are produced by placing the ingredients in a mold and then firing the mixture in a furnace. For use as a high-temperature heat shield on a space shuttle, Tobin et al. (Refs. 7 and 8) have developed a closed-pore ceramic foam insulation made with a low-cost raw

material (fly ash, obtained from the combustion of coal) which has negligible water absorption because of the noninterconnecting network of cells and which has a high emittance for radiation heat transfer. Basically, a face sheet of closed-pore foam insulation (up to 0.5 in. thick) is supported by a lightweight metallic honeycomb, with the cells of the honeycomb being filled with lightweight refractory fibers (such as microquartz). The ductile honeycomb core tends to isolate the brittle closed-pore foam insulation from the rigid backside metallic structure which is in turn attached to the primary structure. The cenospheres (which are spherical, hollow glass particles) are heated in a mold in air or any inert atmosphere at firing temperatures in the range of between 2500 to 3000 F, and the cenospheres then shrink together to form a closed-pore ceramic foam. The two problems with the closed-pore foam insulation are a relatively high density and the tendency to develop hairline stress cracks in pieces with the thickness necessary to provide sufficient heat retardation. Stated another way, the thermal conductivity of this foam insulation is too high, and the thickness of the foam insulation must therefore be increased to provide sufficient heat transfer retardation.

Another high-temperature insulating material is carbonized granulated cork (Ref. 9) that has been molded to the desired shape. The cork particles are placed in a mold and are then heated at a temperature of about 570 F. This temperature level effects the flow of the lignin (naturally found in cork) which acts as a binder. Then the bound cork granules are carbonized in an inert atmosphere such as argon or helium. The carbonized cork material may then be graphitized, at a suitable temperature of about 5400 F. One application for this graphite cork material is to insulate heat sources in radio-isotopic thermoelectric generators for space applications, and an important feature of this material is that its thermal conductivity does not increase with temperature, in contrast to the temperature dependence of carbon foam and fibrous carbon.

Graphite flakes and fibers have also been developed for high-temperature heat transfer retardation devices. Graphite flakes (Ref. 10) are placed in fibrous thermal insulation to increase the opacity of the composite insulation to radiation. Thin graphite flakes are oriented in the fibrous insulation with the maximum dimension of each flake being approximately perpendicular to the expected direction of heat flow through the composite. A mixture of water and starch particulates is used as the binder to secure the flakes to the fibers. The resulting slurry of fibers, graphite flakes and the water and starch is vacuum formed into the desired configuration. The slurry is then heated to gelatinize the starch, and then the dried mixture is heated further so that the starch is converted to carbon which thereby joins the fibers together. Composite insulation fabricated by this approach was tested at temperatures above 3800 F in a vacuum.

In another approach to decreasing heat transfer by radiation, Deschamps and Bernier (Ref. 11) coat the insulation, either a fiber base or spheres, with a thin layer of highly heat-reflective, low emissivity material. In the case of spheres in a vacuum atmosphere, the point contact between the spheres results in poor heat transfer by conduction, and the vacuum conditions substantially eliminate convection heat transfer. Then, if the spheres are coated with reflective material, the radiation mode of heat transfer is also substantially eliminated. A fibrous base material can also be used instead of the spheres. For example, Min-K can be used with the fibers coated with a thin layer of highly heat reflective, low emissivity material, preferably a metal which can be applied by a vacuum sputtering technique to deposit a film on each fiber in a mass of fibers.

Asbury and Googin (Ref. 12) have developed an inorganic thermal insulation that is made from minute particles of silicon oxide mixed with inorganic fibers, an organic wetting agent, and octanoic acid that will act as a binder for the silicon oxide particles. The mixture is heated, ground, pressed into a mold with the desired configuration, and then lightly sintered in an inert atmosphere. The thermal conductivity of the resulting material was measured at temperatures as high as 2700 F.

Vogan and Trumball (Ref. 13) have investigated metal-ceramic composites with a magnesia foam backing for use on nose caps and leading edges of re-entry vehicles. Alumina with metal honeycomb reinforcements was evaluated, and the preferred system is a partially crushed honeycomb structure in which the honeycomb is bonded to the desired backing material and partially filled with a fibrous insulating material. The rest of the structure is filled with an alumina-binder mix which is pressed into place and cured at 800 F. Chemically-bonded zirconia has also been examined and found to work very well as the ceramic. Superalloy honeycomb materials were found to be satisfactory for temperatures of up to 3000 F, even though some melting can occur at the surface. The ceramic retention is considerably improved by partially crushing the honeycomb. This crushing is accomplished without buckling the honeycomb by fitting it with a matrix material that is removed after the honeycomb has been compressed. The metal honeycomb reinforcements primarily serve to control thermal shock and to limit subsequent crack growth. Ceramic foams were developed as an insulating backing to the metal-ceramic honeycomb structures, in order to protect the support structure from heat. The best zirconia foams were produced by a chemical blowing process, where the pores in the ceramic are produced by a gas generated through a chemical reaction between zirconium metal and phosphoric acid. Mechanically whipped foams were also investigated, because satisfactory chemically blown magnesia foams could not be developed within their time schedule. Three methods of reinforcing the ceramic bodies were investigated: the metal honeycomb discussed above, wires, and flame-sprayed backings. Ceramic samples containing magnesia and wire reinforcements were prepared by pressing them at 12,000 psi and then sintering them in an argon atmosphere for 20 hrs at 2200 F. The samples

containing tantalum and tungsten wires cracked during sintering, but the samples with platinum, molybdenum or Rene 41 did not crack. Cracking in the tantalum sample was attributed to differential thermal expansion between the two materials. Flame-sprayed backings were also investigated because the resistance to spalling shown by the magnesia body indicated that metal reinforcement might not be needed throughout the ceramic phase. Three samples were tested, but cracks occurred in one and delamination of the flame-sprayed surface occurred with the other two samples.

An amorphous carbon-layered composite has been developed by Allen and Lysher (Ref. 14). This thermal insulation consists of separate layers of particulate material selected from materials with low thermal conductivity above 1800 F and from materials with low thermal conductivity below 1800 F. These layers are separated by one or more layers of metal sheets, which act as radiation shields and internal structural support for the particulate layers and as barriers to transverse fracturing. The insulation layers are composed of unbonded particles which have a lower thermal conductivity than materials with particles that are physically or chemically bonded together. For example, in a three-layer composite, the outer layer could be amorphous carbon black which has low thermal conductivity above 1800 F. The middle layer of metal could be a sheet of tantalum foil, while the inside layer could be zirconia which has low thermal conductivity below 1800 F.

Thin thermal barrier coatings have been investigated for the protection of cooled rocket nozzles and gas turbine components (Ref. 15). A thermal barrier coating is a thin layer of ceramic applied, for example, to the hot-section components of a gas turbine. The basic concept of heat barrier coatings is that the thermal resistance of the coating reduces the heat flux through the chamber wall (in the instance of a rocket engine), thereby keeping the metal surface temperature below the acceptable limits. The selection of the optimum thermal resistance is generally a compromise between the coating thickness and the required thermal protection. Thick coatings are to be avoided for three reasons: economics, convenience in applying the coating, and minimization of thermal shock. Typically, coating thicknesses of 0.015 in. are used, but coatings this thin can provide only modest levels of heat transfer retardation because the thermal conductivity of ceramic metals such as yttria-stabilized zirconia are relatively high.

Research at United Technologies/Pratt and Whitney Division (Refs. 16, 17 and 18) has investigated plasma-sprayed yttria-stabilized zirconia (ceramic) for use in gas turbine blade-tip seals for operation at temperatures up to 2400 F. These seals have a ceramic thickness of 0.15 in. The weight fraction of the zirconia spray powder can be varied to tailor the thermal conductivity of a material designed for use at a given maximum temperature. The blade-tip seals have a dual

function of not only providing a gas-path seal in the turbine but also providing thermal protection for the support structure.

Pechman and Beasley (Ref. 19) describe ceramic glaze coatings which are nonporous and impervious to moisture and which can withstand repeated exposures to alternating high and low temperatures. The coatings were applied to fibrous silica insulation which has a low coefficient of thermal expansion and a low emissivity. If a suitable ceramic glaze coating is not used, fibrous insulations can readily absorb moisture.

An extensive investigation of thermal protection system was conducted by Hurwicz and Mascola (Ref. 20) for use on the exterior of glide reentry vehicles. Their study concentrated on radiation and radiation/ablation systems for thermal protection. Extensive performance studies were conducted on the weight of radiation shields, including the effect of backface cooling, as a function of idealized material properties (density, thermal conductivity, and specific heat), for typical reentry glide vehicle heating rates and stagnation enthalpy. Similarly, extensive performance studies were conducted for radiation/ablation shields as a function of idealized material properties, including the ablation temperature and the heat of ablation. Models of radiation shields were made, in the form of flat plates, of pyrolytic graphite and also of molybdenum with the front face coated by a chromium diffusion process for oxidation protection. Radiation/ablation models in the shape of spherical-radius blunt-nosed cylinders were made of four different materials: X4000 and X5000 (experimental materials under development at the time by Avco); Teflon; and a zirconia matrix filled with polymethylmethacrylate.

Many candidate ablation materials have been studied for various applications, depending upon the heat rates and their duration. Weinberg (Ref. 21) developed an ablating material which consists of a char-forming polymer and a mixture of a solid noble-gas fluoride and sulfur. The heat generated during reentry by friction between the earth's atmosphere and the heat shield causes the sulfur and the fluoride to react thereby forming gases which are discharged into the aerodynamic flow field of the spacecraft. These gases act as a quenching agent that protects the spacecraft from the heat generated during reentry. The ablating material is formed in a mold of the desired shape and is then cured in an oven at approximately 300 F.

Three classes of materials have generally been found to be suitable for ablative thermal protection systems on reentry vehicles: refractories and ceramics, plastics, and composites. Graphite systems have been examined for reentry vehicles because of their relatively low ablation rates, which result in low levels of material loss and shape change in areas subject to high heating rates such as small-radius leading edges and ballistic missile nose tips. Graphite sublimates at temperatures as high as 6500 F and absorbs or rejects the heat

through the combined mechanisms of radiation, oxidation, sublimation, and sensible heating. Pyrolytic graphite, formed by the deposition of graphite layers and hence very anisotropic, has a very low thermal conductivity in the direction normal to the deposition plane. The major drawbacks to using graphite are its brittleness and low resistance to thermal stress, which mean that thick pieces can not be used. Also, delamination of pyrolytic graphite can occur at high temperature and high thermal stresses, and pyrolytic graphite is difficult and expensive to manufacture.

Ceramic-based ablators have problems with thermal stress failures, but this problem can be lessened by placing the ceramic in a metallic honeycomb. Resin-impregnated porous ceramics (Ref. 22) have better ablation characteristics because the resin component increases the composite strength and the thermal shock resistance. Further the thermal conductivity is reduced and high environmental temperatures can be handled without exceeding the melting or decomposition temperature of the ceramic. The possible porous ceramics include silica, zirconia, alumina, magnesia, thoria, carbides, borides and silicides. Candidate resin impregnants include the phenolics, epoxies, acrylics, and polystyrenes. Metal-base ablators (Ref. 23) have also been studied. A porous refractory skeleton, tungsten for example, is filled with a metallic infiltrant, such as copper or silver, that has a lower melting point.

Plastic-base ablators, such as teflon for low-temperature applications, are widely used because of their high heat shielding capability and low thermal conductivity, but their disadvantages are high erosion rates when exposed to high gasdynamic shear forces and their inability to handle very high heat loads. The mechanisms by which plastic-base ablators handle the heat vary: depolymerization and vaporization for teflon; pyrolysis and vaporization for phenolics and epoxy resins; and decomposition, melting, and vaporization for nylon-fiber-reinforced plastic.

Composites, in the form of charring-ablator heat shields, are of great interest to designers of thermal protection systems. This type of heat shield can be made of a thermosetting resin (such as the phenolics, epoxies, or silicones) and a refractory fiber (such as glass, asbestos, graphite, or nylon). When the heat shield is heated, the resin begins to decompose (pyrolyze) and releases gaseous products, leaving a porous carbonaceous residue. The gaseous products diffuse through the porous char to the surface, decomposing further and absorbing heat from the char. The gases exit into the boundary layer where they act as a transpirant. The fibers add strength to the char and thereby reduce its removal which could be caused by mechanical shear and/or by spalling. A thick char, primarily carbonaceous, acts as an insulation barrier and radiates heat from the surface, as well as being an efficient ablation material.

### I.1.2 Experimental Data on Heat Transfer Retardation Characteristics

Because the heat transfer retardation characteristics of most suitable materials have to be determined experimentally, most of the investigators of the materials discussed in the previous section have run some sort of experiments to determine these characteristics. These measurements could include density, thermal conductivity, specific heat and emissivity, and, for ablation materials, ablation temperature and heat of ablation.

The type of experiments that have been conducted can be generally divided into two classes: experiments with a composite heat transfer retardation device, and experiments on individual materials that have been developed for subsequent incorporation into a heat transfer retardation device.

Experiments with composite heat transfer retardation devices have been run on test sections developed for highly specific applications. Giemza et al. (Ref. 1) conducted extensive experiments to develop a composite reinforced ceramic-foam heat shield-sandwich structure for a superorbital reentry environment and temperatures in excess of 3000 F for a period of up to one hour. Tobin et al. (Ref. 7) tested a closed-pore insulation material with plasma arc jet tests to simulate entry heating conditions for external insulation on the space shuttle. An arc-driven supersonic wind tunnel was used by Hurwicz and Mascola (Ref. 20) to test both radiation models (made of pyrolytic graphite and of molybdenum) and also radiation/ablation models (made of Teflon, of zirconia impregnated with polymethylmethacrylate, and of two experimental materials being developed by Avco at that time). Martynenko et al. (Ref. 6) tested the high-alumina wool tubing under actual operating conditions of carrying molten bronze alloy at approximately 1800 F.

Erosion-shield tiles made of D-36 Columbian tiles and felt insulation on the cold side were tested by Clawson (Ref. 24) under conditions to simulate the heat loading of a radiation-cooled hot-structure reentry vehicle. Radiant heat lamps were used to heat the tile surface only, and control was by temperature rather than heat flux. Temperature-time data was obtained for a thermocouple on the back side of the columbian tile.

In addition to the experiments described above for composite heat transfer retardation devices, other investigators have developed and tested individual materials that may be suitable for incorporation into composite multi-layered heat transfer retardation devices. Rolinski et al. (Ref. 3) measure the thermal conductivity of a number of low-density fibrous insulations for use in reusable reentry and hypersonic cruise vehicles. Chapman (Ref. 5) conducted experiments to investigate the integrity of rigidized ceramic fibers with a high-emittance coating at conditions twice as severe as predicted shuttle reentry. Klett (Ref. 9) measured the density, thermal conductivity, crush stress, and modulus of elasticity for the carbonized granulated cork that he developed. Ardary et al.

(Ref. 10) measured the density, thermal conductivity, compressive strength, and modulus of elasticity of the material containing graphite flakes and fibers that they developed. The thermal conductivity and density of the inorganic thermal insulation made from silicon oxide particles and inorganic fibers was measured by Asbury and Googin (Ref. 12). Allen and Lysher (Ref. 14) measured the thermal conductivity of the amorphous carbon-layered composite that they developed.

Extensive tests were conducted by Vogan and Trumball (Ref. 13) in their development program for metal-ceramic composite heat transfer retardation materials. Thoria and magnesia bodies were tested for thermal shock resistance using oxyacetylene and plasma torches. The modulus of rupture, thermal expansion, relative emittance, foam compressive strength and impact strength were measured for the various thoria, magnesia, and zirconia metal-ceramic composites that they examined.

The ablation characteristics of many materials suitable for radiation/ablation heat shields have also been measured. For example, Straus (Ref. 22) tested impregnated alumina, zirconia, and silica foams in an oxyacetylene torch facility to determine the back-face temperature rise for various heating rates. Further tests were also done in a high-mass-flow hot-gas facility to measure the strength, erosion resistance, and thermal shock resistance of impregnated ceramics. Weinberg (Ref. 21) tested the char-forming polymer ablating heat shield material that he developed, with a high-temperature, high-velocity gas to simulate conditions for spacecraft reentry. Maloof (Ref. 23) tested a tungsten-based composite ablation material in an arc-plasma generator.

### I.1.3 Analyses of Retardation Characteristics

Heat transfer analyses have been conducted for a number of heat transfer retardation devices. Generally, many of these analyses have been computerized numerical analyses for a specific protection device subjected to the transient heating profile for the reentry vehicle being developed. Clawson (Ref. 24) used a large digital-computer program for the transient two-dimensional and three-dimensional thermal analyses of insulated panels for a glide reentry vehicle, with the temperature-altitude combinations used in the analyses typical of those expected.

Extensive parametric system studies were conducted by Hurwicz and Mascola (Ref. 20) for radiation heat shields and radiation-ablation heat shields, both with and without backface cooling. Specific reentry environments were selected, and the thermophysical properties of idealized materials were varied to see the parametric effect on heat shield performance in terms of required heat shield weight for the mission. The analytical results were used to aid the design of the experimental test sections that were subsequently tested.

A digital computer code was developed by Rathjen (Ref. 25) for the analysis of two-dimensional transient heating of hypersonic vehicles. The aerodynamic heating boundary conditions are calculated by the code based on the input flight trajectory, and the method of solution is a hybrid analytical-numerical technique. This solution method is computationally more efficient than conventional explicit finite-difference methods when structures with small time constants are analyzed over long flight trajectories.

A different approach to heat shield design was taken by Garcia and Fowler (Ref. 26). They investigated optimal entry trajectories for the space shuttle that minimize the weight of the thermal protection system. Two types of thermal protection systems were considered: a metallic system, with insulation behind the metal panel; and also a reusable surface-insulation thermal protection system. Optimal entry paths were generated using the maximum orbiter nose temperature as a parameter.

Giemza et al. (Ref. 1) conducted parametric analyses to optimize the structural honeycomb cell size of their composite heat shield structure. Their study was mainly concerned with the development of manufacturing processes for the composite reinforced ceramic-foam heat shield structure, but stress analyses were also conducted as a part of the study.

Generally, two types of analyses have been conducted by previous investigators. The first type is an extremely detailed numerical thermal analysis, usually two-dimensional and sometimes three-dimensional, where the performance of a specific design is intensively studied for its transient retardation response for specific reentry trajectories and/or thermal loadings. This type of analysis normally requires a computerized code to obtain the detailed numerical results of temperatures at the numerous nodes as a function of time. The second type of analysis is a more generalized heat flow network and does not examine the response to specific thermal loads such as a reentry trajectory. Rather, a one-dimensional heat flow network is used to compare various proposed thermal retardation devices on the basis of the overall thermal resistance of the composite geometry. Actually, many heat loads will be applied in a nearly one-dimensional pattern.

Furthermore, for new materials that have been recently developed, the specific application may not have been identified with its specific thermal loading, but it is still necessary to compare the heat transfer retardation characteristics of the composite retardation device incorporating the new material to other candidate configurations/composites. Hence, the one-dimensional network analysis can be very useful for basic comparisons between candidate retardation devices without getting deeply involved in the detailed calculations and the specifics of the transient thermal load. Later, for the purposes of detailed designs preparatory to fabricating the actual retardation device for a specific application,

detailed two- or three-dimensional thermal analyses of the proposed device would be extremely desirable.

#### I.1.4 Crucial Problems Related to Heat Transfer Retardation

On the basis of the survey of the literature described above, the following problems have been identified as crucial in the development and design of heat transfer retardation devices for high-temperature applications. Generally the crucial problems can be grouped into three areas: the temperature capability of available materials, the retardation and weight characteristics, and the stress and attachment problems.

The purpose of a heat transfer retardation device is to protect equipment and load-carrying structures from thermal loads which would otherwise compromise the integrity of the equipment and the structure. Thus the retardation device must provide thermal protection and also maintain its integrity by not cracking after exposure to the severe operating environment. The strain in the load-carrying structure being protected must be compatible with the strain allowable in the retardation device, and the retardation device must also be able to handle the thermal strain induced by the environment. Fatigue strength may also be a factor, depending upon the duration and cyclicity of the combined loading, both thermally induced and structural contributions. Further, some materials may have potential spalling problems that must be addressed, depending upon the combination of environmental characteristics.

One of the most critical factors in the design of a heat transfer retardation device is the match between the thermal expansion of the retardation device and that of the adjacent structure if a rigid bond is used. On the other hand, the use of a flexible bond here would greatly reduce the problems associated with differential thermal expansion, but the availability of flexible bonds that can handle wide temperature ranges is very limited. These bonding related problems have resulted in the development of composite configurations where the retardation device also provides the necessary structure.

Another major design factor for thermal retardation devices for reentry vehicles is shape retention, particularly small-radius surfaces such as leading edges and nose tips where erosion can occur and/or ablation can change the shape. Shape changes, could result in changes in the aerodynamic and/or thermal loading characteristics.

A third important design factor is the manufacturability of the retardation device. The materials of construction must be transformable into the designed shape of the retardation device. The inclusion of the bonding materials must also be considered in the design of the retardation device, as these materials may require a curing process after the composite has been assembled.

### I.1.5 Passive Laser Countermeasures

When a laser beam impinges upon an opaque target material, the beam is absorbed in a thin surface layer and heat is developed in this thin layer. Simultaneously heat is conducted into the interior of the material, but heat conduction can not provide a sufficient outlet for the large incident laser energy fluxes that are likely to be encountered in passive laser countermeasure applications. At these high energy fluxes, the surface of the target material will melt and a fusion interface will propagate into the interior of the material. The heating rate is determined by the heat flux which can be lower than the optical flux density at the surface of the target because part of the incident beam may be reflected by the surface. The heat flux into the target is equal to  $(1-R)$  times the optical flux density of the beam, where  $R$  is the reflectance of the surface and is a strong function of factors such as the surface finish of the target material (including its state of oxidation), the temperature of the target surface, and the wavelength of the incident beam.

The power levels relevant to passive laser countermeasures are indicated in Fig. I.2, based on information from Ref. 27. Current ablative technology is judged to be in the range of 10 to 20 kilojoules/cm<sup>2</sup>, while current military laser technology at a distance of 2200 miles is judged to be less than approximately 5 kilojoules/cm<sup>2</sup>. Based on these energy levels then, the anticipated laser power levels of interest and the duration of the beam can be inferred. For long-distance lasers in the range of 10 kW/cm<sup>2</sup>, the duration of the beam is likely to be measured in seconds, at current technology levels. Furthermore, as shown in Fig. I.3, the elapsed time before surface melting of a slab of ATJ graphite commences will be measured in fractions of a second for laser power levels greater than 5 kW/cm<sup>2</sup>.

## I.2 Definition of Candidate Structural Configurations

Candidate structural configurations for heat transfer retardation should be selected to minimize the heat transfer rate in terms of the heat transfer modes operative at the expected temperature levels. The possible modes of heat transfer through the retardation device would include: radiation through porous structures; conduction through the solid and also the working gas if the structure is porous; and possibly even natural convection if the cells of the porous structure are open and large. Candidate structural configurations should minimize heat transfer by all relevant modes. Other important considerations include weight characteristics, maximum operating temperatures including cognizance of any time-at-temperature limitations, and mechanical strength and thermal shock characteristics. Specifics concerning the effective thermal conductivity, the effective density, and the maximum operating temperatures of candidate materials will be discussed in Section I.3 - Physical Properties of Candidate Materials.

Structural configurations of retardation materials for hot-gas applications can be grouped into five general categories, as shown in Table I.1. These five categories are: fibrous, ceramic foam, ceramic composite, radiation/layered, and powder materials.

### I.2.1 Fibrous Configurations

Fibrous insulations are a familiar type and generally have the lowest values of effective thermal conductivity ( $k$ ) and effective density ( $\rho$ ). The low effective thermal conductivity can be attributed to the poor thermal contact between the individual fibers that make up the insulation and that are roughly aligned in planes perpendicular to the direction of heat transfer. If the pore size of the insulation is extremely small, then the heat transfer rate by molecular conduction through the gas phase is very low. The fibers themselves scatter the radiant energy and thereby limit heat transfer by radiation. The low effective density can be attributed to the high porosity of the collection of fibers that form the overall insulation.

### I.2.2 Ceramic Foams

Ceramic foams are essentially ceramic materials into which small voids have been introduced. Two techniques have been used in the past to produce these foams: chemical blowing and mechanical whipping. Chemically blown foams can be produced by gas generated in a chemical reaction throughout the substance which starts as a liquid suspension of ceramic particles. The substance with the entrapped bubbles is then cured to form the hard ceramic foam. Mechanically whipped foams are produced by mechanical agitation of a liquid suspension of

ceramic particles, thereby entrapping air to produce the voids in the ceramic foam upon curing. Ceramic foams generally have higher values of the effective thermal conductivity and effective density than those of fibrous insulations. The conductivity is higher, in part, because of solid conduction through the cell walls and therefore the absence of internal contact resistance that exists in fibrous insulations. However, foamed materials have structural advantages that the structure-less fibrous materials do not have.

### I.2.3 Ceramic Composites

Glass matrix composites with high-strength fibers have been under development in recent years for gas-turbine applications. The use of fibers exhibiting high strength and stiffness can successfully reinforce low-modulus glass matrices, but limitations on use temperature occur. The more recent development of high-silica glass matrix composites resulted in higher thermal stability, but these higher use temperatures resulted in significantly greater fabrication problems than those of materials with lower use temperatures, because of the much higher viscosity of the higher temperature glass matrix during composite consolidation. To reduce these fabrication problems, a glass-ceramic was used as the composite matrix, with the resultant combination of high use temperature and simpler fabrication. Composite densification can occur while the matrix is maintained in a low viscosity glass state while composite structural use can take place after the matrix has been crystallized for thermal stability. Thus far, ceramic composites have been reproducibly fabricated with exceptional mechanical and thermal properties to temperatures of approximately 1800 F. However, accompanying the excellent mechanical and thermal properties which are useful for structural purposes, the effective thermal conductivity and density of ceramic composites are relatively high for insulation applications, in part because the ceramic composites are solid materials.

### I.2.4 Radiation/Layered Configurations

The fourth category of candidate structural configurations is radiation/layered, where thin layers of metallic foil such as tantalum are wrapped with fibrous layers. The purpose of the metallic foil is to reduce radiation through the insulation layer, but experimental data (Ref. 28) suggests that the effective thermal conductivity of the combination at high temperature increases over time because of reactions between the foil and the fibrous layer. The deteriorated values of the effective thermal conductivity of the combination are higher than the values of purely fibrous insulations. If radiation/layered materials were experimentally developed, then these materials could be advantageously used to provide efficient insulation. Nevertheless, radiation/layered materials are difficult to use in real systems that have curved surfaces or small dimensions.

### I.2.5 Powders

The last category of candidate structural configurations is powders, which are used in cryogenic applications and medium-temperature applications where thin metal structures can be used to contain the powders. For high-temperature applications, several problems arise for the potential use of powders. Metals can not be used for containment at high temperatures in hot-gas applications, and most powder materials have undesirable sintering and compaction (or shrinkage) behavior and also can be typically several times as dense as ceramic foam. Solid conduction is limited in powder materials because of the thermal resistance at the many contact points, and the fine powder also scatters and attenuates thermal radiation thereby reducing heat transfer by this mode through the insulation.

### I.2.6 Summary of Candidate Structural Configurations

Generally speaking, the following statements can be made about the candidate structural configurations for hot-gas applications, and details on the physical properties of candidate materials for these structural configurations will be discussed in Section I.3. Currently, the maximum operating temperature of insulation materials available in the open literature is 3000 F or less. The fibrous materials generally have the lowest values of effective thermal conductivity and density, primarily because of their porosity, but they provide no mechanical rigidity and have maximum operating temperatures of 2700 F or less - generally quite a bit less than 2700 F for most fibrous materials. Ceramic foams have values of effective thermal conductivity and effective density that are higher than fibrous materials. Foams do have mechanical structure and some have maximum operating temperatures of 3000 F. Ceramic composites have excellent mechanical and thermal properties but are currently limited to maximum operating temperatures of approximately 1800 F because of oxidation problems. Composites also have a relatively high thermal conductivity and density when compared with ceramic foams or fibrous insulations. Radiation/layered materials have undesirable reactions at high temperatures between the metallic layers and the fibrous layers, which reactions result in an adversely increasing effective thermal conductivity. Powder materials have containment problems in hot-gas applications, and also undesirable compaction and sintering occurs.

### I.2.7 Structural Configurations for Passive Laser Countermeasures

Candidate configurations for passive laser countermeasures could involve several mechanisms of heat transfer, as indicated in Fig. I.4. The laser beam impinges upon the outside surface of the passive countermeasure device and is partially reflected by the thin reflective layer. The laser energy that is not reflected can burn through this outside layer and then begin to burn through the ablative layer. If the ablative layer is thick enough to outlast the relatively short duration of the laser attack, then this layer would remain intact but be at

a high temperature, for example 4000 F. The insulating layer inside the ablative layer would then protect the thermal wave from penetrating and overheating the underlying metal structure and/or electronics. At these temperature levels, both conduction through the solid and radiation heat transfer will be contributing modes if the insulating layer is porous, which is the case for fibrous insulations and ceramic foam insulations. Furthermore, if there is gas within the porous insulation layer, then gas conduction will also occur, in addition to conduction through the solid portion of the insulation.

### I.3 Physical Properties of Candidate Materials

Candidate materials for heat transfer retardation in hot-gas applications have been identified for the candidate structural configurations discussed above in Section I.2. Table I.2 summarizes these candidate materials in terms of their structural configuration. Powder materials are not included because of obvious containment problems for hot-gas applications, not to mention the undesirable sintering and compaction problems of powders at high temperatures. In this section, the thermophysical properties of candidate materials for heat transfer retardation configurations have been examined using data from the literature.

#### I.3.1 Insulation Performance Factor

The effective thermal conductivity of candidate materials is obviously important for the prediction of heat loss and the temperature drop through a given thickness of that material. But material density is also an important consideration if the retardation device is to be lightweight. A simple thermo-physical factor that combines density and thermal conductivity can be developed to rate the candidate insulation materials in terms of relative weight and thereby to select the material for each layer of a multi-layer retardation device that has the lowest relative weight.

The Fourier conduction law can be used to describe the heat transfer ( $q/A$ ) across a thickness of insulation:

$$q/A = \frac{k}{\delta} (T_1 - T_2) \quad (I.1)$$

where  $k$  is the effective thermal conductivity,  $\delta$  is the thickness of insulation in the direction of heat flow across the temperature differential. Hence, by rearrangement:

$$\delta = \frac{k}{(q/A)} (T_1 - T_2) \quad (I.2)$$

The weight of insulation per unit face area ( $Wt/A$ ) is given by the expression:

$$Wt/A = \rho\delta \quad (I.3)$$

where  $\delta$  is the effective density of the insulation. By combining Eqs. I.2 and I.3 to eliminate  $\delta$ , then the following expression for the unit weight of the insulation material is obtained:

$$Wt/A = \rho k \left( \frac{T_1 - T_2}{q/A} \right) \quad (I.4)$$

Therefore, with a given temperature difference across the material and a specified heat loss, the relative weight of an insulating material is proportional to the factor,  $\rho k$ . In other words, for a lightweight heat transfer device, materials with low values of  $\rho k$  are desirable.

Figure I.5 shows the effective thermal conductivity of selected materials as a function of mean temperature of the material. The effective thermal conductivity of a material is a measured value and therefore includes all operative modes of heat transfer across the material, at the temperature level of interest. This thermal conductivity data is re-plotted in Fig. I.6 as the insulation performance factor,  $\rho k$ , and the relative position of some of the insulation materials changes because of their density. For example, Min-k insulation has a very low value of effective thermal conductivity, as seen in Fig. I.5, but its value of the insulation performance factor is not as relatively favorable, as seen in Fig. I.6. The selected materials of construction in Figs. I.5 and I.6 will be discussed in more detail in the text following, in groups according to their structural configurations.

### I.3.2 Fibrous Materials

Candidate fibrous materials considered for use in high-temperature heat transfer retardation devices include: Dynaquartz (silica), alumina, zirconia, graphite, and Min-k. Dynaquartz fibrous insulation, manufactured by the Manville Corporation, has a very low value of thermal conductivity and also a very low value of the insulation performance factor ( $\rho k$ ), as seen in Fig. I.6. This insulation has a maximum operating temperature of 2700 F, according to test results (Ref. 28).

Alumina fibrous insulation may be stable up to about 3200 F, but it is quite costly as compared to Dynaquartz and the effective thermal conductivity is about 30 percent higher than that of Dynaquartz (Ref. 29). Zirconia fibrous materials have major problems with undesirable shrinkage and reaction at temperatures over 2500 F (Refs. 29 and 30). Tests (Ref. 30) with "Saffil Zirconia HT" in the form of fibercakes showed less than 15 percent linear shrinkage for a time period on the order of only 100 hours at 2550 F, and the same material in the form of

fibrous blankets showed 15 percent shrinkage in less than 25 hours at 2550 F. Either period of time is too short for relatively long-term applications such as protection walls in gas turbine combustors and nozzles. Graphite has a relatively high thermal conductivity for use as an insulation material, and it can not be used in an oxidizing atmosphere.

Fibrous insulation Min-k, manufactured by the Manville Corporation, has a medium value of the  $pk$  product, but it has a maximum long-term use temperature of 1800 F. Actually, the thermal conductivity of Min-k is very low, but its density is too high for light-weight applications. For applications where weight is not a prime consideration, Min-k is a familiar insulation in the form of a fibrous blanket for applications at 1800 F or lower.

### I.3.3 Ceramic Composites

Ceramic composites have been under development (Ref. 31) in recent years as a structural material for high-temperature hot-gas applications. The term, ceramic composites, refers to materials where fibers exhibiting high strength and stiffness are used to reinforce a low-modulus glass matrix. Fibers made of graphite, alumina, or silicon carbide have been utilized. The glass matrix composite using SiC fiber was found to be capable of achieving excellent mechanical properties at temperatures of up to 1100 F (Ref. 32), but the borosilicate glass matrix that was used did not allow the high temperature potential of the SiC fibers to be realized. In response to this need for higher use temperatures, high-silica glass (Ref. 33) was tried as the matrix and, while higher use temperatures were achieved, this approach resulted in significantly greater fabrication problems because of the higher viscosity of this glass during composite consolidation. To reduce the fabrication problems, a glass-ceramic was used as the composite matrix, which use resulted in a combination of high composite use temperature and also fabrication ease, because composite densification can occur while the matrix is maintained in a low-viscosity glass state while the composite can be used structurally after the matrix has been crystallized for thermal stability.

Currently, ceramic composites have been developed for maximum operating temperatures of 1800 F, with the limitation occurring because of oxidation problems. The ceramic composite consisting of SiC yarn reinforced lithium aluminosilicate glass ceramic has an effective thermal conductivity of 1.1 BTU/hr-ft-F (in a direction perpendicular to the fibers) at 1800 F, which value is high compared to the thermal conductivity of Dynaquartz of 0.098 BTU/hr-ft-F at the same temperature. Further, although light when compared with metals, ceramic composites are relatively heavy (with a density of 156 lbm/ft<sup>3</sup>) when compared to the values for Dynaquartz of 4 to 6 lbm/ft<sup>3</sup>. Thus the insulation performance factor ( $pk$ ) of ceramic composites is too high for their use as an insulation, but ceramic composites do have excellent mechanical properties that

the ceramic foams lack. And ceramic composites have the structure that fibrous insulations lack. If the maximum use temperature of ceramic composites were to be increased to the neighborhood of 3000 F by continued development, then a thin layer of ceramic composite could provide structure as the outer layer of a multi-layer retardation device, with the internal fibrous layer(s) providing the bulk of the resistance to heat transfer.

#### 1.3.4 Ceramic Foam Materials

There are several candidate materials in the category of ceramic foams: All-Alumina foam, Alumina foam, and SiC foam. In general, although the foams have structure, they are quite brittle. Values of the effective thermal conductivity for these three foams are shown in Fig. I.5. The All-Alumina foam, a high-purity foam made by RIM Products Corporation, has the lowest conductivity of the three foams in the temperature range of interest. The conductivity of the SiC foam is more than twice as high as the value for either of the alumina foams, which circumstance greatly reduces interest in SiC foam as a potential insulating material.

The insulation performance factor is shown in Fig. I.6 for these three ceramic foams. Because the alumina foam (manufactured by Norton with a porosity of 88 percent) has a density that is about twice that of the All-Alumina foam, the All-Alumina foam has an insulation performance factor that is favorably lower than that of the alumina foam, as well as much lower than the value for the SiC foam. Hence the ceramic foam with the most interest for high-temperature retardation applications is the All-Alumina foam.

#### 1.3.5 Radiation/Layered Materials

Several radiation/layered materials, consisting of alternate layers of a fibrous or paper insulation and of a metal foil, have been tested (Ref. 28). One of the configurations tested was formed with alternate layers of an insulating paper ("Dexiglas" paper, which is about 50 percent  $\text{SiO}_2$ ) and aluminum foil (0.002 in. thick). The other configuration tested was formed with alternate layers of an insulating paper ("Fiberfrax" paper, which has almost equal portions of  $\text{Al}_2\text{O}_3$  and  $\text{SiO}_2$ ) and tantalum foil (0.0005 in. thick).

However, both configurations encountered problems caused by temperature at about the 2500 F level on the hot side. The aluminum foil apparently melted in the one configuration, while reactions between the tantalum foil and the aluminum silicates in the paper were the apparent cause of the deterioration of the second configuration. Basically, the effective thermal conductivity showed about a 50 percent increase for the data taken after the maximum hot side temperature had been reached. However, before the deterioration occurred, the thermal

conductivity of the tantalum configuration was about 30 percent lower than that of the Dynaquartz fibrous insulation (Ref. 28).

Hence, if a multi-foil insulation could be developed to eliminate this deterioration, it would be a promising insulation. One problem would still be the density of the fibrous layer, because "Fiberfrax" has a density of about 15 lbm/ft<sup>3</sup>, as compared to the Dynaquartz density of 4 to 7 lbm/ft<sup>3</sup> depending on the compaction. Thus the insulation performance factor of Dynaquartz would still be lower than that of a radiation/layered insulation that had a paper layer with a density on the order of 15 lbm/ft<sup>3</sup>.

### I.3.6 Materials for Passive Laser Countermeasures

As mentioned above in Section I.1.5, the reflectivity of the target is important in laser countermeasures applications because high reflectivity favorably reduces the amount of energy that is absorbed by the retardation device. Typical reflectivity values (from Ref. 34) for metals with smooth surfaces are shown as a function of beam wavelength in Fig. I.7. CO<sub>2</sub> lasers have a wavelength of 10.6 microns, where the reflectivity is high for all these metals with polished smooth surfaces. Rough surface finishes and surface oxides (which can be formed while the surface is being heated) will reduce the reflectivity. The effect of temperature on surface reflectivity is shown in Fig. I.8 (adapted from Ref. 35). For aluminum, the reflectivity falls from a high value (in excess of 0.98 at room temperature) to a much lower value as the aluminum approaches its melting temperature, and then abruptly falls when the metal melts. Thus even though the reflectivity of the outer surface material can be very high if the thin surface layer is made of polished aluminum, if the incident laser beam is of sufficiently high intensity, then the surface will begin to heat and the surface reflectivity will then fall. If the beam lasts long enough, then the thin reflective layer will be burned through and the underlying ablative layer will begin to ablate.

Experimental data for laser penetration rates compiled from the literature (Refs. 36, 37 and 38) are shown in Fig. I.9 for selected materials as a function of beam intensity. The two materials with the lowest penetration rates are the ATJ graphite and the carbon/epoxy material, which both have relatively low densities of approximately 100 lbm/ft<sup>3</sup>. These materials have sublimation temperatures in the vicinity of 7000 F. Because of their low laser penetration rates, these two materials are strong candidates for the ablative layer of the retardation device.

A parallel approach to using the ablative materials discussed above would be to use an ablative material with capsules that are embedded in the ablative material and that contain a gas, as shown schematically in Fig. I.10. The gas selected would be released by the laser ablation of the outer edge of the

ablative layer (and hence the capsule shell) and would absorb the rest of the laser's energy above the retardation device. One candidate gas for the capsules would be  $SF_6$ . An added feature of the capsule approach would be that the ablative layer at that spot would not be destroyed beyond the thickness necessary to release the gas, and hence the ablative layer with its capsules would largely remain intact at that location in case another laser beam attack were to hit that exact spot.

With sublimation (or ablation) temperatures potentially as high as 7000 F and with the relatively high thermal conductivity of the candidate ablative materials with the lowest laser penetration rates (such as carbon- or graphite-based materials), an insulating layer behind the ablative layer is required to protect the underlying structure and/or electronics from the transient temperature response that will occur even after the actual laser beam attack has ended. For example, Fig. I.11 shows the temperature response of a one-half-inch thick slab of zirconia foam that is suddenly exposed to a high-temperature heat source. Because of the low thermal conductivity of the foam, time is required for the heat to penetrate this insulation. Fig. I.12 shows the bulk average temperature of this slab as a function of time and indicates that, even though the laser beam attack may last only a few seconds, there is a significant increase in the heat content of the foam insulating slab.

The effective thermal conductivity of selected insulating materials was shown earlier in Fig. I.5, and the insulation performance factor and maximum operating temperature were shown in Fig. I.6. The insulating material with the lowest value of  $pk$  is Dynaquartz which has a maximum operating temperature of 2700 F.

## I.4 Selection of Configuration and Materials Combinations

Combinations of retardation configuration types and their materials of construction have been selected for analysis of their retardation characteristics in terms of their overall resistance to heat transfer. The selection criteria are lightweight configurations with high resistance to heat transfer. The possible operating limits of these selected combinations of configuration and materials have been identified in terms of maximum operating temperatures, working fluids, and erosion and corrosion problems.

### I.4.1 Selected Combinations for Hot-Gas Applications

Based on the discussion of candidate materials in Section I.3, multi-layer combinations of retardation configuration types and their materials of construction have been selected for hot-gas applications, for analysis of their overall retardation characteristics relative to their weight characteristics. As already discussed, materials that have low values of the insulation performance factor ( $\rho k$ ) are the best in terms of providing high resistance while being relatively lightweight.

Because of the characteristics of the individual materials, multi-layer configurations provide the best approach to heat transfer retardation. The class of materials with the lowest values of the insulation performance factor are fibrous materials, as seen earlier in Fig. I.6, and the fibrous material with the lowest value of the insulation performance factor is Dynaquartz. But fibrous insulations do not provide a hard and relatively smooth gas flowpath for hot-gas applications, and the fibrous material could be torn off by the shearing forces of the flowing gas. Further, fibrous insulations have only limited structural capabilities and must be supported by other materials.

To sidestep these problems while still retaining the excellent insulating characteristics of the fibrous materials, an outer layer of ceramic foam (or ceramic composite for some hot-gas applications with lower temperatures) is proposed to provide both the gas flowpath and structural support for the inner fibrous layer(s). Figure I.13 shows the rationale of this multi-layer approach. Because ceramic foams and ceramic composites have values of  $\rho k$  that are much higher than those of fibrous insulations such as Dynaquartz, the outer layer of ceramic foam or composite should be made as thin as is structurally possible in order to keep the relative overall weight of the retardation device as low as possible.

If a certain thickness of ceramic foam is required, one possible way to reduce the weight of the required thickness would be to incorporate either machined slots or axial holes cast into the ceramic foam, as shown conceptually in Fig. I.14. However, while these large uniform voids would reduce the

effective density of the foam, the fabrication cost of such foam would probably be significantly higher than that of plain ceramic foam.

Shown in Fig. I.15 are the multi-layer combinations (for hot gas applications) of retardation configuration types and their materials of construction that have been selected for analysis, based on the groundwork discussed in Sections I.2 and I.3. In general, the outer layer of the retardation devices selected is hard and relatively smooth, in order to provide a gas flowpath, and the outer layer also provides support for the relatively limp fibrous layers. The interior of the device consists of fibrous insulation that provides the bulk of the heat transfer resistance because of the lower effective thermal conductivity of the fibrous materials.

Of the six candidate combinations selected for analysis, three have outer layers made of All-Alumina foam, which has the lowest  $\rho k$  value of the available foam materials and which can operate at temperatures of up to 3000 F. The remaining three combinations have outer layers made of COMGLAS™, a ceramic composite, which has excellent mechanical properties at temperature but is currently limited to only 1800 F because of oxidation problems. However, future developments in ceramic composites may result in increases in the maximum operating temperatures well beyond the current allowable levels.

Four of the six combinations selected have a single layer of fibrous insulation inside the outer layer, while the other two combinations have two layers of fibrous insulation inside the outer layer. The single fibrous layer in these combinations is made of materials with the lowest  $\rho k$  values: Dynaquartz and Cerablanket insulation. The Dynaquartz insulation has the advantageously lower  $\rho k$  value of these two insulations and has a maximum operating temperature of 2700 F. On the other hand, Cerablanket has a lower maximum operating temperature of 2400 F, so that Dynaquartz is the more desirable choice of these two fibrous insulations. The maximum temperature of the hot side of this fibrous layer (either Dynaquartz or Cerablanket) will be varied in the analysis to see the effect of this limitation on the heat transfer and weight characteristics, but the temperature in an actual design would be limited to the maximum operating temperature recommended by the producer in order to avoid deterioration of the insulation.

The remaining two (of the six total combinations selected for analysis for hot-gas applications) have a second inner layer (which is made of Min-k insulation), for a total of three layers in each of these two retardation configurations. Min-k has the lowest thermal conductivity of the fibrous insulations when operating in air, but its maximum operating temperature is only 1800 F and it has a  $\rho k$  value that is above that of Dynaquartz (because of the higher density of Min-k). Min-k is a familiar insulation, and its maximum operating temperature on the hot side of this layer will be varied in the analysis to see its effect on

the heat transfer and weight characteristics, but in an actual design the maximum operating temperature will be limited to this 1800 F.

However, because the  $\rho k$  value of Min-k is higher than that of either Dynaquartz or Cerablanket, it is expected that the three-layer configurations with Min-k as the cold-side layer will be heavier, at the same level of heat transfer through the configuration, than the two-layer configurations with either Dynaquartz or Cerablanket and the same hot-side layer (of either All-Alumina foam or COMPGLAS™ ceramic composite). As discussed earlier, Dynaquartz insulation has been found to be an effective insulation, and can provide the same amount of heat transfer resistance at less weight than Min-k insulation.

#### I.4.2 Operating Limits

The insulating materials selected for analysis have operating limits, some of which have been mentioned in the above paragraphs. Possible limits include maximum operating temperatures and system working fluids which in turn can be related to possible erosion and corrosion problems.

##### I.4.2.1 Temperature Limits

In general, the insulating materials selected will deteriorate over time if they are used at temperatures above their maximum temperature limit. Therefore, the recommended maximum operating temperature has been established by testing. In tests conducted by A. D. Little (Ref. 28), the maximum operating temperature of Dynaquartz, manufactured by The Manville Corp., is approximately 2700 F. Cerablanket, also manufactured by The Manville Corp., has a maximum operating temperature of 2400 F (Ref. 39). Min-k insulation, also manufactured by The Manville Corp., has a maximum operating temperature of 1800 F (Ref. 40). The All-Alumina foam, manufactured by the RIM Corp., has a maximum operating temperature of almost 3000 F (Ref. 41). The COMPGLAS™ ceramic composite has a current maximum operating temperature of 1800 F (Ref. 31), but future development work on this family of ceramic composites may eventually increase this maximum temperature.

##### I.4.2.2 Other Operating Limits

The insulation materials selected are all generally suitable for hot-gas applications because they have been developed for and previously used in furnaces that contain air. In general, oxidation or shrinkage problems did not occur with these materials if they were used at or below their recommended maximum operating temperature. Above this temperature level as determined by testing for each specific material, the material would deteriorate in time.

The main potential problem with erosion would seem to occur with the fibrous insulations, where the shear force caused by the flowing gas could tear off fibers if the layer is directly exposed to this gas. To avoid this potential problem, a multi-layer structure has been selected, with the outer layer made of ceramic foam or ceramic composite to shield the fibrous material.

Problems with water corrosion are not expected because condensation of water from the combustion products can not occur in the hot section. Possible corrosion problems can sometimes occur at high temperatures where a ceramic material comes into contact with a metal. For example, problems can occur in radiation/layered materials with reactions between the fibrous layers and the metal foil, but radiation/layered materials have been ruled out for retardation in hot-gas applications in order to avoid this problem and also the problem of forming this material for curved surfaces and areas with small radii.

#### I.4.3 Candidate Combinations for Passive Laser Countermeasures

Based on the considerations in Section I.3.6, a number of candidate combinations of configurations and materials were identified for application to heat transfer retardation devices for laser countermeasures applications. A layered approach is used, because there does not seem to be one material that possesses all three desirable characteristics of high reflectivity, low laser penetration rate, and low effective thermal conductivity. Figure I.16 summarizes the candidate combinations of configurations and materials, in terms of three-layer configurations, two-layer configurations, and one-layer configurations. The one-layer configurations selected essentially isolate the laser energy absorption characteristics, in terms of the laser ablation process or the absorption of laser energy by interaction with a gas (such as  $SF_6$ ) which is envisioned as being released when the outer edge of its containment capsule is burned off by the incident laser energy.

The two-layer configurations consist of an outer ablative layer and an inner insulating layer which is included to protect the underlying structure and/or electronics from the thermal wave that will still be a potential problem even after the duration of the laser beam. For two of the two-layer candidate configurations, the ablative layer includes a metallic ingredient. In one case, the metallic ingredient is in the form of a metallic foil which would be sandwiched in layers in the carbon/epoxy ablative layer. The aim of the metallic foil would be to increase the reflectivity of the inner mass of the ablative layer. Whether the reflectivity would actually remain high during the ablation process is a moot point for two reasons. First, as seen earlier in Fig. I.8, as the temperature of the metal (such as aluminum) increases, the reflectivity will decrease from its room-temperature value. And second, the ablation process will not be very orderly, with melted and/or charring ablation material sticking to the metallic foil and thereby obfuscating the purpose of the metallic foil. In

the case of the second of the two-layer candidate configurations, metallic flakes (again such as aluminum) would be incorporated into the ablative layer with the same aim of increasing the internal reflectivity of the ablative layer. Whether or not the metallic flakes would work is again a moot point for the same two reasons given above for the metallic foil.

The three-layer configurations have a thin reflective layer (of polished aluminum, for example) as the outside skin over the ablative and insulation layers. At the high laser intensities, the aluminum layer would be rapidly heated, but the rapid heating rate would still be slower than if the outer layer were a material with a lower reflectivity. The materials proposed for each layer of the candidate configurations offer the best capability of the materials available in the literature to handle the mode of heat transfer expected at each layer of the configuration: high reflectivity for the outer layer; high resistance to laser-induced ablation in the middle layer; and high resistance to thermal conduction through the inside insulating layer.

The parameters that could be varied for experiments with the candidate configurations will now be discussed in the following paragraphs. The high reflectivity of the outside layer is essentially a surface effect, so that the thickness of the outside layer is not expected to be a factor in the experiments. Polished aluminum is the most economical choice, because the reflectivity of either gold or silver is only slightly higher according to the reflectivity data of Fig. I.7.

The ablative layer should be made of a lightweight material with a high resistance to laser-induced ablation, such as graphite or carbon/epoxy. The thickness of this layer can then be designed, using the data on laser penetration rates shown in Fig. I.9 for example, to meet the anticipated intensity and duration of the laser beam hypothesized to be encountered in the attack. For the ablative layers that include metallic ingredients, the spacing of the layers of metallic foil should be varied in the experiments, and the average spacing of the metallic flakes should be varied. Apparently, no ablation data exists for materials containing such metallic ingredients, so that reasonable judgements would have to be the guiding factor in the design of the experimental pieces containing either of these metallic ingredients. For the ablative material with gas capsules embedded in it, the capsule diameter and the average capsule spacing are variables of interest. The gas selected, such as SF<sub>6</sub> or water vapor, would also be expected to have a large effect on the laser absorption characteristics of this layer.

The primary variables in the design of the inner layer of insulation for the test pieces will be the thickness and the geometric pattern such as grooves that could be used to reduce the weight and possibly the thermal conductivity of the insulating layer. Possible geometric patterns were discussed in more detail in the section on heat transfer retardation devices for hot-gas applications.

## I.5 Analysis of Retardation Characteristics

A model of heat transfer has been formulated for the analysis of the retardation configurations selected above for hot-gas applications and has been used to estimate the heat transfer retardation characteristics in terms of an overall thermal resistance through the configuration. The unit weight of the overall configuration has also been estimated for use in identifying lightweight combinations of configuration types and their materials of construction. The assumptions made to simplify the heat transfer model and the resulting limitations in the model are discussed.

### I.5.1 Model of Heat Transfer

A simplified model of heat transfer through the configurations selected for hot-gas applications has been formulated using the effective thermal conductivity of each layer of insulation in the multi-layer retardation devices. The effective thermal conductivity is the quantity measured when thermal conductivity tests are conducted on porous media at high temperature, and the effective thermal conductivity thereby measured accounts for all modes of heat transfer across the insulation at the temperature level of interest: conduction through the solid and the gas in the pores, and thermal radiation through porous insulation.

Figure I.17 is a schematic representation of the steady-state heat transfer model of retardation configurations for hot-gas applications. Allowance is made for contact resistance between the layers, although the contact between a fibrous layer and a ceramic foam can not be described well, and in fact this less-than-intimate contact between the fibers in the body of the fibrous insulation is the principal basis for the lower thermal conductivity of the fibrous insulation. In any event, the existence of contact resistance in retardation applications would be advantageous, in contrast to many applications where the contact resistance would form an unwanted barrier to heat transfer.

To model the multi-layer configurations, the combined heat transfer through each of the layers will be considered. Using the Fourier conduction law, the combined heat flux ( $q/A$ ) through layer 1 (the layer exposed to the flowing gas) can be written as:

$$q/A = \frac{k_1}{\delta_1} (T_{Hot} - T_{Cl}) \quad (I.5)$$

where  $k_1$  is the effective thermal conductivity of layer 1 as discussed above, and  $\delta_1$  is the thickness of layer 1.

The hot-side temperature of the layer is used as the descriptive variable instead of the gas temperature, because there is a wide range of flow conditions that would determine the temperature drop through the gas film. Predictions presented later can be used to estimate this temperature drop for possible operating conditions. However, with forced convection flow past the outer layer, the temperature drop through the gas film will generally be quite small as compared with the temperature drops through the low-conductivity layers of insulation, so that the hot-side temperature ( $T_{Hot}$ ) will actually be nearly equal to the gas temperature ( $T_{Gas}$ ) in many cases of interest for hot-gas applications.

The heat flux through the contact resistance between layers 1 and 2 can be represented in terms of a contact resistance ( $h_{c12}$ ):

$$q/A = h_{c12} (T_{C1} - T_{mid}) \quad (I.6)$$

Similarly, the equations for the combined heat transfer through layer 2, for the contact resistance between layers 2 and 3, and for the combined heat transfer through layer 3 to the cold-side temperature ( $T_{Cold}$ ) can be written as follows:

$$q/A = \frac{k_2}{\delta_2} (T_{mid} - T_{C2}) \quad (I.7)$$

$$q/A = h_{c23} (T_{C2} - T_{Min-k}) \quad (I.8)$$

$$q/A = \frac{k_3}{\delta_3} (T_{Min-k} - T_{Cold}) \quad (I.9)$$

where  $k$  is the effective thermal conductivity of the specific material selected for each layer at the average temperature of that layer. The above five equations can be combined in such a manner as to eliminate the internal temperatures, with the result being the heat flux through the entire retardation configuration in terms of the overall temperature difference ( $T_{Hot} - T_{Cold}$ ):

$$q/A = \frac{T_{Hot} - T_{Cold}}{\frac{\delta_1}{k_1} + \frac{1}{h_{c12}} + \frac{\delta_2}{k_2} + \frac{1}{h_{c23}} + \frac{\delta_3}{k_3}} \quad (I.10)$$

The overall resistance, the R-factor, is defined as:  $R \equiv \Delta T/(q/A)$ . Thus the overall R-factor for a 3-layer configuration can be written as:

$$R = \frac{\delta_1}{k_1} + \frac{1}{h_{c12}} + \frac{\delta_2}{k_2} + \frac{1}{h_{c23}} + \frac{\delta_3}{k_3}$$

The ratio of the temperature drops in each of the layers can be obtained by manipulating Eqns. I.5 to I.9:

$$\frac{T_{Hot} - T_{mid}}{T_{mid} - T_{C2}} = \frac{k_2}{\delta_2} \left( \frac{\delta_1}{k_1} + \frac{\delta_3}{h_{c12}} \right) \quad (I.11)$$

$$\frac{T_{Hot} - T_{mid}}{T_{mid} - T_{C2}} \cong \frac{k_2}{k_1} \frac{\delta_1}{\delta_2} \quad \text{for } \frac{\delta_1}{k_2} \gg \frac{1}{h_{c12}} \quad (I.11a)$$

$$\frac{T_{Hot} - T_{mid}}{T_{Min-k} - T_{Cold}} = \frac{k_3}{\delta_3} \left( \frac{\delta_1}{k_1} + \frac{1}{h_{c12}} \right) \quad (I.12)$$

$$\frac{T_{Hot} - T_{mid}}{T_{Min-k} - T_{Cold}} \cong \frac{k_3}{k_1} \frac{\delta_1}{\delta_3} \quad \text{for } \frac{\delta_1}{k_1} \gg \frac{1}{h_{c12}} \quad (I.12a)$$

For a given application where  $T_{Hot}$  and  $T_{Cold}$  are fixed by given constraints, then the internal temperature levels can be varied in the analysis by changing the thickness of the layers relative to each other ( $\delta_1/\delta_2$ ), once specific materials have been chosen for each layer (in order to set  $k_2/k_1$ ).

Conversely, the effect of varying the internal temperatures on the relative thicknesses can be examined by rearranging Eqs. II.11a and I.12a into the

following form (which applies for cases of relatively low contact resistance, as will be discussed below):

$$\frac{\delta_2}{\delta_1} = \frac{k_2}{k_1} \left( \frac{T_{\text{mid}} - T_{\text{C2}}}{T_{\text{Hot}} - T_{\text{mid}}} \right) \quad (\text{I.13})$$

$$\frac{\delta_3}{\delta_1} = \frac{k_3}{k_1} \left( \frac{T_{\text{Min-k}} - T_{\text{Cold}}}{T_{\text{Hot}} - T_{\text{mid}}} \right) \quad (\text{I.14})$$

Then if the total thickness of the configuration ( $\delta_{\text{TOT}}$ ) is set, the thickness of the individual layers can be determined from the following identity:

$$\delta_{\text{TOT}} = \delta_1 + \delta_2 + \delta_3 \quad (\text{I.15})$$

or

$$\delta_1 = \frac{\delta_{\text{TOT}}}{1 + \frac{\delta_2}{\delta_1} + \frac{\delta_3}{\delta_1}} \quad (\text{I.16})$$

In practice, the maximum value of the hot-side temperature of each layer will be set by the maximum operating temperature of that layer, as specified by the producer of that insulation.

#### I.5.1.1 Interfacial Contact Resistance

Figure I.18, which is from "The Handbook of Heat Transfer" (Ref. 42), shows the level of contact conductance ( $h_c$ ) that can be expected between combinations of the gap fluid (or vacuum) and various metals. Heat transfer across an interfacial gap occurs through the combined mechanisms of solid conduction (across actual contact points), conduction across the gas or fluid in the gap, and thermal radiation across the gap. And these are the same mechanisms by which heat is transferred through porous insulations. So the point at which the heat transfer resistance of the insulation can be distinguished from the contact

resistance is not clear because both resistances are so similar in their heat transfer mechanisms.

In Figure I.18, for curves that correspond to interface gaps that contain air (Curves 4 to 6 and 16 to 18) as will be the case in hot-gas applications, the contact conductances are all higher than 300 BTU/hr-ft<sup>2</sup>-F which is much higher than the conductance ( $k/\delta$ ) for the insulation materials and their thicknesses anticipated for the retardation layers. In other words, for hot-gas retardation applications, the contact conductance is high enough relative to the conductance of the insulation layers that the assumption of  $(\delta/k) \gg (1/h_c)$  is valid.

#### I.5.1.2 Surface Boundary Conditions

In order to be able to handle the possible wide range of surface boundary conditions, the surface temperature of the hot-side layer was selected as the variable. For various levels of forced convection over a flat plate, the heat transfer coefficient between the gas and the surface can be estimated as a function of the gas velocity and the other operating conditions.

The local Nusselt number ( $Nu_x$ ) for subsonic turbulent flow over flat plates is given by the expression:

$$Nu_x = 0.029 Re_x^{0.8} Pr^{1/3} \quad (I.17)$$

where  $Re_x$  is the local Reynolds number of the flow based on flow length ( $x$ ) and  $Pr$  is the Prandtl number of the gas. The transition Reynold number for a flat plate is approximately  $3.2 \times 10^5$ , above which the flow is turbulent. For lower Reynolds numbers where the flow is laminar, the local Nusselt number is given by the expression:

$$Nu_x = 0.332 Re_x^{0.5} Pr^{1/3} \quad (I.18)$$

Hence the local forced convection heat transfer coefficient can be estimated, using these expressions based on the Reynolds number of the flow:

$$h_{conv} = \frac{k}{x} Nu_x \quad (I.19)$$

In combination with forced convection heat transfer, radiation heat transfer also occurs. An effective radiative heat transfer coefficient ( $h_{\text{rad}}$ ) can be calculated with the expression (Ref. 43):

$$h_{\text{rad}} = \frac{\epsilon_s \sigma T_g^4 - T_s^4}{T_g - T_s} \quad (\text{I.20})$$

where  $T_g$  is the temperature of the gas;  $T_s$  is the surface temperature;  $\sigma$  is the Stefan-Boltzman constant ( $\sigma=0.1713 \times 10^{-8}$  Btu/ft<sup>2</sup>-hr-R); and  $\epsilon_s$  is the emissivity of the surface, which has a value of approximately 0.2 (Ref. 28). A simplified expression for the effective radiative heat transfer coefficient can be deduced from Eq. I.20:

$$h_{\text{rad}} \cong 4 \epsilon_s \sigma T_{\text{mean}}^3 \quad (\text{I.20a})$$

which is valid for cases where the surface temperature is not much lower than the gas temperatures (i.e., cases where the heat flux to the wall is low because the wall is insulated).

Then by assuming parallel paths of heat transfer for the convective contribution and the radiative contribution, the total heat transfer coefficient between the gas and the surface can be taken as the sum of these two coefficients:

$$h_{\text{TOT}} = h_{\text{conv}} + h_{\text{rad}} \quad (\text{I.21})$$

Figures I.19 and I.20 show estimates, based on Fig. I.20, of the temperature drop through the gas film as a function of heat flux, gas velocity, and temperature level. The heat flux levels of interest for hot-gas retardation applications will be on the order of 3500 Btu/hr-ft<sup>2</sup>-F. This number can be deduced from the relationship:  $q \sim k\Delta T/\Delta X$ . A typical value of  $k$  for insulation is 0.08 BTU/hr-ft-F (see Fig. I.4);  $\Delta T$  is the temperature drop across the insulation, on the order of 1800 F for a hot-side temperature of 3000 F and a cold-side temperature of 1200 F; and  $\Delta X$  is the thickness of insulation, perhaps 0.5 in. for a typical installation. Hence the heat flux through the insulation corresponding

to these values of the parameters would be 3500 BTU/hr-ft<sup>2</sup>. The heat flux through the boundary layer would also be this value, which would require a temperature drop through the boundary layer of less than 40 F, as can be seen in Fig. I.19 or I.20.

### I.5.1.3 Two-Layer Model

To obtain the corresponding heat transfer expressions for a two-layer configuration, as shown schematically in Fig. I.21, just set  $\delta_3=0$  and  $h_{c23} = \infty$  (because there is now no contact resistance) in the above analysis and the following equations result:

$$q/A = \frac{T_{\text{Hot}} - T_{\text{Cold}}}{\frac{\delta_1}{k_1} + \frac{1}{h_{c12}} + \frac{\delta_2}{k_2}} \quad (\text{I.22})$$

$$R = \frac{\delta_1}{k_1} + \frac{1}{h_{c12}} + \frac{\delta_2}{k_2} \quad (\text{I.23})$$

Similarly, the ratio of the temperature drops in each layer of a two-layer configuration is given by the expression:

$$\frac{T_{\text{Hot}} - T_{\text{mid}}}{T_{\text{mid}} - T_{\text{Cold}}} = \frac{k_2}{\delta_2} \left( \frac{\delta_1}{k_1} + \frac{1}{h_{c12}} \right) \quad (\text{I.24})$$

$$\frac{T_{\text{Hot}} - T_{\text{mid}}}{T_{\text{mid}} - T_{\text{Cold}}} \cong \frac{k_2 \delta_1}{k_1 \delta_2} \quad \text{for} \quad \frac{\delta_1}{k_1} \gg \frac{1}{h_{c12}} \quad (\text{I.24a})$$

### I.5.2 Unit Weight of Retardation Configuration

The total weight of the insulation per unit face area is determined by the thicknesses of each of the individual layers:

$$Wt/A = \rho_1 \delta_1 + \rho_2 \delta_2 + \rho_3 \delta_3 \quad (I.25)$$

Generally, for a specified heat loss, the lighter-weight multi-layer configuration will result from using the maximum thickness possible of the insulation with the lower value of  $\rho k$ , and the maximum thickness will occur if the hot-side temperature of that layer of insulation is set at the maximum operating temperature for that insulation.

### I.5.3 Simplifying Assumptions

The simplifying assumptions made to formulate the heat transfer retardation model discussed above will be summarized here. First, the effective thermal conductivity is used to describe the heat transfer across a layer of insulation. This is a logical approach because thermal conductivity is a measured parameter, which means that all of the operative modes of heat transfer are accounted for in their actual relationship at the various temperature levels.

Second, the contact resistance between layers of insulation with air in the gap is low relative to the resistance of the insulating layers. This is a reasonable assumption, based on the experimental data shown in Section I.5.1.1. Further, the presence and magnitude of contact resistance can be erratic and should not be relied upon to provide retardation in the performance predictions of retardation configurations.

Third, the model is one-dimensional. The presence of struts to hold the outer layer in place relative to the inner layer could result in localized reductions in retardation. But a one-dimensional analysis is deemed to be suitable for ranking combinations of configurations and materials of construction because these struts would probably be required in all configurations.

### I.5.4 Estimated Retardation Characteristics

Using the model formulated above, the heat transfer characteristics in terms of the overall thermal resistance of the configurations selected for hot-gas applications (Fig. I.15) have been estimated, as well as the unit weights of these configurations. The contact resistance is assumed to be zero in the calculations, as was discussed earlier.

Shown in Figs. I.22 through I.25 are the retardation and weight characteristics, as a function of the interface temperature, of a two-layer retardation device which consists of All-Alumina foam as the outer layer and Dynaquartz

fibers as the inner layer. The operating conditions for these calculations are a hot-side temperature of 3000 F and a cold-side temperature of 1200 F.

Figure I.22 shows the heat loss through the insulation as a function of interface temperature, which is the hot-side temperature of the inner layer. This interface temperature is varied by changing the relative thicknesses of the two layers. Along lines of equal weight, the heat loss decreases as the interface temperature increases, because the thickness of the inner layer relative to the outer layer is increasing and the inner layer (Dynaquartz) in this combination has both a lower effective thermal conductivity and a lower effective density than the outer layer (All-Alumina foam). Along lines of constant thickness of the inner layer, the heat loss increases as the interface temperature is increased, because a larger proportion of the overall temperature drop is then being taken by the inner layer and the thickness of the outer layer must therefore be decreased relative to the thickness of the inner layer and the heat loss rises as a result.

Shown in Fig. I.23 is the decrease in total thickness as the interface temperature is increased, along lines of constant thickness of the inner layer. Figure I.24 shows the overall R-factor ( $R \equiv \Delta T/(q/A)$ ) as a function of the interface temperature. Along lines of constant thickness of the inner layer, the resistance decreases as the interface temperature is increased because the outer layer is becoming thinner and hence the total thickness of insulation is smaller.

Similarly, as seen in Fig. I.25, the weight of the insulation per unit face area decreases as the interface is increased. Along lines of equal heat transfer, the weight decreases as the interface temperature is increased, because the material (Dynaquartz) with the advantageously lower value of the insulation performance factor ( $pk$ ) is being added while the material with the higher value (All-Alumina foam) is being subtracted.

Figure I.26 shows the overall R-factor and weight of the same two-layer combination as a function of the total thickness of insulation ( $\delta_1 + \delta_2$ ). At a constant total thickness, the unit weight of the insulation decreases as the interface temperature ( $T_{mid}$ ) is increased, because the thickness of the inner layer which has a lower density is being increased (see Fig. I.27). And the overall R-factor increases slightly as the interface temperature is increased, at a constant value of the overall insulation thickness. Figure I.28 shows the same type of results for a different grade of Dynaquartz insulation (which has a lower value of  $pk$  — slightly higher conductivity, but lower density) in combination with the same All-Alumina foam for the outer layer. To provide the same overall R-factor, the overall thickness is approximately seven percent thicker, but the unit weight is approximately 13 percent lower. Figure I.29 shows the relative thickness for this combination as a function of interface temperature ( $T_{mid}$ ).

The overall R-factor and unit weight of a two-layer retardation device are shown in Fig. I.30, with the outer layer made of the same All-Alumina foam but with the inner layer made of Cerablanket (fibrous) insulation. Because the maximum operating temperature of the Cerablanket is only 2400 F, the outer layer of foam must be thicker than the foam thickness for the two-layer combination of All-Alumina foam and Dynaquartz discussed above. At a given total thickness, the overall R-factor increases when the interface temperature ( $T_{mid}$ ) decreases because the effective thermal conductivity of Cerablanket is higher than that of the All-Alumina foam, as was seen earlier in Fig. I.5. But the unit weight of the two-layer device also increases when the interface temperature is decreased because the relative thickness of the foam layer must be increased to provide more temperature drop in the outer layer and the effective density of the foam is almost five times as high. Figure I.31 shows the relative thickness of the two layers as a function of  $T_{mid}$ , and as expected the trend is that the relative Cerablanket thickness decreases when the interface temperature decreases.

Shown in Fig. I.32 are the overall R-factor and unit weight of a three-layer device which is the same as the first two-layer configuration discussed above but with the addition of an inner layer of Min-k fibrous insulation. The maximum operating temperature of Min-k insulation is 1800 F. As the temperature at the interface between the foam layer and the Dynaquartz is increased, the relative thickness of the foam layer decreases (as seen in Fig. I.33) and the overall R-factor increases slightly because the effective thermal conductivity of Min-k is lower (even though the effective thermal conductivities of the Dynaquartz and the All-Alumina foam are virtually identical in the temperature range of interest), and the unit weight of the overall combination decreases because the effective density of the Dynaquartz insulation is substantially lower than that of the All-Alumina foam which is being displaced.

Generally, as compared with the two-layer All-Alumina foam/Dynaquartz combination discussed earlier, at the same total thickness, the three-layer combination offers about nine percent higher resistance (because Min-k has a lower effective thermal conductivity of the Dynaquartz that it is displacing), but the unit weight of the three-layer combination is about 12 percent higher because Min-k is more than four times as dense as the Dynaquartz.

Configurations employing COMPGLAS™ ceramic composite as the outer layer were also selected for analysis, but COMPGLAS™ is currently limited to only 1800 F because of oxidation problems that occur at higher temperatures. Nevertheless, calculations have been done with a hypothetical ceramic composite to see its effect on the heat transfer and unit weight characteristics of multi-layer retardation devices, by extrapolating the thermal conductivity of COMPGLAS™ to the temperature levels of 3000 F for hot-gas applications. Thus the assumption has been made that future developments will result in a ceramic composite (with their excellent mechanical properties) that can operate at higher temperatures.

Besides the current temperature limitation, COMPGLAS™ also has a high effective density and a high effective thermal conductivity relative to other insulating materials suitable for high-temperature operation, so that the main advantage of such a ceramic composite would seem to be in its excellent mechanical properties.

Shown in Fig. I.34 are the overall R-factor and unit weight of a two-layer configuration that uses a hypothetical ceramic composite (with an extrapolated thermal conductivity similar to COMPGLAS™) as the outer layer and Dynaquartz as the inner layer. The ceramic composite is labelled "hypothetical" because no current ceramic composite can operate at 3000 F yet. As the interface temperature ( $T_{mid}$ ) is increased, the relative thickness of the outer layer (hypothetical ceramic composite) decreases as seen in Fig. I.35, and the overall R-factor increases because the assumed effective thermal conductivity of the outer layer is much higher than that of Dynaquartz, and the unit weight of the combination decreases because the assumed density of the ceramic composite is much higher than that of Dynaquartz.

The overall R-factor and the unit weight of the hypothetical ceramic composite/Cerablanket combination are shown in Fig. I.36, and the relative layer thickness of this combination is shown in Fig. I.37. This combination exhibits the same trends as existed in the hypothetical ceramic composite/Dynaquartz combination discussed above because the effective thermal conductivities and densities of the two material pairs bear the same relationship to each other.

The remaining combination selected for analysis is the same as the first ceramic composite combination discussed above except with the addition of an inner layer of Min-k insulation. The same trends exist in the estimates of the overall R-factor and the unit weight (Fig. I.38) and in the relative layer thickness (Fig. I.39). As the outer interface temperature ( $T_{mid}$ ) is increased, the overall R-factor increases because the low-conductivity Dynaquartz displaces the hypothetical ceramic composite, and the unit weight decreases because Dynaquartz has a lower effective density. The other three-layer combination (All-Alumina foam/Dynaquartz/Min-k) discussed previously has, at the same total thickness, both a higher overall R-factor and a lower unit weight because the outer layer of All-Alumina foam has more favorable values of the effective conductivity and density for heat transfer retardation.

## I.6 Lightweight Retardation Configurations

Based on available high-temperature insulating materials, performance analyses of selected configurations have been conducted in terms of their geometric parameters to determine their effect on heat transfer retardation, using the analyses developed in Section I.5, and lightweight multi-layer retardation configurations for hot-gas applications have been identified. The effect of material properties on both retardation and weight characteristics has been investigated, and the fractions of the total heat loss that are represented by the different modes of heat transfer through the configuration have been identified.

### I.6.1 Effect of Materials

The effects of thermal conductivity and density are first-order effects because of their prominence in the governing equations. Figure I.40 shows a comparison between two density grades of Dynaquartz as the inner layer behind a layer of All-Alumina foam. The heavier Dynaquartz ( $6.2 \text{ lbm/ft}^3$ ) has an effective thermal conductivity that is approximately eight percent lower than that of the higher Dynaquartz ( $4.5 \text{ lbm/ft}^3$ ). The net result of these factors is that a two-layer configuration employing the heavier Dynaquartz as the inner layer is approximately 24 percent heavier and has an overall R-factor that is approximately eight percent higher, at the same total thickness.

Similarly, Fig. I.41 shows the comparison between using All-Alumina foam (density of  $14 \text{ lbm/ft}^3$ ) as the outer layer, as compared to a hypothetical ceramic composite (density of  $156 \text{ lbm/ft}^3$ ). Because the ceramic composite is estimated to have a density more than ten times as large, the configuration with this hypothetical material, at the same total thickness, weighs much more (by a factor of 16), because the relative thickness of the hypothetical material must be increased in order to provide the same temperature drop - the assumed thermal conductivity of this composite is much higher (by a factor of seven) than that of the All-Alumina foam. And the relatively high conductivity of the hypothetical composite results in an overall thermal resistance (R-factor) that is only half as large. Therefore any justification for the use of this hypothetical material with these assumed properties would have to be based on the superior mechanical properties that some ceramic composites possess at high temperatures.

### I.6.2 Effect of Temperature Level

Temperature level has an effect on the thermal conductivity of the materials and also the temperature difference if only one temperature is changed. Generally the effective thermal conductivity of the porous insulations of interest for hot-gas applications increase with temperature, in part because the contribution of radiation through the material increases. Figure I.42 shows the

effect of changing the cold-side temperature, on the overall R-factor and unit weight of a two-layer combination of All-Alumina foam and Dynaquartz. The hot-side temperature is set at 3000 F, and the interface temperature is also held constant, in the vicinity of 2700 F because this is the maximum allowable temperature for Dynaquartz and it has already been seen that it is advantageous (for this combination of materials) to increase this temperature to the maximum allowable operating temperature. When these two temperatures are fixed and the cold-side temperature is then increased, the relative thickness of the foam layer increases because a larger fraction of the total temperature drop is now taken through the foam layer. Thus the overall R-factor drops because a larger fraction of the total thickness then consists of the higher-conductivity foam, while the unit weight increases because the foam is denser than the Dynaquartz.

Temperature also has an effect on the effective thermal conductivity. Wechsler and Kritz (Ref. 29) have proposed a simple decoupled model that adequately correlates the effective thermal conductivity of many porous insulations

$$k = (1-P)k_s + Pk_g + 4\sigma T_{\text{mean}}^3 d \quad (I.26)$$

where  $k_s$  is the thermal conductivity of the solid material in the porous insulation,  $k_g$  is the thermal conductivity of the gas present in the interstices of the porous material,  $P$  is the porosity,  $d$  is the pore diameter, and  $T_{\text{mean}}$  is the mean temperature (at which  $k_s$  and  $k_g$  are evaluated).  $\sigma$  is the Stefan-Boltzman constant. The term,  $(1-P)k_s$ , represents the contribution to the total heat transfer of conduction through the solid; the term,  $Pk_g$ , represents the gas-conduction contribution; while the radiation contribution is represented by the remaining term,  $4\sigma T_{\text{mean}}^3 d$ . In the case of the All-Alumina foam, however, the predicted radiation contribution seems to be too large as compared to the experimental data unless the radiation term is multiplied by the emissivity of the foam (which is approximately 0.2 according to Ref. 28). So, for the purpose of estimating the relative contributions of the three modes of heat transfer to the overall thermal conductivity, the last term of Eq. I.26 can then be simply modified:

$$k = (1-P)k_s + Pk_g + 4\epsilon\sigma T_{\text{mean}}^3 d \quad (I.26a)$$

Based on this modified formulation, Fig. I.43 shows the relative contributions of the heat transfer modes as a function of temperature, for an assumed porosity of 95 percent, an assumed pore diameter of 0.020 in., and an assumed emissivity of 0.2. Under these conditions at a mean temperature of 2900 F, the conduction through the solid ligaments carries approximately 56 percent of the heat, the radiation contribution is approximately 27 percent of the total, while the contribution from gas conduction is approximately 17 percent.

### I.6.3 Preferred Retardation Configurations

Based on the preceding discussions, the preferred retardation configurations employing available materials can be identified. A two-layer configuration is the simplest that can take hot-side temperatures of 3000 F and that also offers a hard and relatively smooth outer layer and a low-conductivity inner layer. Of the available materials, All-Alumina foam is the preferred material for the outer layer and Dynaquartz is the preferred material for the inner layer, because each has the lowest value of the insulation performance factor ( $\rho k$ ) in its class.

If better mechanical properties are needed for the outer layer, then ceramic composites can offer more structure, but maximum operating temperatures of this type of material are currently limited to only 1800 F. The overall combination that employs a ceramic composite as the outer layer will be significantly heavier than one that uses a ceramic foam as the outer layer, unless the density of ceramic composites can be significantly reduced. Currently available composite materials have a density of approximately 156 lbm/ft<sup>3</sup>, which is a factor of approximately ten higher than the density of All-Alumina foam, for example.

The inclusion of a third layer on the inside adds complexity to the overall configuration. The main advantage of a third layer would be if the material has a lower value of its insulation performance factor but is otherwise restricted in its use to the colder side because of limitations in its maximum operating temperature. Because this additional layer would require its own attachment geometry, the third layer would appear to be worthwhile only if there were a significant advantage in its insulation performance factor at the lower temperatures over the material of the middle layer.

## REFERENCES

1. Giemza, C. J., W. B. Hunter et al.: Final Report on Structural Heat Shield for Reentry and Hypersonic Lift Vehicles - High Temperature Composite Structure. Report No. ML-TDR-64-267, Part I, Vols. 1 and 2, 1965.
2. Scanlon, R. J.: U. S. Patent 3,802,145, assigned to Rohr Corporation, April 9, 1974.
3. Rolinski, E. J., et al.: Development of High-Temperature Insulation Systems. AIAA Paper No. 66-43, 1966.
4. Kummer, D. L. and G. B. Bilow: Refractory Materials and Insulation. AIAA Paper No. 68-1128, 1968.
5. Chapman, A. J.: Evaluation of Reusable Surface Insulation for Space Shuttle Over a Range of Heat-Transfer Rate and Surface Temperature. NASA TM X-2823, 1973.
6. Martynenko, V. V. et al.: Heat Insulation of High-Alumina Wool. Refractories, Vol. 19, No. 7-8 July-August 1979, p. 472-473.
7. Tobin, A., et al.: Development of a Closed Pore Insulation Material. NASA Report CR-2254, 1973.
8. Tobin, A. G.: U. S. Patent 4,016,229, assigned to Grumman Aerospace Corporation, April 5, 1977.
9. Klett, R. D.: U. S. Patent 3,914,392, assigned to U. S. ERDA, October 21, 1975.
10. Ardary, Z. L., D. H. Sturgis, and C. D. Reynolds: U. S. Patent 3,793,204, assigned to the U. S. AEC, February 19, 1974.
11. Deschamps, N. H. and G. L. Bernier: U. S. Patent 3,769,770, assigned to the Sanders Nuclear Corp., November 6, 1973.
12. Asbury, J. J. and J. M. Googin: U. S. Patent 3,634,563, assigned to the U. S. AEC, January 11, 1972.

## REFERENCES (Cont'd)

13. Vogan, J. W. and J. L. Trumball: Metal-Ceramic Composite Materials. Report No. ML-TDR-64-83, 1964.
14. Allen, R. D. and W. M. Lysher: U. S. Patent 3,715,265, assigned to McDonnell Douglas Corporation, February 6, 1973.
15. Nainiger, J. J.: Effect of Thermal Barrier Coatings on The Performance of Steam- and Water-Cooled Gas Turbine-Stream Turbine Combined Cycle Systems. NASA Report TM-79057, 1968.
16. Shiembob, L. T.: Development of a Plasma Sprayed Ceramic Gas Path Seal for High Pressure Turbine Applications. NASA Report CR-135183, 1977.
17. Shiembob, L. T.: Development of a Plasma Sprayed Ceramic Gas Path Seal for High-Pressure Turbine Application. NASA Report CR-135387, 1978.
18. Shiembob, L. T.: Development of Improved High Pressure Turbine Outer Gas Path Seal Components. NASA Report CR-1519801, 1980.
19. Pechman, A. and R. M. Beasley: U. S. Patent 3,955,034, assigned to NASA, May 4, 1976.
20. Hurwicz, H. and R. Mascola: Thermal Protection Systems - Application Research of Materials Properties and Structural Concepts. Report No. ML-TDR-64-82, 1965.
21. Weinberg, E. K.: U. S. Patent 3,725,282, April 3, 1973.
22. Strauss, E. L.: Structural and Heat Transfer Characteristics of Resin-Impregnated Porous Ceramics. American Ceramic Society Bulletin, Vol. 42, 1963, pp. 444-447.
23. Maloof, S.: Tungsten-Base Composites. Astronautics, Vol. 6, No. 4, April, 1961, p. 36.
24. Clawson, J. F.: Thermal Correlation of Heat Protection System. Report AFFDL-TR-65-167, 1965.
25. Rathjen, K. A.: CAVE: A Computer Code for Two-Dimensional Transient Heating Analysis of Conceptual Thermal Protection Systems for Hypersonic Vehicles. NASA Contractor Report 2897, 1977.

## REFERENCES (Cont'd)

26. Garcia, F., and W. T. Fowler: Thermal Protection Optimization for the Space Shuttle, AIAA Paper No. 72-977, 1972.
27. Robinson, C. A.: Laser Technology Demonstration Proposed. Aviation Week and Space Technology, February 16, 1981, pp. 16-19.
28. Wechsler, A. R. and P. E. Glaser: Investigation of the Thermal Properties of High-Temperature Insulation Materials. Technical Documentary Report No. ASD-TDR-63-574, 1963.
29. Wechsler, A. R. and M. A. Kritz: Investigation and Development of High Temperature Insulation Systems. Technical Report AFML-TR-138, 1965.
30. Strauss, R. L.: Evaluation of Low Cost/High Temperature Insulation. NASA CR-134902, 1975.
31. Brennan, J. J. and K. M. Prewo: Silicon Carbide Fibre Reinforced Glass-Ceramic Matrix Composites Exhibiting High Strength and Toughness. J. Materials Science, Vol. 17, 1982, p. 2371.
32. Prewo, K. M. and J. J. Brennan: J. Materials Science, Vol. 15, 1980, p. 463.
33. Prewo, K. M. and J. J. Brennan: J. Materials Science, Vol. 17, 1982, p. 1201.
34. Ready, J. F.: Laser Applications in Metal Working. Society of Manufacturing Engineers Paper No. MRR75-06, 1975.
35. Schriempf, J. T.: Response of Materials to Laser Radiation: A Short Course. Naval Research Laboratory Report 7728, 1974.
36. Lundell, J. H. and R. R. Dickey: Response of Heat-Shield Materials to Intense Laser Radiation. In "Outer Planet Entry Heating and Thermal Protection", R. Viskanka, ed. Vol. 64 in "Progress in Astronautics and Aeronautics", 1979.

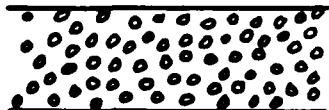
## REFERENCES (Cont'd)

37. Crane, K. C. A. and J. R. Brown: Laser-Induced Ablation of Fibre/epoxy Composites,. J. Phys. D: Appl. Phys., Vol. 14, 1981, p. 2341-9.
38. Crane, K. C. A., R. K. Garnsworthy, and L. E. S. Mathias: Ablation of Materials Subjected to Laser Radiation and High-Speed Gas Flows. J. Appl. Phys., Vol. 51, No. 11, November, 1980, pp. 5954-61.
39. Cerablanket Aerospace Insulation Product Brochure. Manville Corporation, 1980.
40. Min-k Thermal Insulation Product Brochure. Manville Corporation, 1982.
41. All-Alumina Refractory Fiber Insulation Product Brochure. RIM Products Corporation.
42. Rohsenow, W. M. and J. P. Hartnett, eds.: Handbook of Heat Transfer. McGraw-Hill, 1973.
43. Giedt, W. H.: Principles of Engineering Heat Transfer. Van Nostrand, 1957.

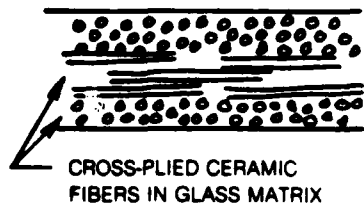
**TABLE I.1  
CANDIDATE GEOMETRIC CONFIGURATIONS FOR  
RETARDATION IN HOT-GAS APPLICATIONS**



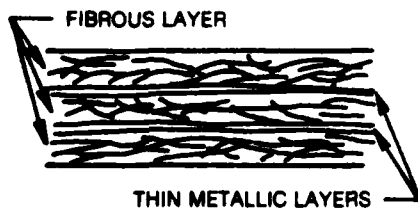
- FIBROUS — GENERALLY LOWEST  $k$  AND  $\rho$



- CERAMIC FOAM — HIGHER  $k$  AND  $\rho$  THAN FIBROUS, BUT FIRM SURFACE EXPOSED TO GAS



- CERAMIC COMPOSITES — CURRENTLY LIMITED IN OPERATING TEMPERATURES; EXCELLENT MECHANICAL PROPERTIES



- RADIATION/LAYERED — MAY NOT BE CHEMICALLY AND PHYSICALLY STABLE



- POWDERS — UNDESIRABLE SINTERING AND COMPACTION PROBLEMS

**TABLE I.2**  
**CANDIDATE MATERIALS VS CANDIDATE CONFIGURATIONS**

**FIBROUS**

- DYNAQUARTZ (SILICA) — MOST EFFECTIVE INSULATION UP TO 2700 F
- ALUMINA — STABLE UP TO 3200 F, BUT HIGH COST
- ZIRCONIA — UNDESIRABLE SHRINKAGE AND REACTION AT TEMPERATURES OVER 2500 F
- GRAPHITE — LIMITED TO VACUUM APPLICATIONS; HIGH k
- MIN-K — LIMITED TO 1800 F

**FOAM**

- ALUMINA — REASONABLY LOW k
- ZIRCONIA — SHRINKAGE AND REACTION PROBLEMS
- SILICON CARBIDE — HIGH k

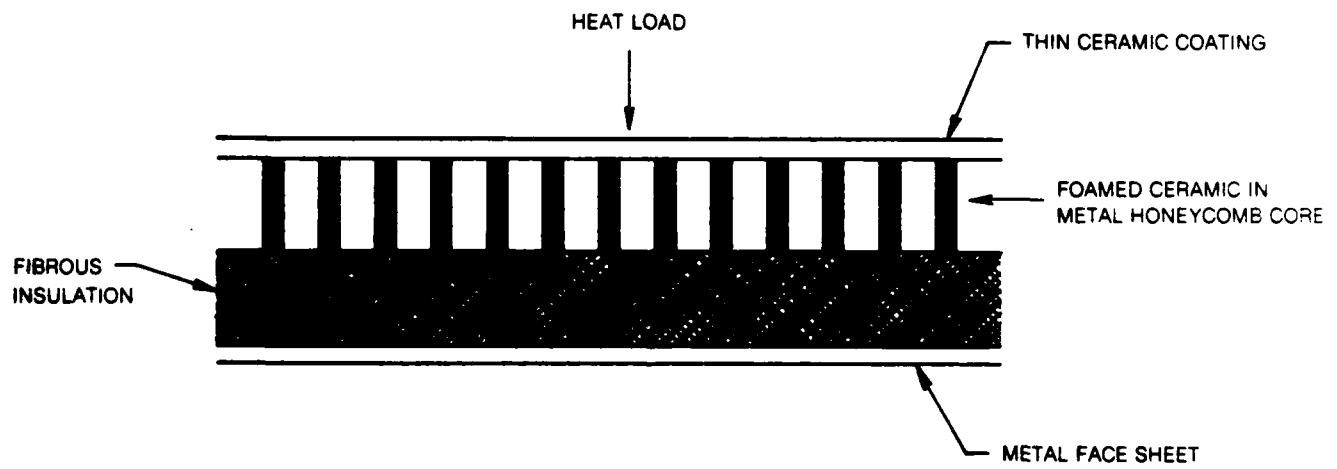
**CERAMIC COMPOSITES**

- COMPGLAS™ — SiC-FIBER REINFORCED GLASS CERAMIC; CURRENTLY LIMITED TO 1800 F BECAUSE OF OXIDATION PROBLEMS

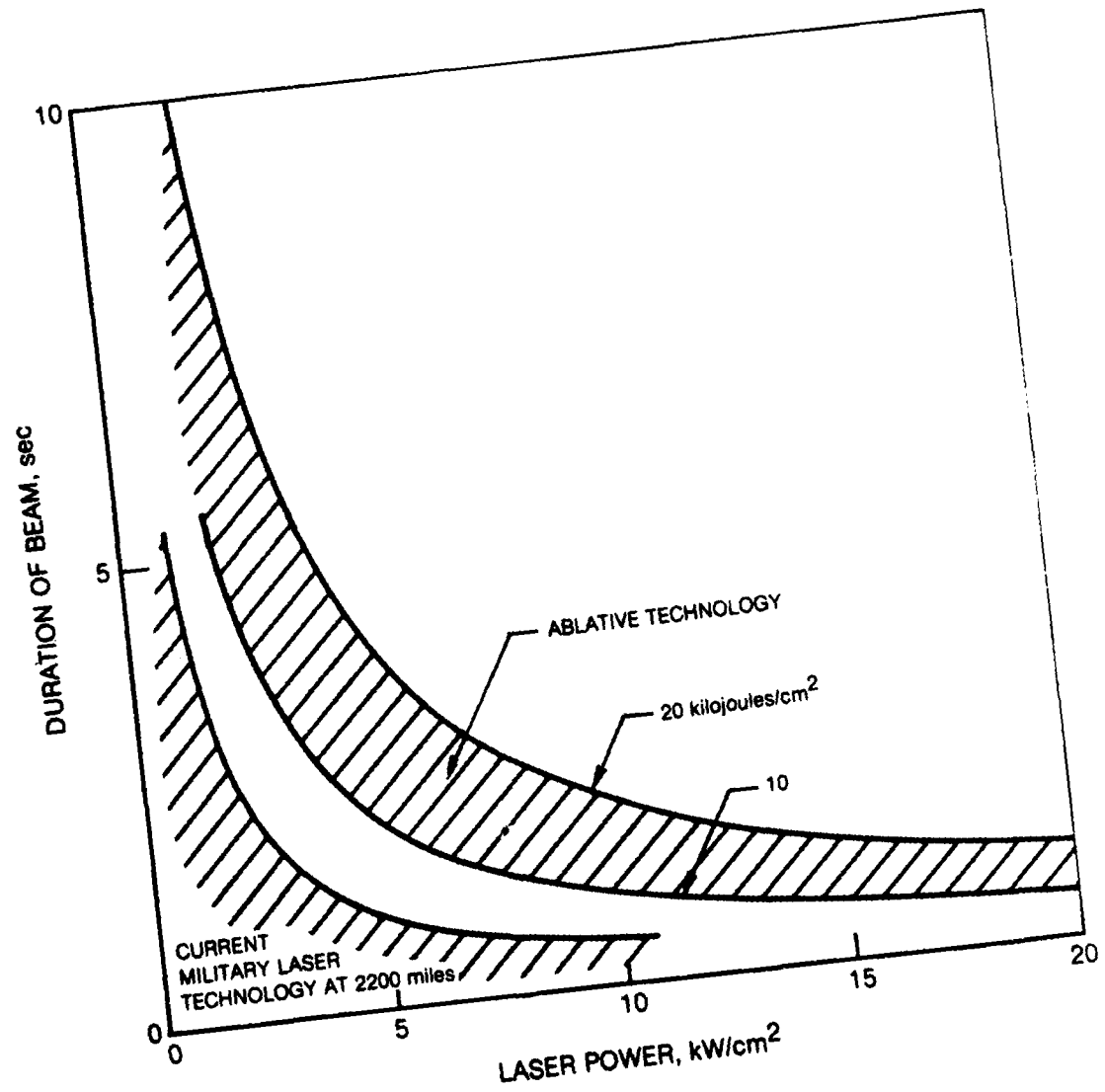
**RADIATION/LAYERED**

- DYNAQUARTZ WITH TANTALUM RADIATION SHIELDS — DIFFICULT TO APPLY IN REAL SYSTEMS WITH CURVED SURFACES OR SMALL DIMENSIONS

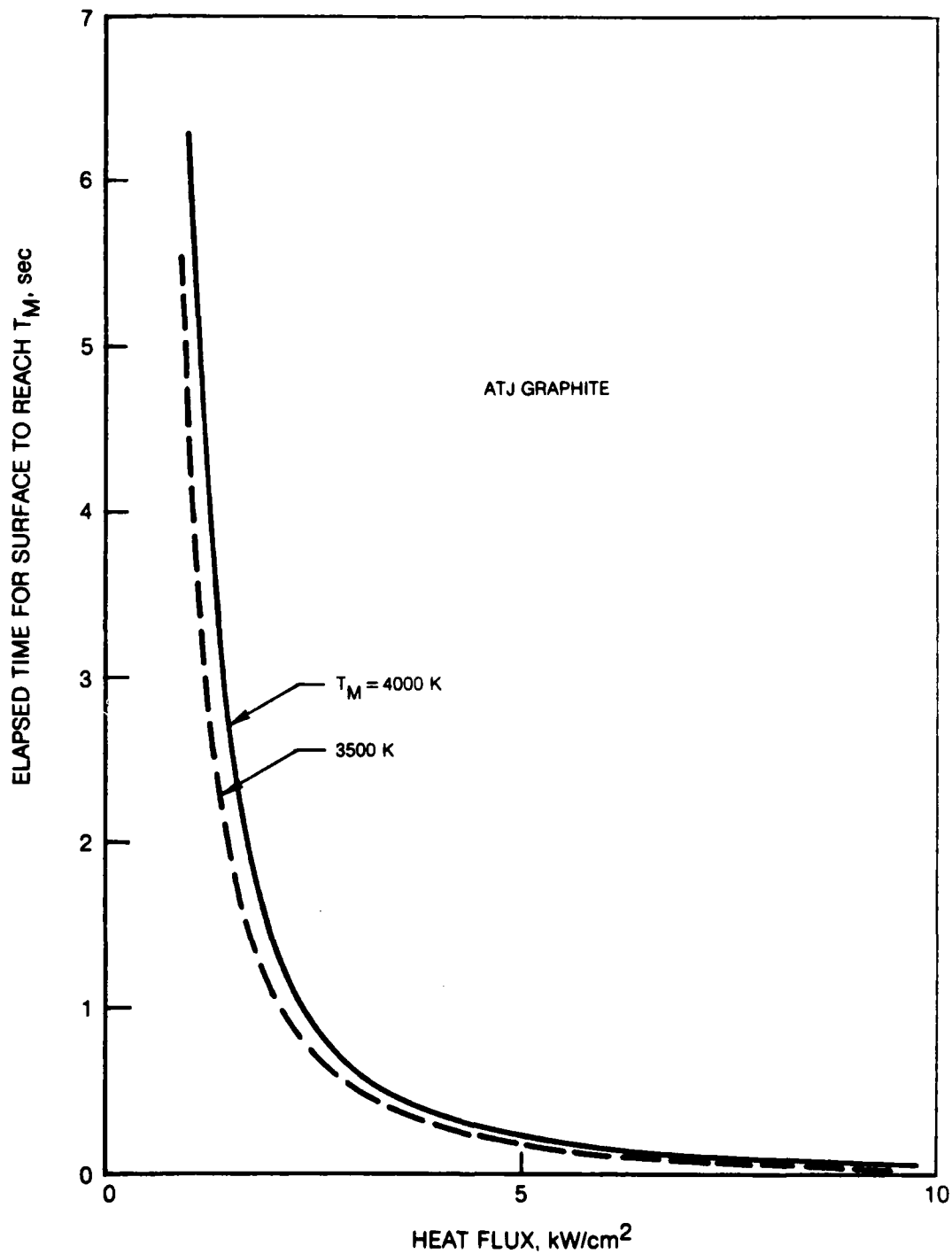
**TYPICAL EXAMPLE OF HEAT TRANSFER RETARDATION DEVICE**



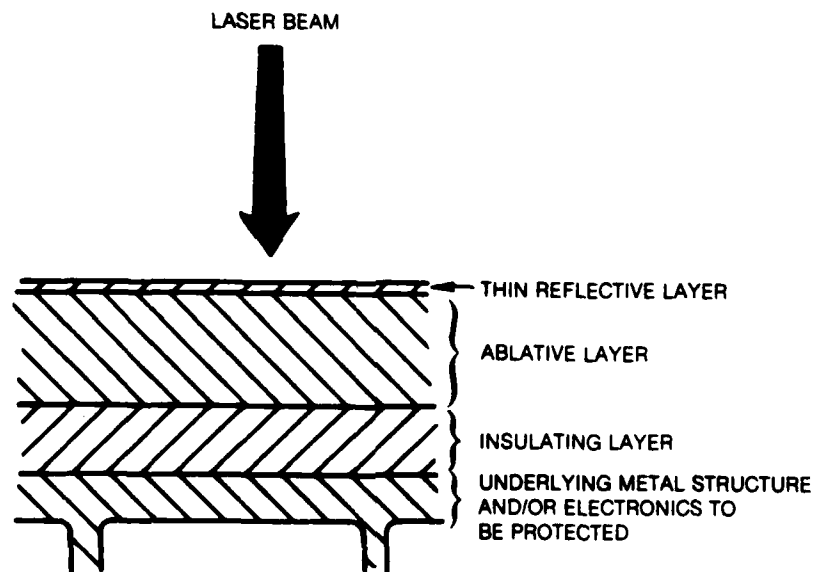
### POWER LEVELS FOR PASSIVE LASER COUNTERMEASURES



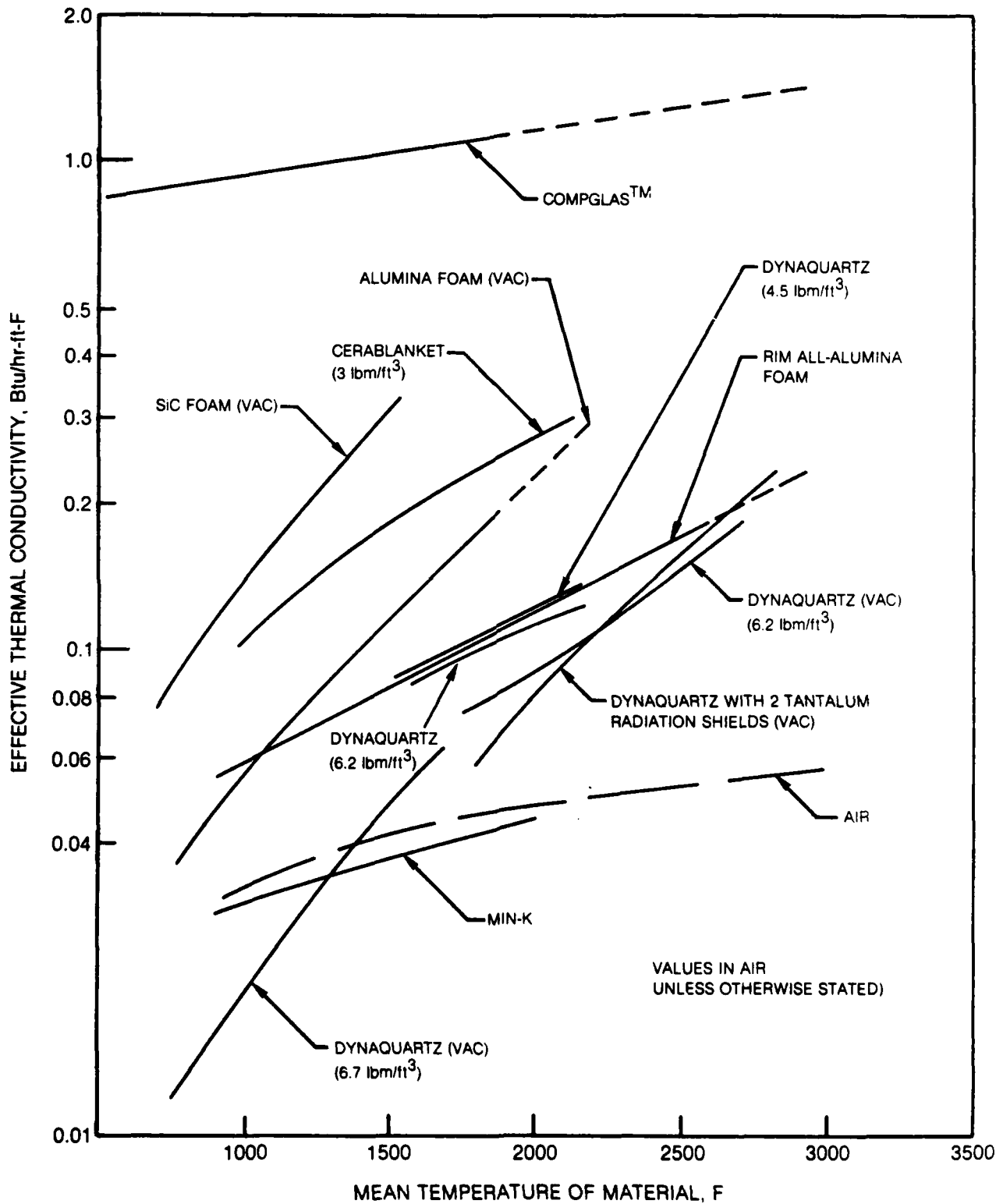
### ELAPSED TIME FOR SURFACE MELTING



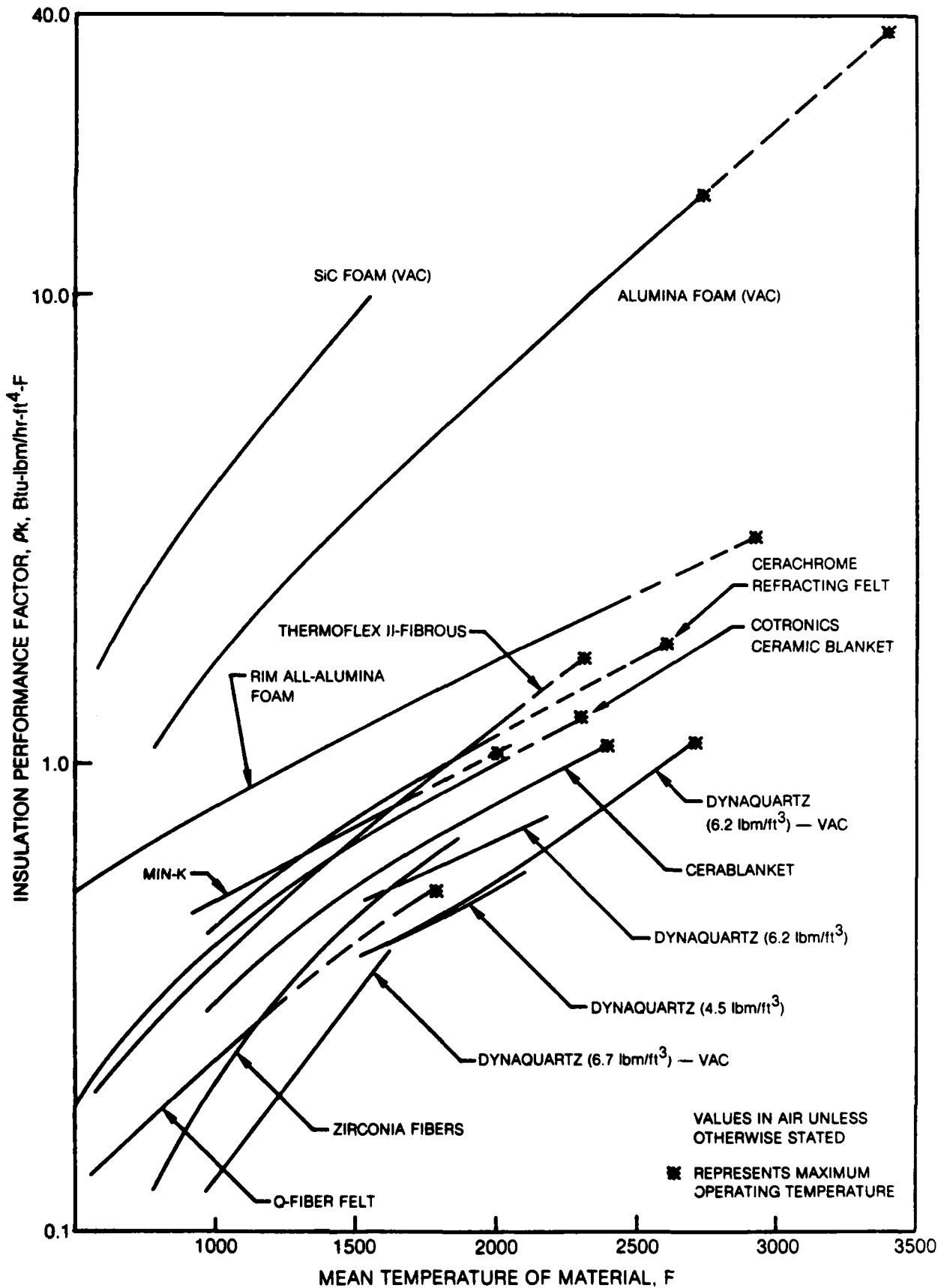
### MECHANISMS OF HEAT TRANSFER IN PASSIVE LASER COUNTERMEASURES

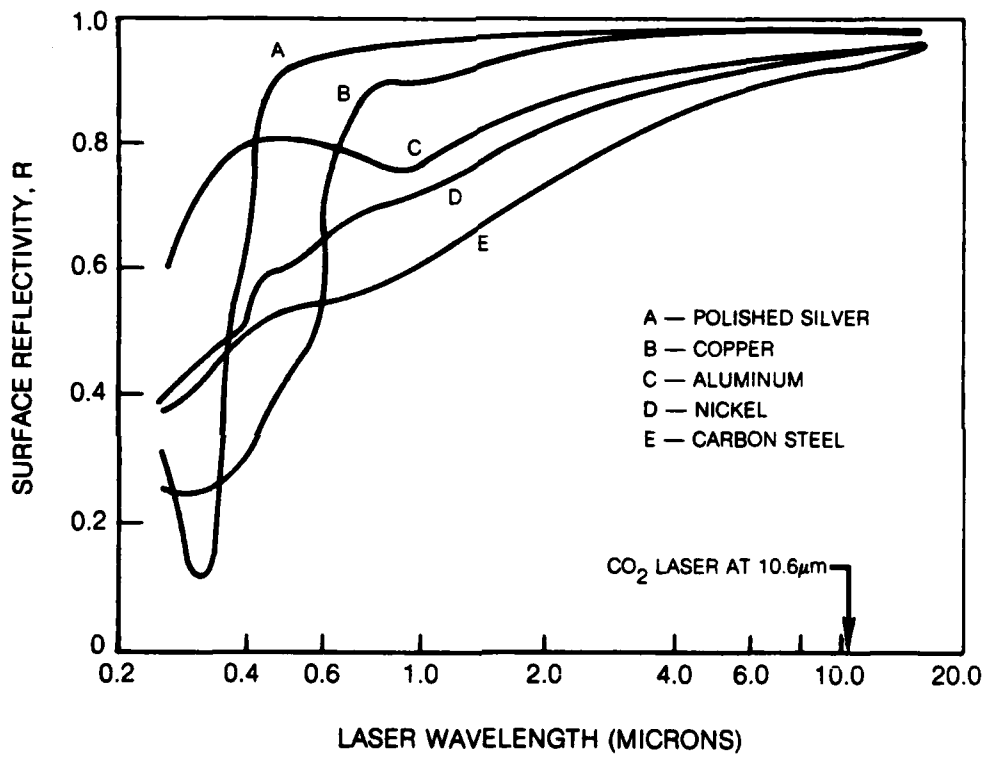


**EFFECTIVE THERMAL CONDUCTIVITY OF SELECTED MATERIALS**

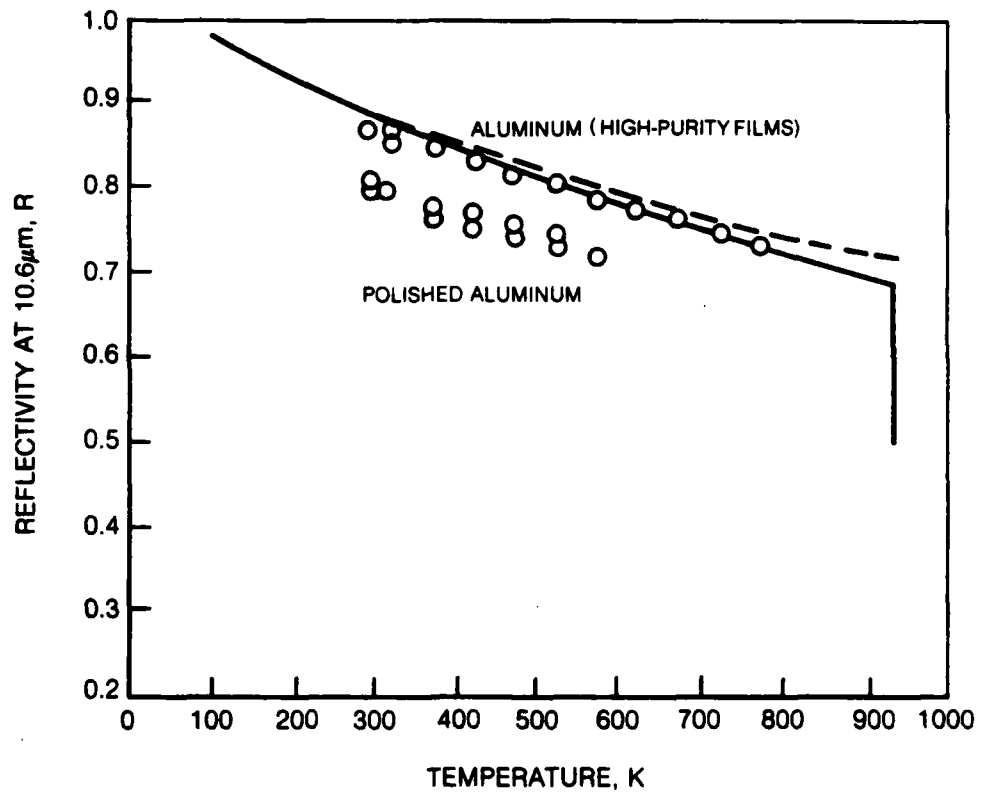


INSULATION PERFORMANCE FACTOR FOR SELECTED MATERIALS

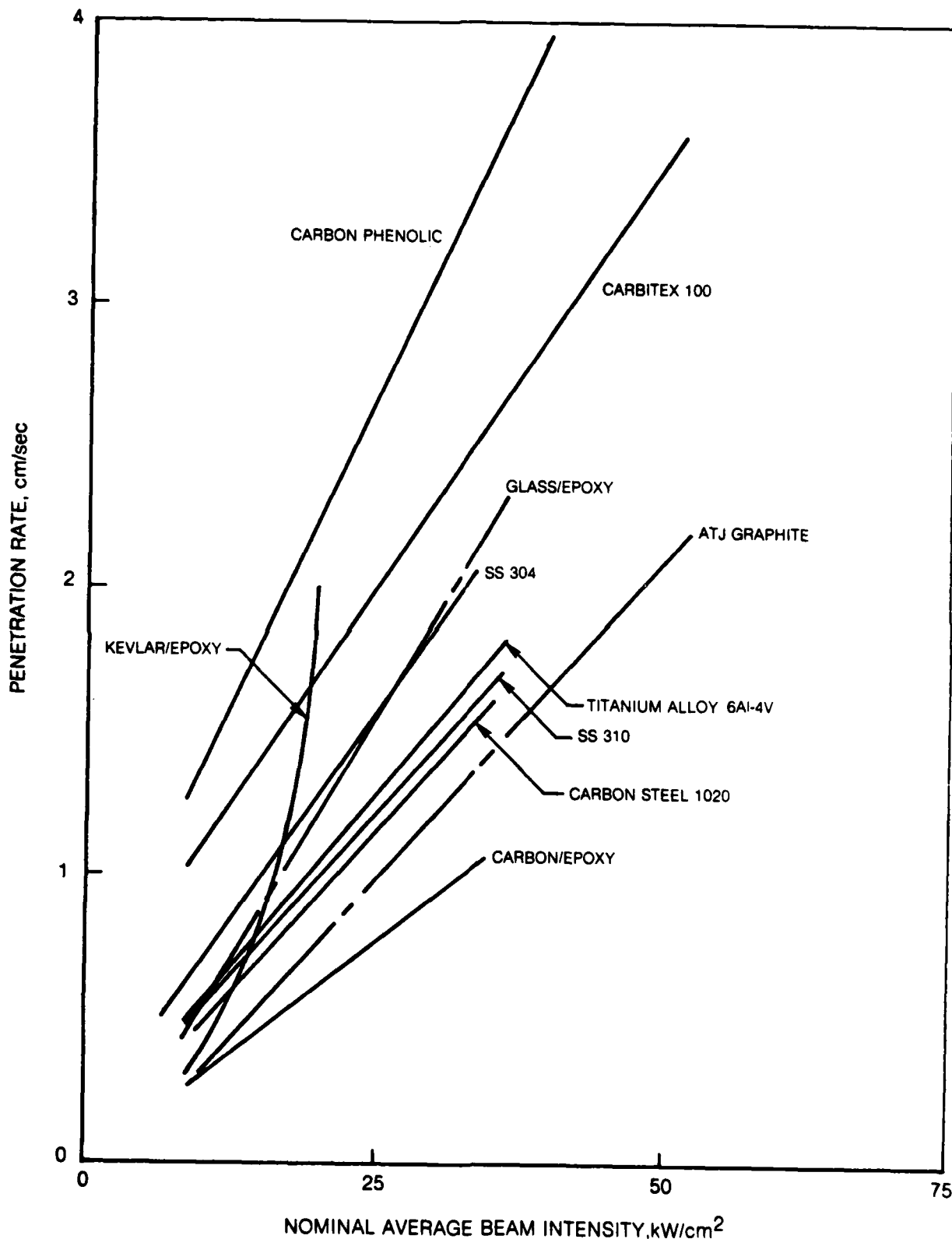




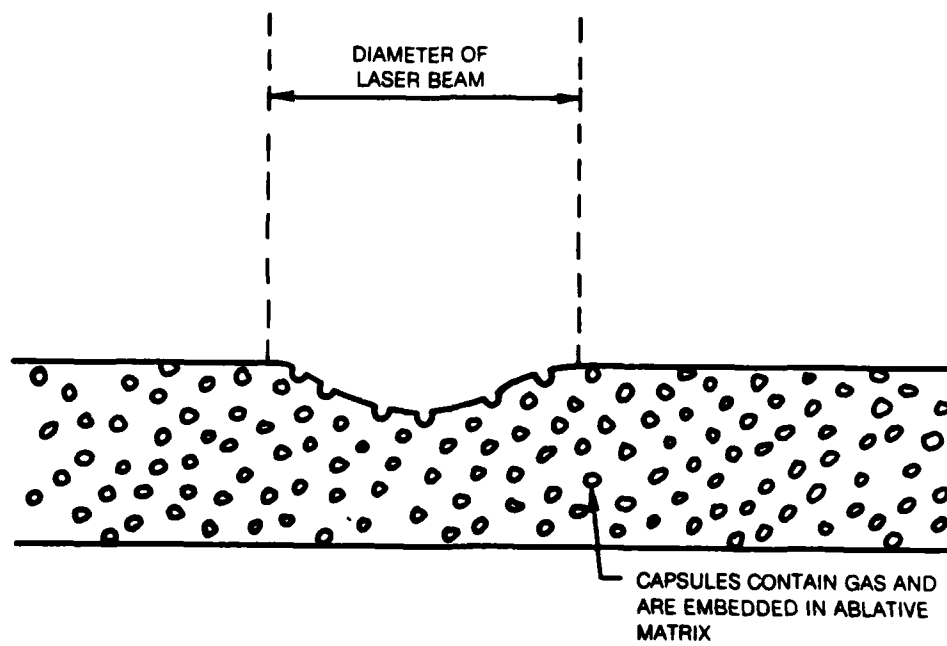
TEMPERATURE DEPENDENCE OF THE REFLECTIVITY OF ALUMINUM



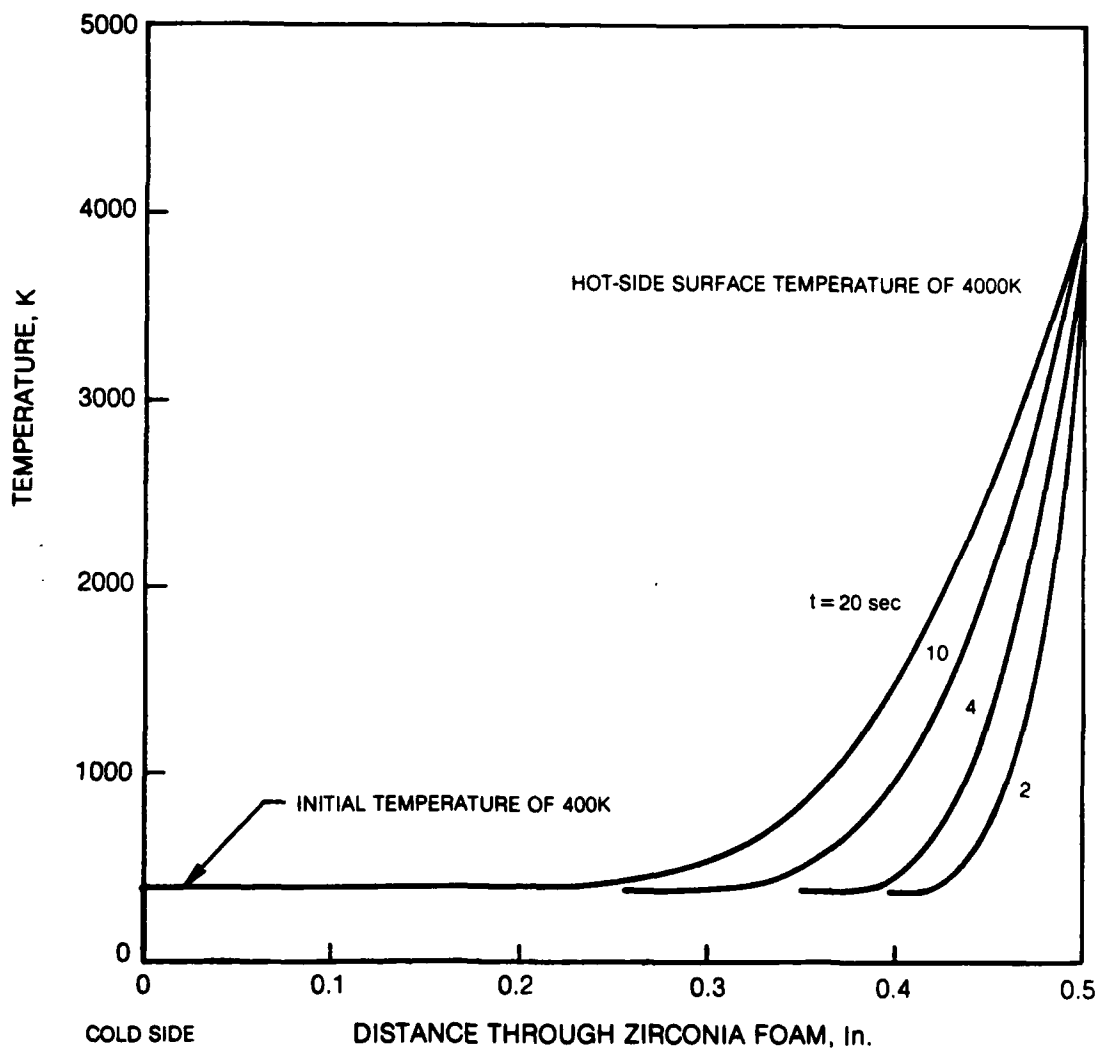
### LASER PENETRATION RATES



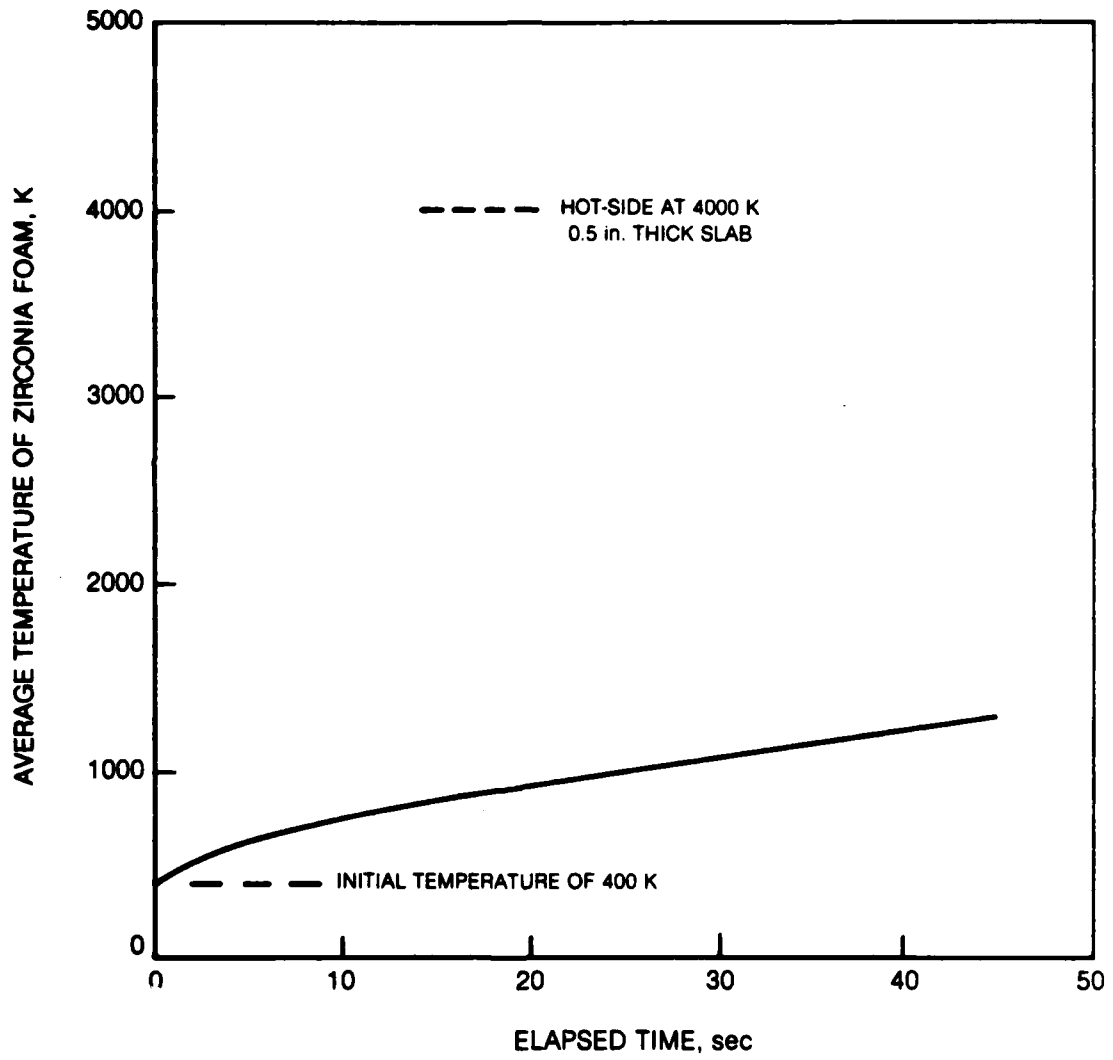
### LASER RETARDATION DEVICE USING GAS CAPSULES



### THERMAL RESPONSE OF ZIRCONIA FOAM



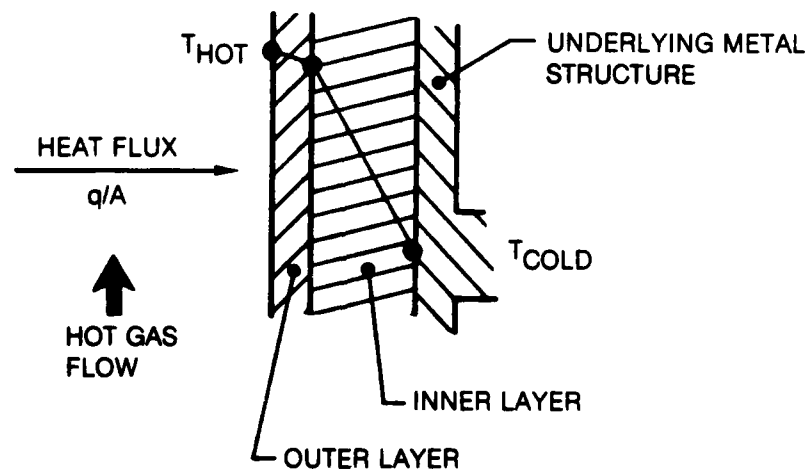
### SPACE-AVERAGE TEMPERATURE OF ZIRCONIA FOAM



### RATIONALE FOR MULTI-LAYER RETARDATION DEVICE

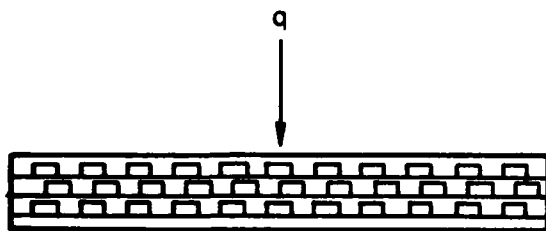
OUTER LAYER: CERAMIC FOAM OR CERAMIC COMPOSITE, SO THAT LOOSE FIBERS WILL NOT BE EXPOSED TO AND TORN OFF BY HIGH-VELOCITY GAS

INNER LAYER(S): FIBROUS, BECAUSE LOWER  $k$  AND  $\rho$  THAN CERAMIC FOAM OR CERAMIC COMPOSITE

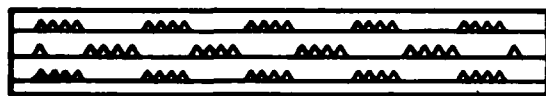


### APPROACHES TO REDUCE DENSITY OF CERAMIC FOAM

STACK OF GROOVED LAYERS

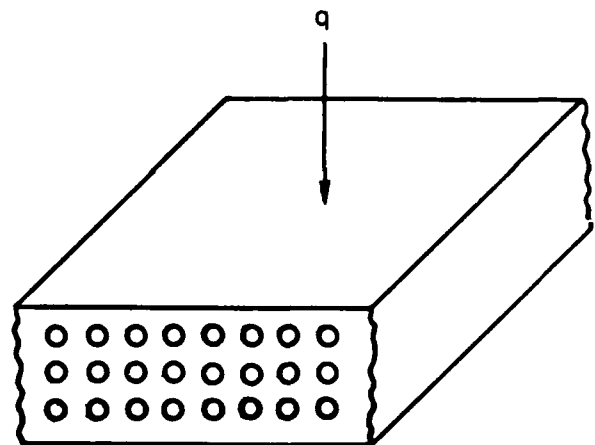


a) RECTANGULAR GROOVES

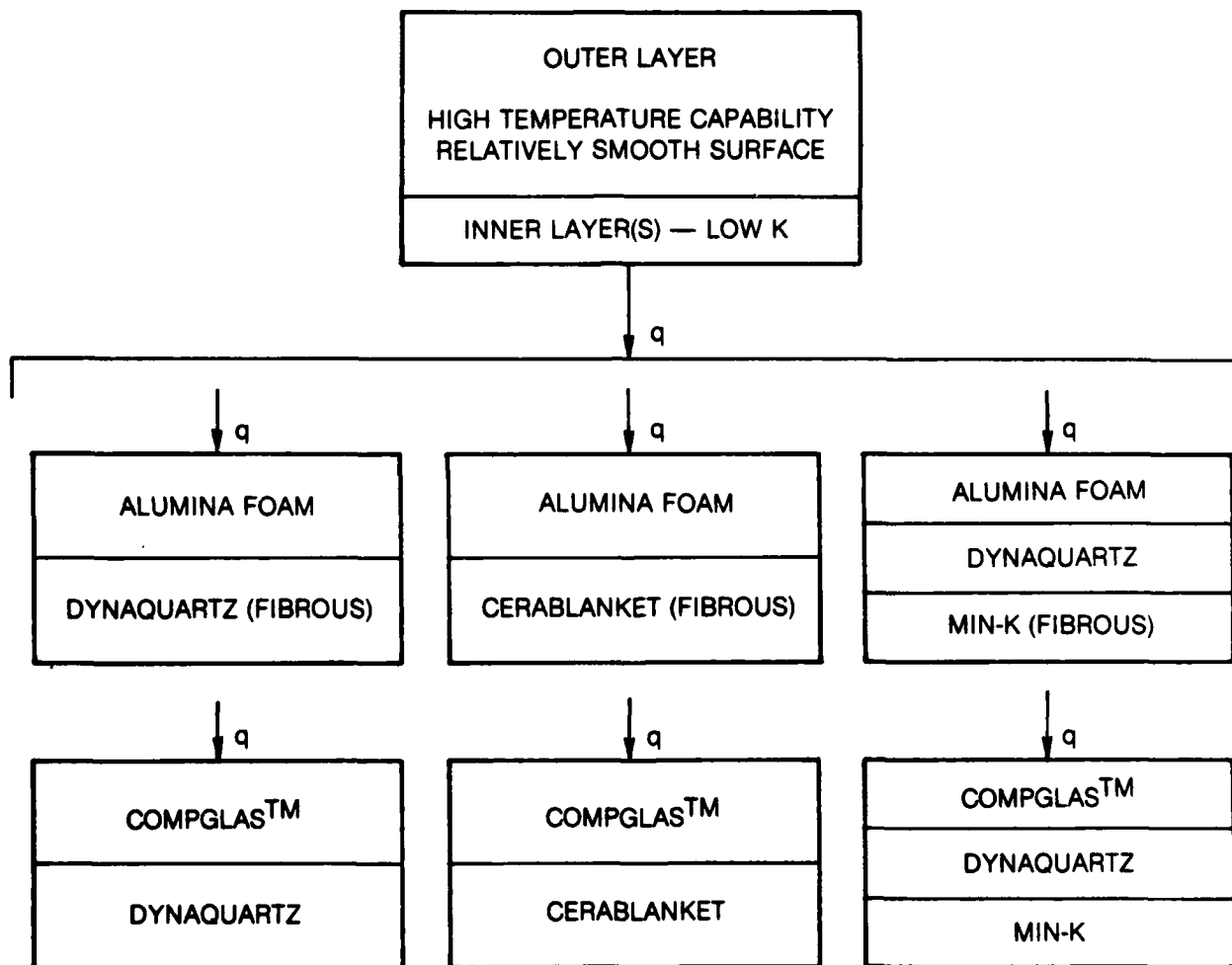


b) TRIANGULAR GROOVES

AXIAL HOLES CAST INTO FOAM

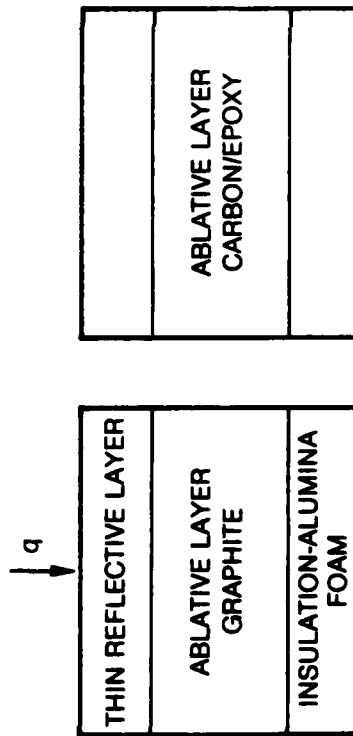


### CANDIDATE MATERIALS/CONFIGURATIONS COMBINATIONS FOR ANALYSIS RETARDATION FOR HOT GAS APPLICATIONS

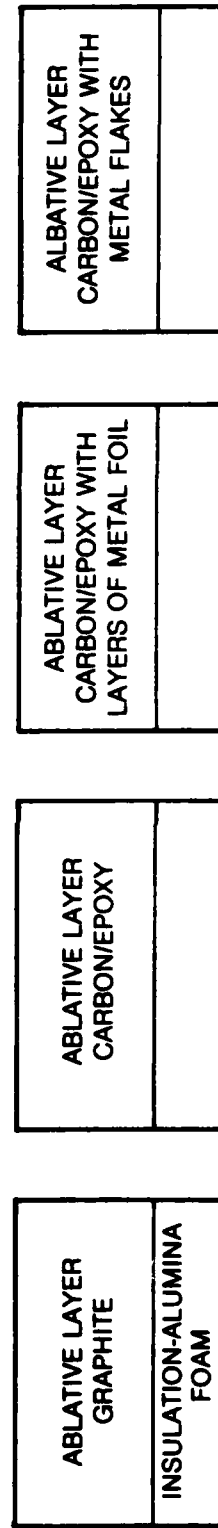


**CANDIDATE MATERIALS CONFIGURATIONS COMBINATIONS FOR LASER EXPERIMENTS**

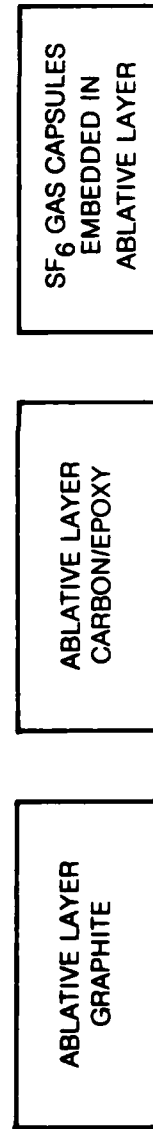
• **THREE-LAYER CONFIGURATIONS**



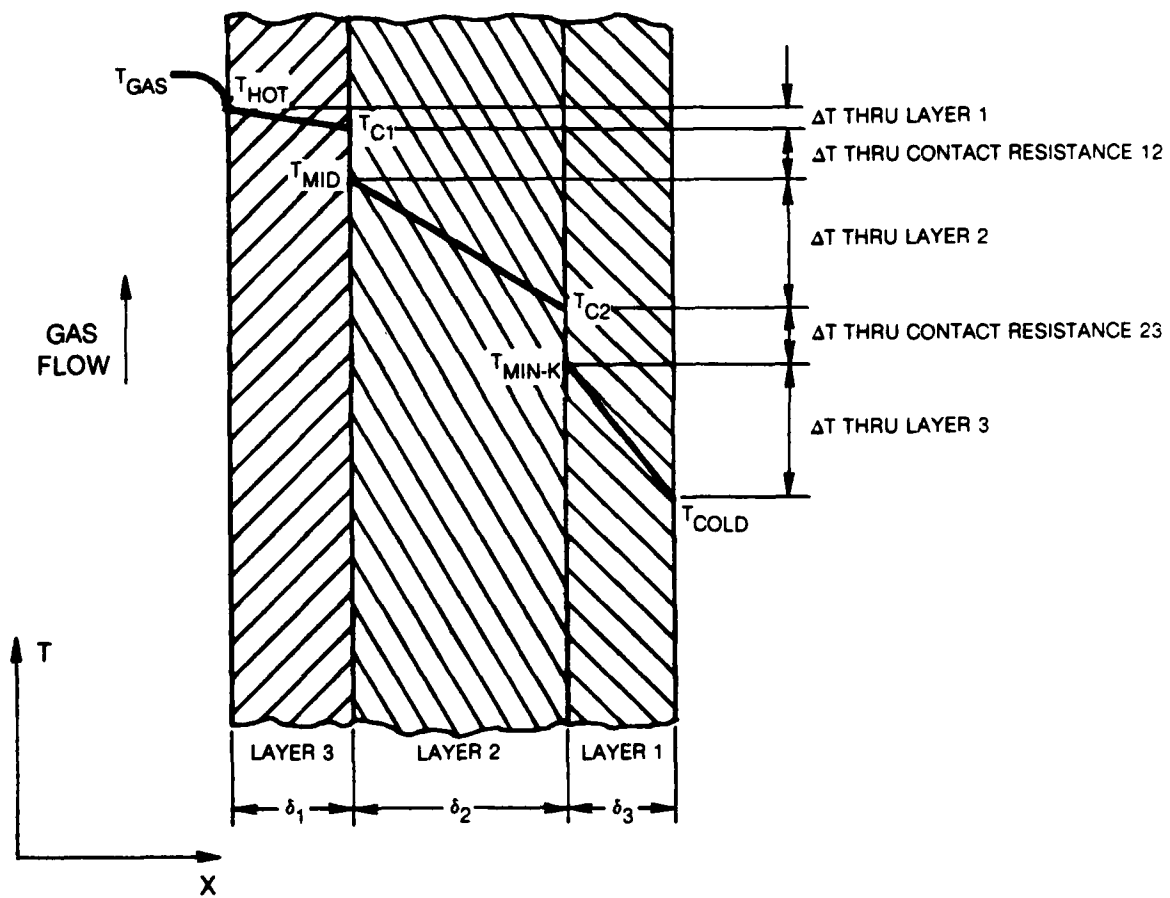
• **TWO-LAYER CONFIGURATIONS**



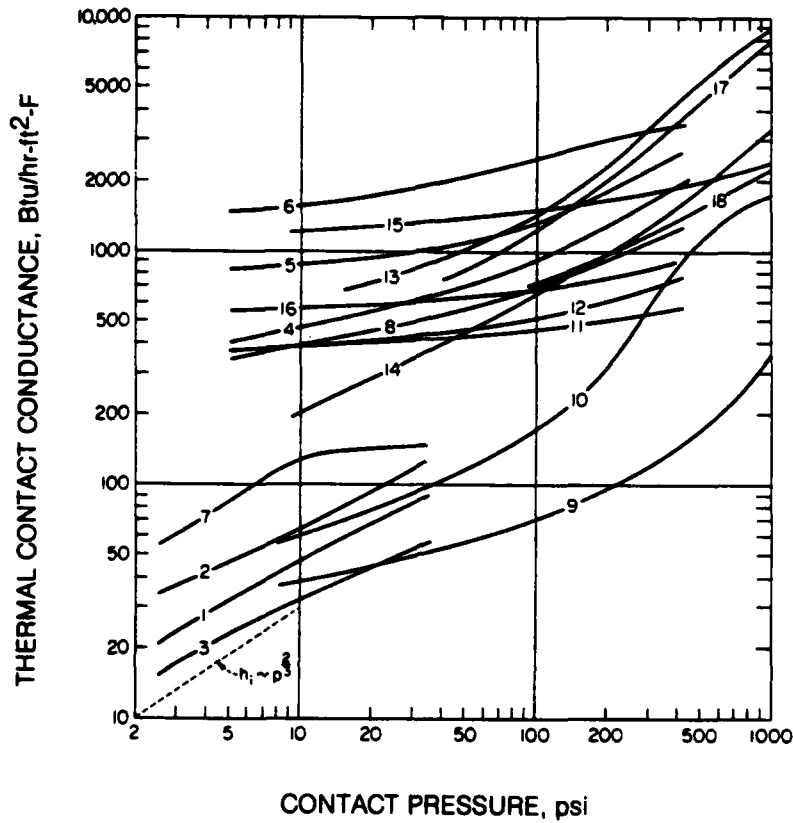
• **ONE-LAYER CONFIGURATIONS**



**HEAT TRANSFER MODEL OF THREE-LAYER RETARDATION DEVICE**

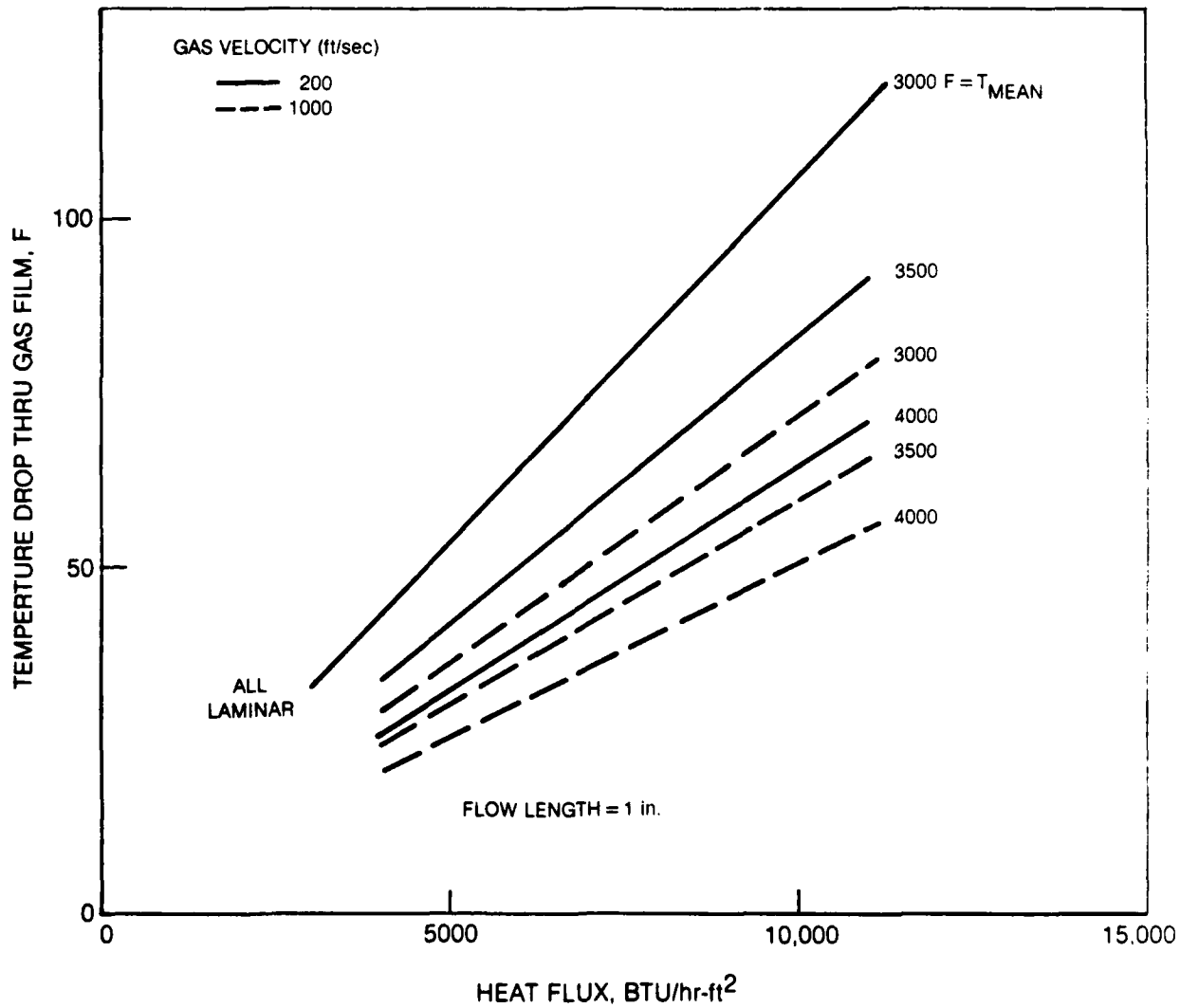


**THERMAL CONTACT CONDUCTANCE**

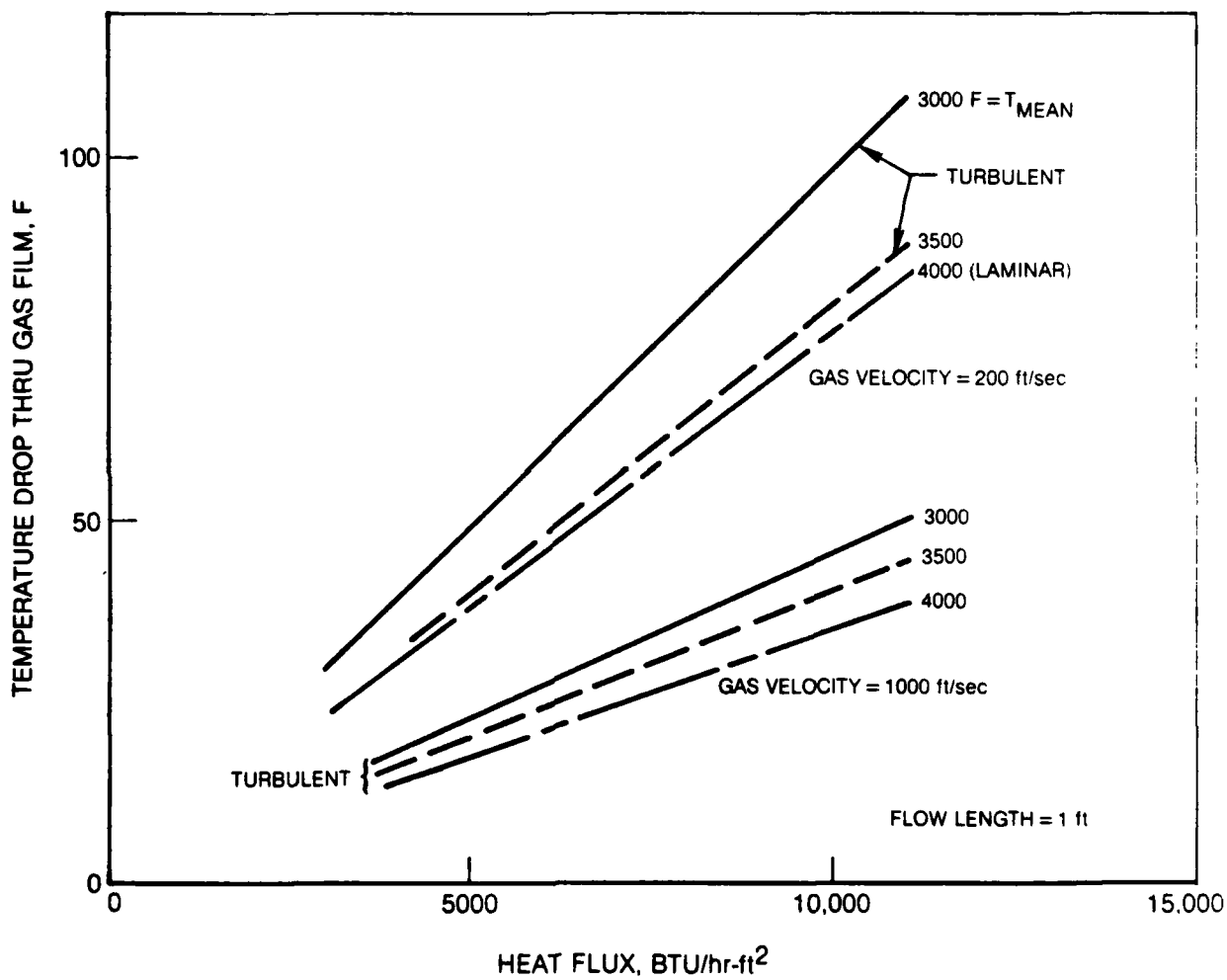


Curve	Material pair	RMS surface finish ( $\mu$ in.)	Gap material	Mean contact temp. ( $^{\circ}$ F)
1	aluminum (2024-T3)	48-65	vacuum ( $10^{-4}$ mm Hg)	110
2	aluminum (2024-T3)	8-18	vacuum ( $10^{-4}$ mm Hg)	110
3	aluminum (2024-T3)	6-8 (not flat)	vacuum ( $10^{-4}$ mm Hg)	110
4	aluminum (75S-T6)	120	air	200
5	aluminum (75S-T6)	65	air	200
6	aluminum (75S-T6)	10	air	200
7	aluminum (2024-T3)	6-8 (not flat)	lead foil (0.008 in.)	110
8	aluminum (75S-T6)	120	brass foil (0.001 in.)	200
9	stainless (304)	42-60	vacuum ( $10^{-4}$ mm Hg)	85
10	stainless (304)	10-15	vacuum ( $10^{-4}$ mm Hg)	85
11	stainless (416)	100	air	200
12	stainless (416)	100	brass foil (0.001 in.)	200
13	magnesium (AZ-31B)	50-60 (oxidized)	vacuum ( $10^{-4}$ mm Hg)	85
14	magnesium (AZ-31B)	8-16 (oxidized)	vacuum ( $10^{-4}$ mm Hg)	85
15	copper (OFHC)	7-9	vacuum ( $10^{-4}$ mm Hg)	115
16	stainless/aluminum	30/65	air	200
17	iron/aluminum	—	air	80
18	tungsten/graphite	—	air	270

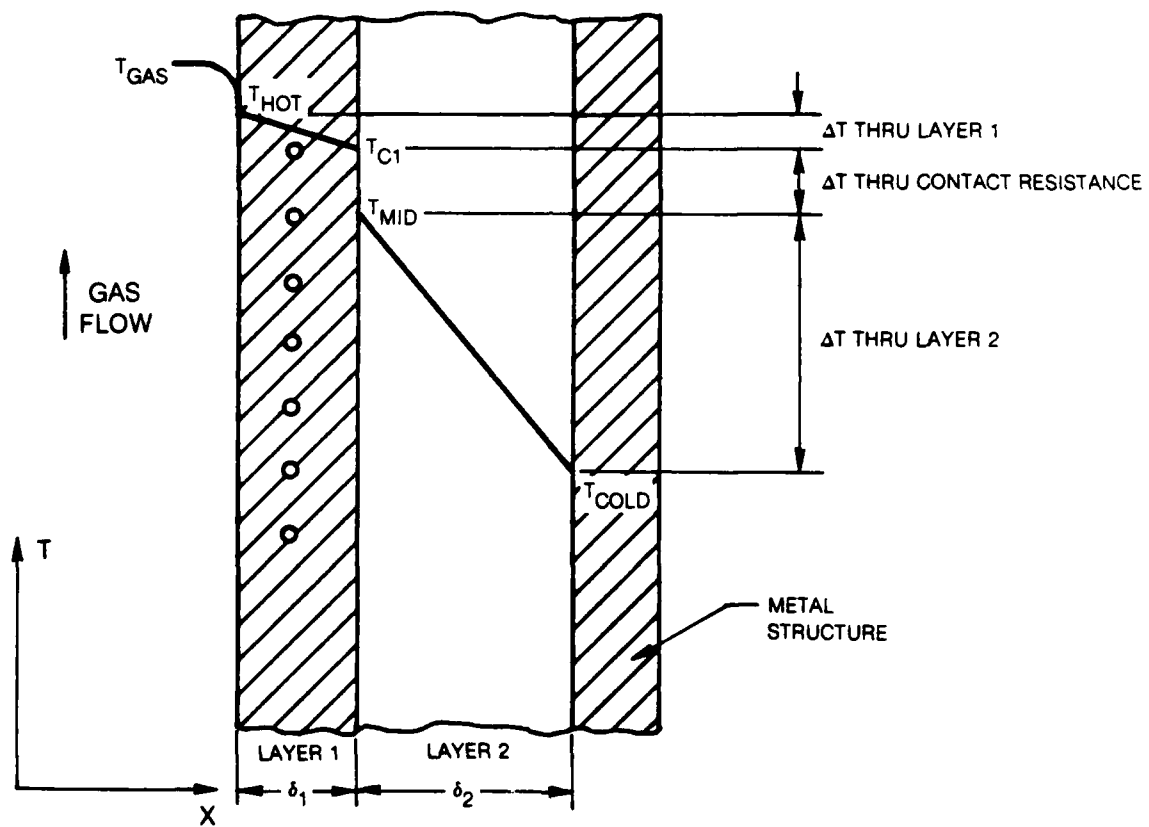
### TEMPERATURE DROP THRU GAS FILM TO OUTER EDGE OF INSULATION LAMINAR REGIME



TEMPERATURE DROP THRU GAS FILM TO OUTER EDGE OF INSULATION

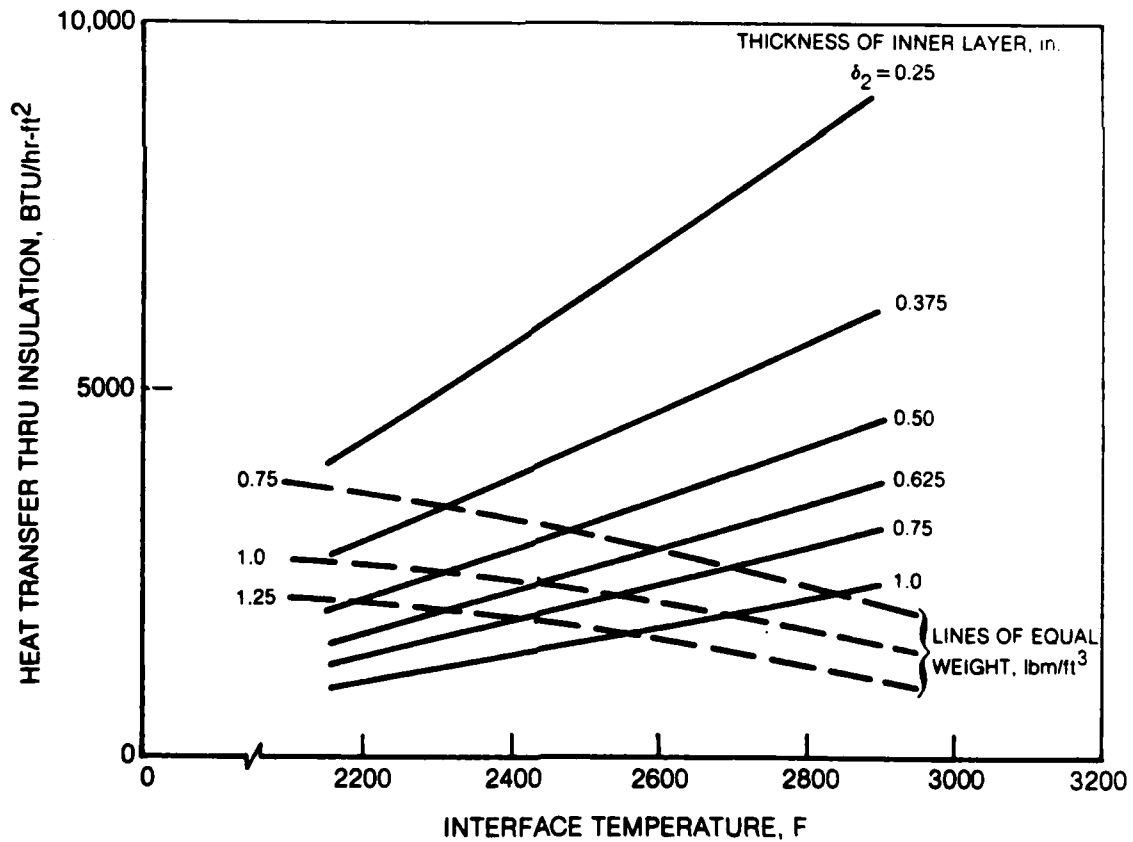
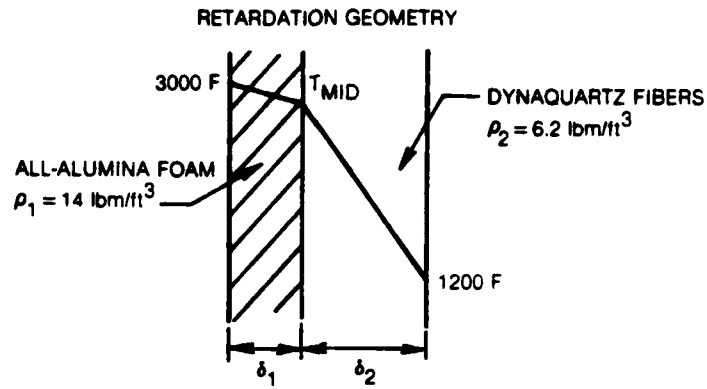


## HEAT TRANSFER MODEL OF TWO-LAYER RETARDATION DEVICE



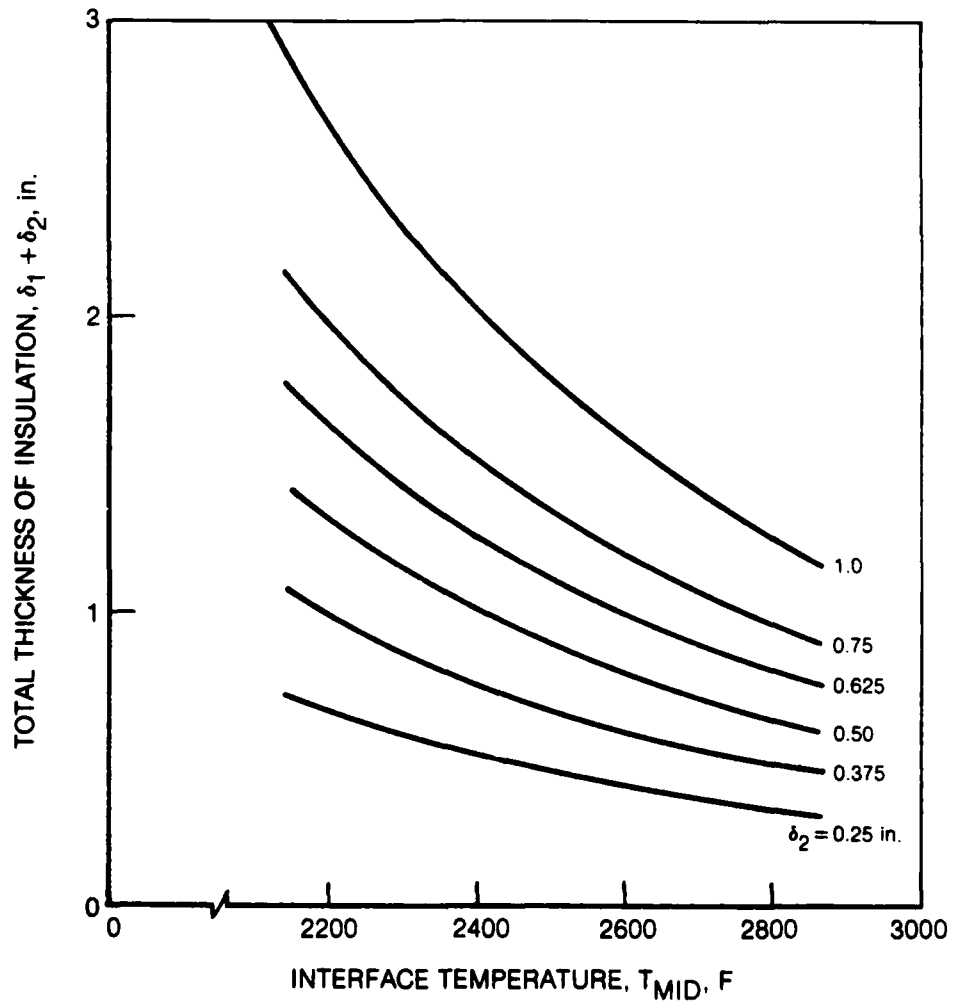
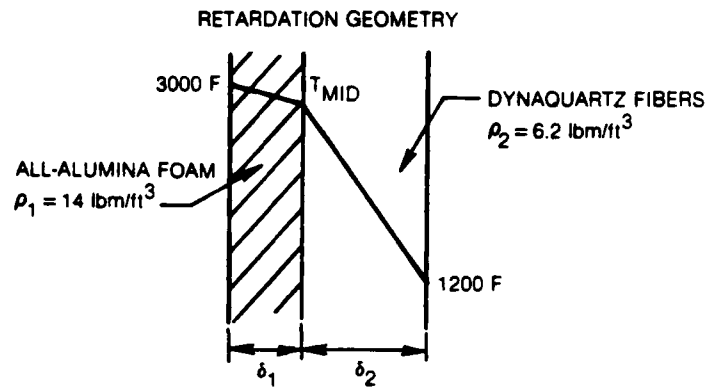
**THERMAL PERFORMANCE OF TWO-LAYER RETARDATION DEVICE**

$T_{HOT} = 3000\text{ F}$

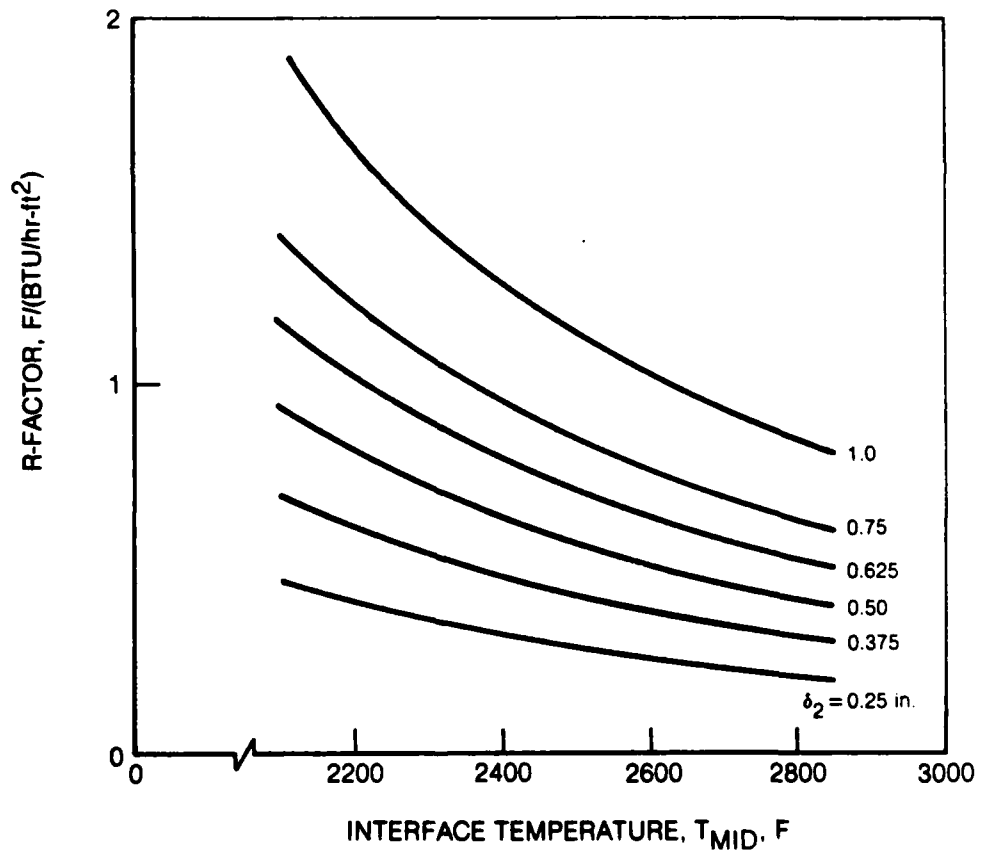
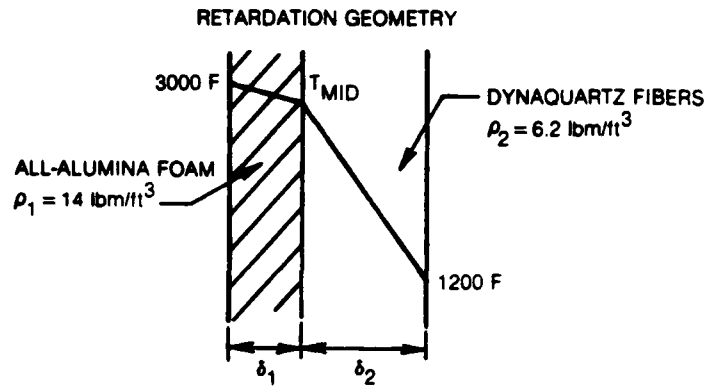


**THICKNESS OF TWO-LAYER RETARDATION DEVICE**

$T_{HOT} = 3000 \text{ F}$

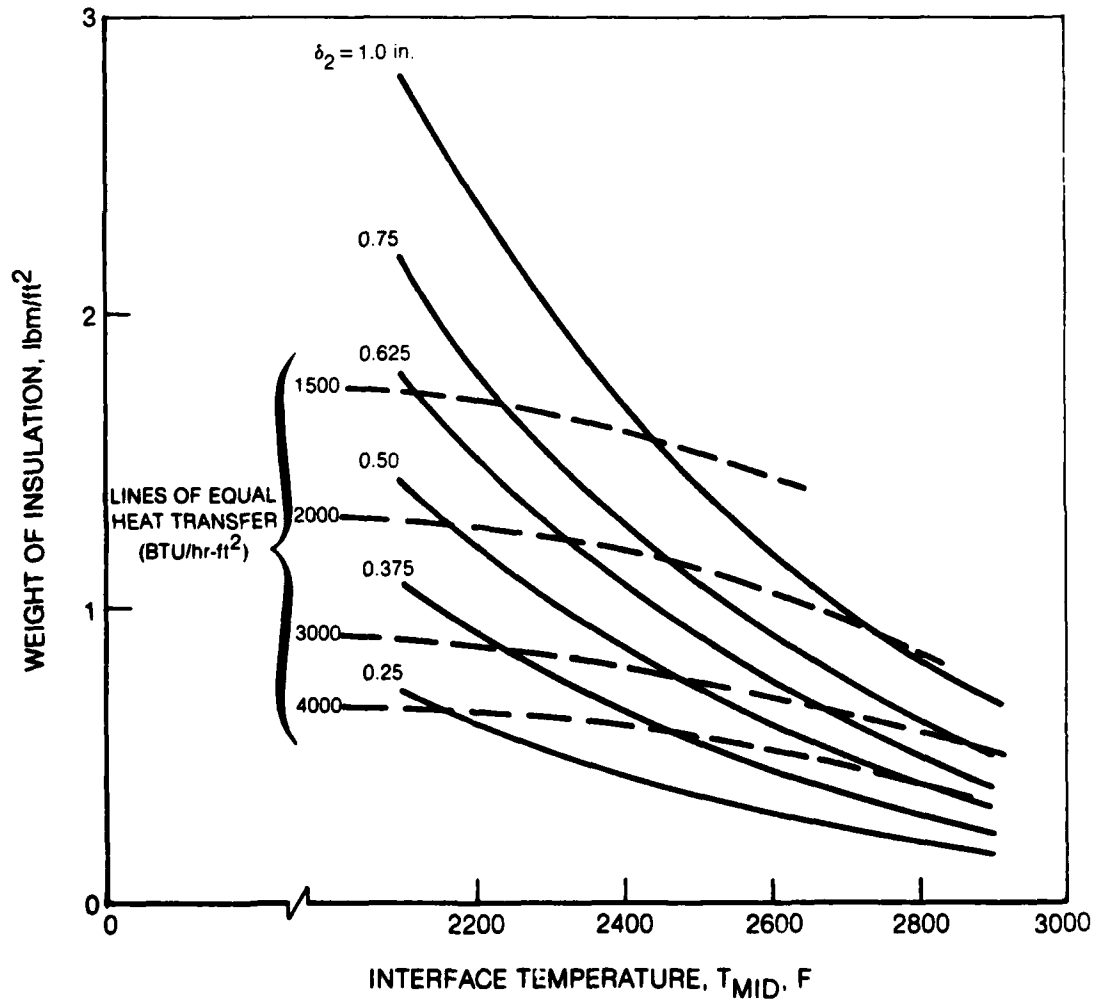
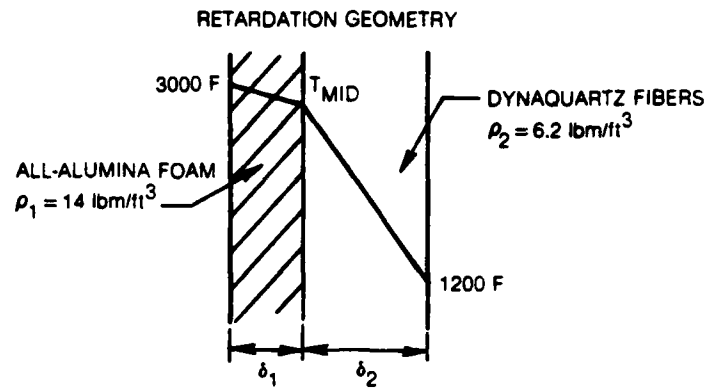


**R-FACTOR OF TWO-LAYER RETARDATION DEVICE**

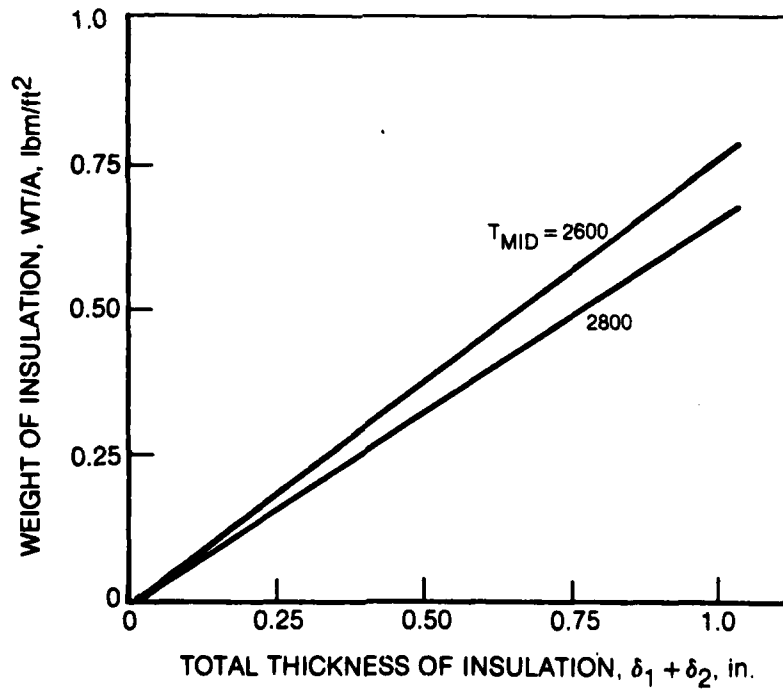
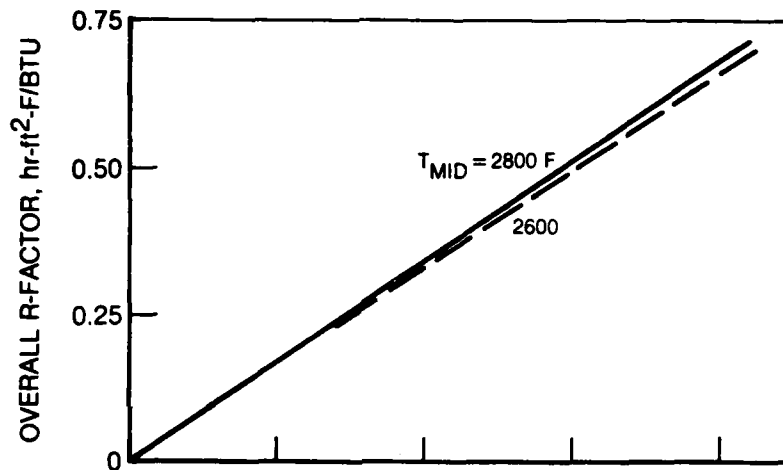
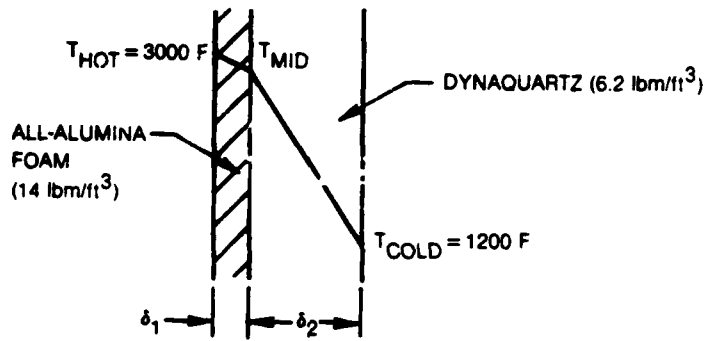


**WEIGHT OF TWO-LAYER RETARDATION DEVICE**

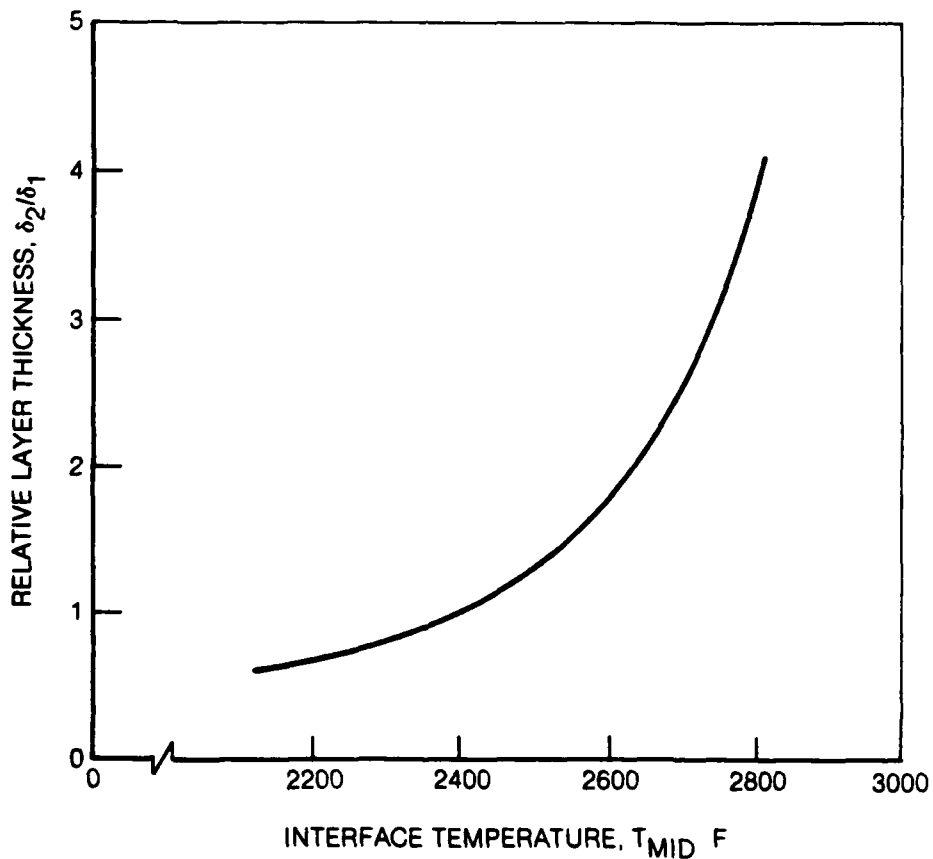
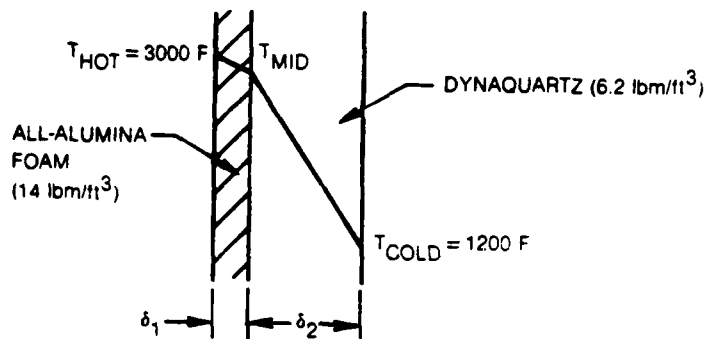
$T_{HOT} = 3000 \text{ F}$



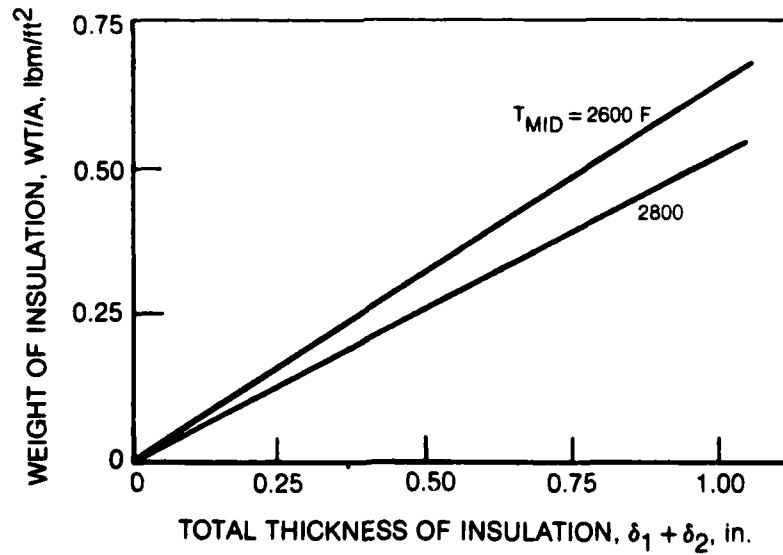
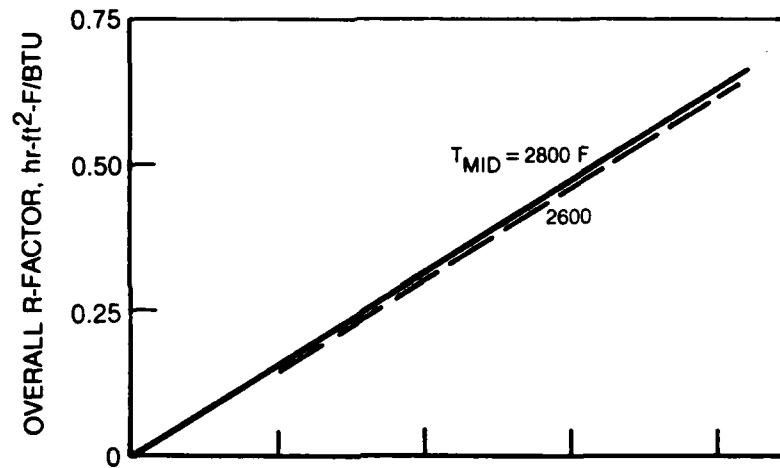
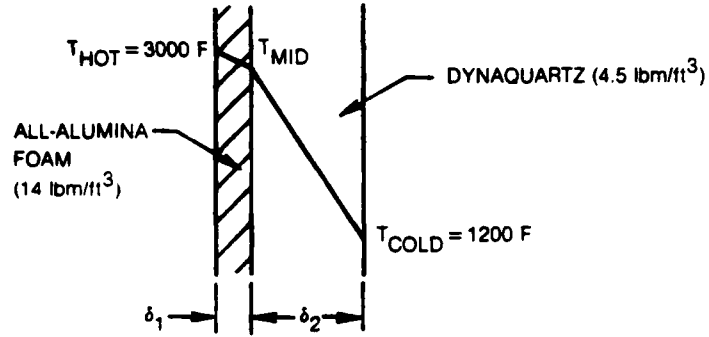
**WEIGHT AND OVERALL R-FACTOR OF TWO-LAYER RETARDATION DEVICE**



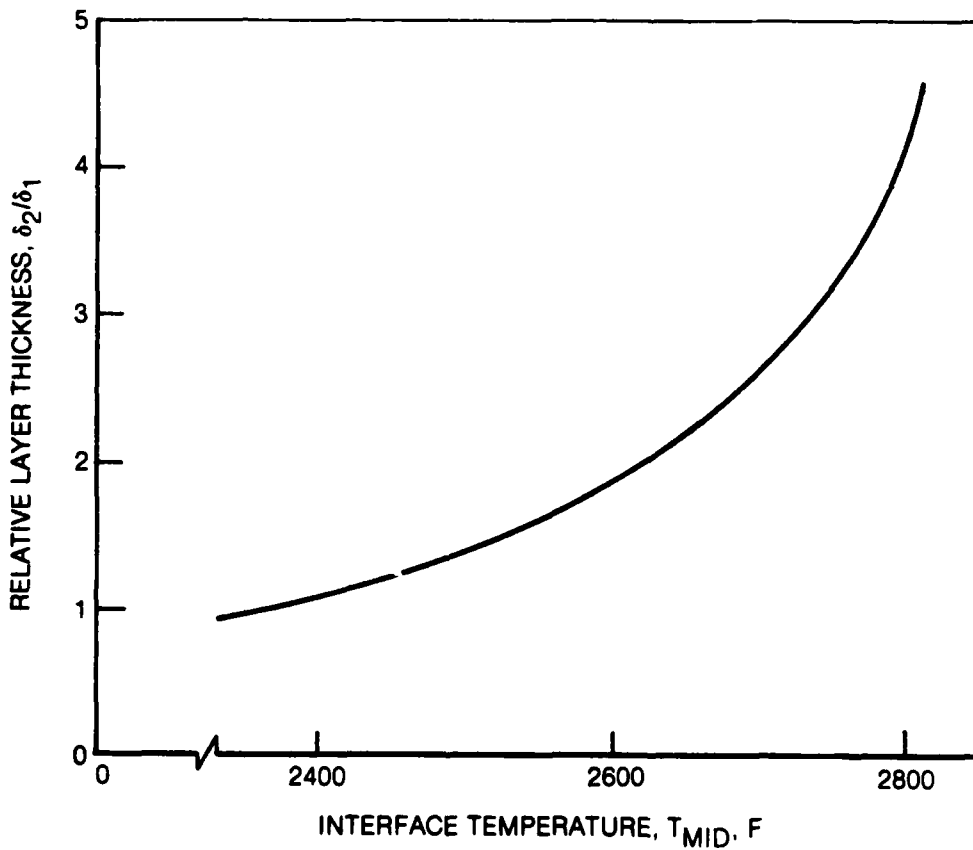
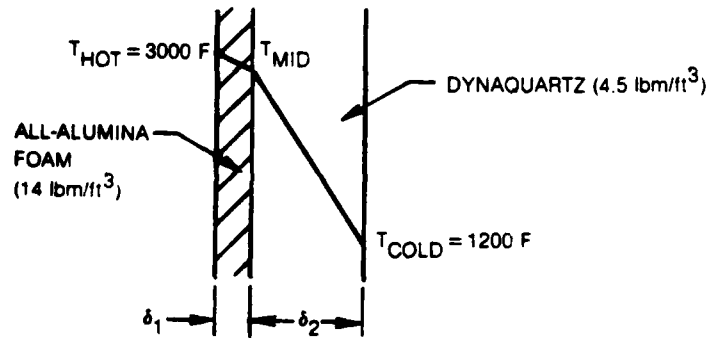
**RELATIVE LAYER THICKNESS FOR TWO-LAYER RETARDATION DEVICE**



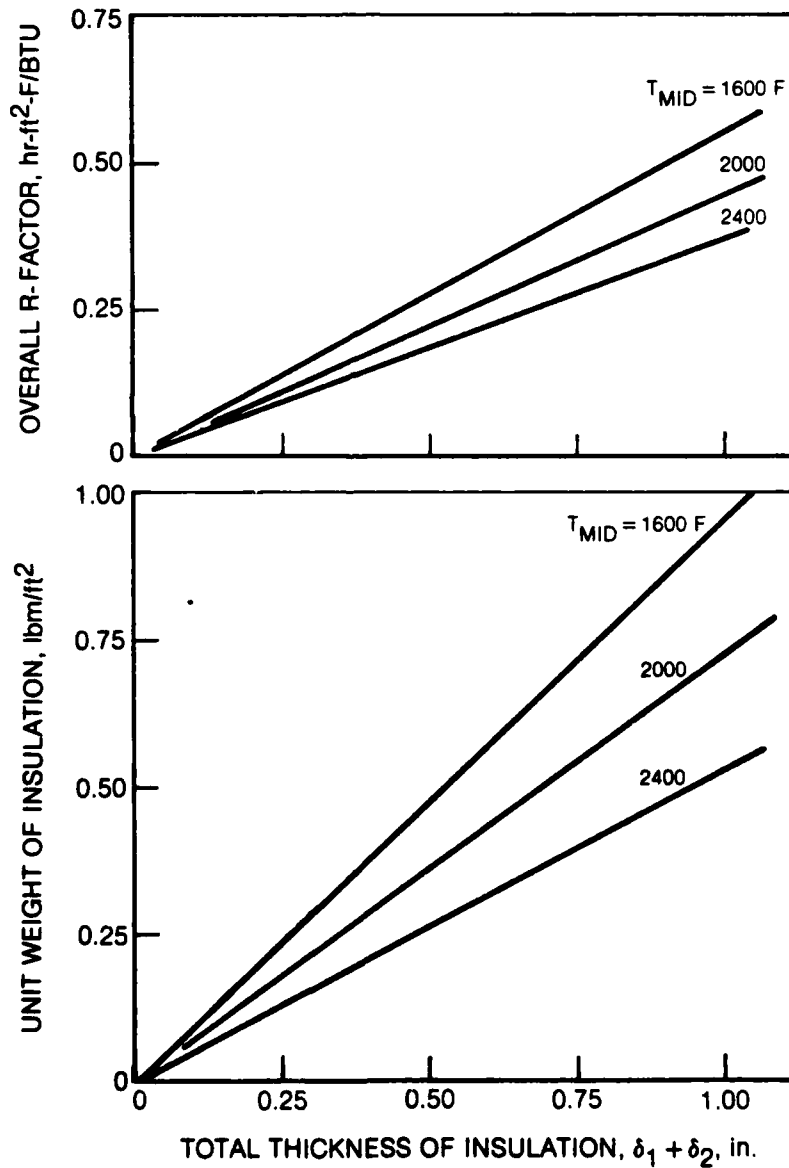
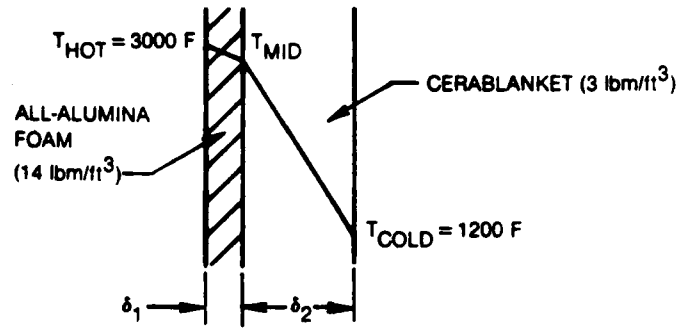
**WEIGHT AND OVERALL R-FACTOR OF TWO-LAYER RETARDATION DEVICE**



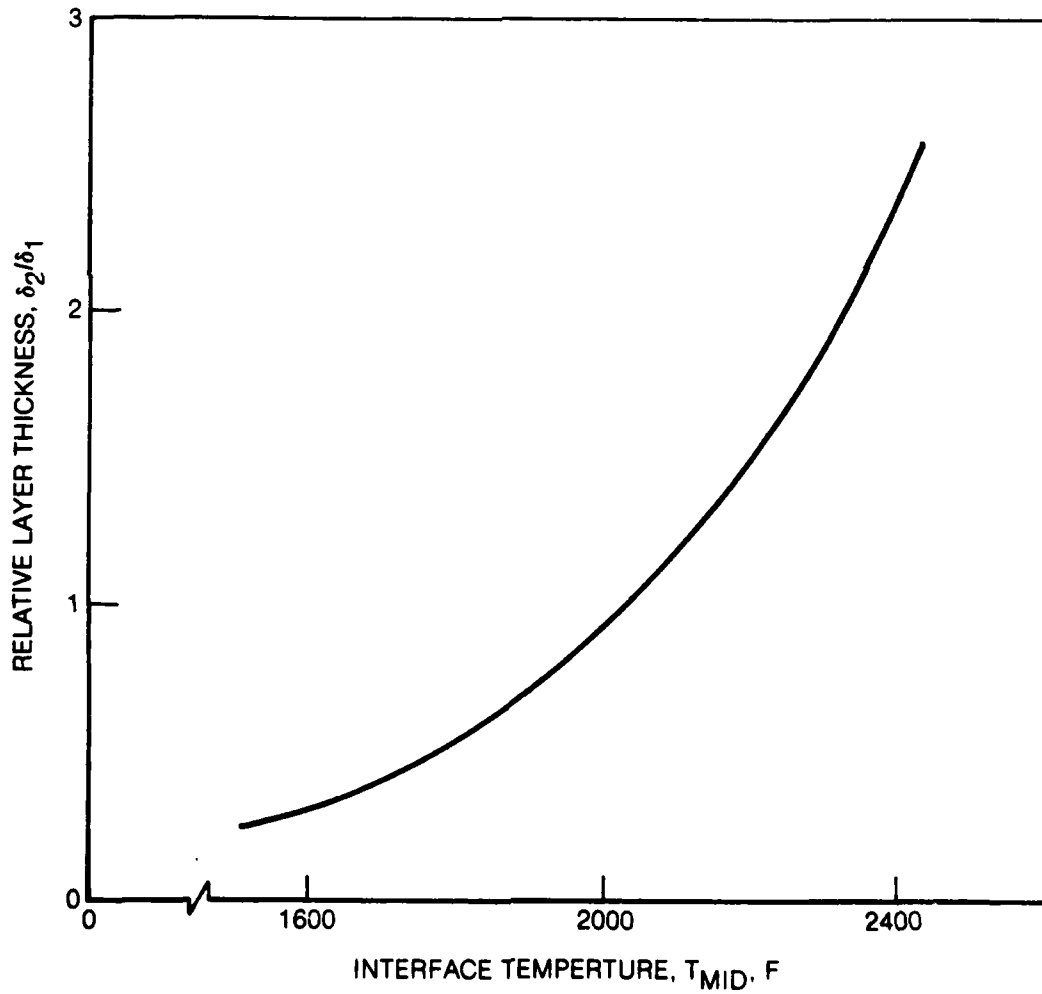
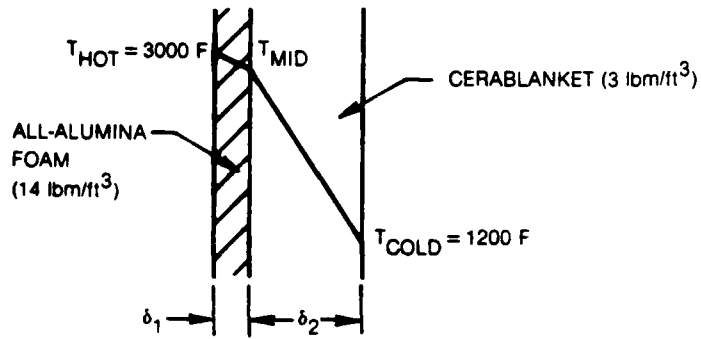
**RELATIVE LAYER THICKNESS FOR TWO-LAYER RETARDATION DEVICE  
ALL-ALUMINA FOAM/DYNAQUARTZ**



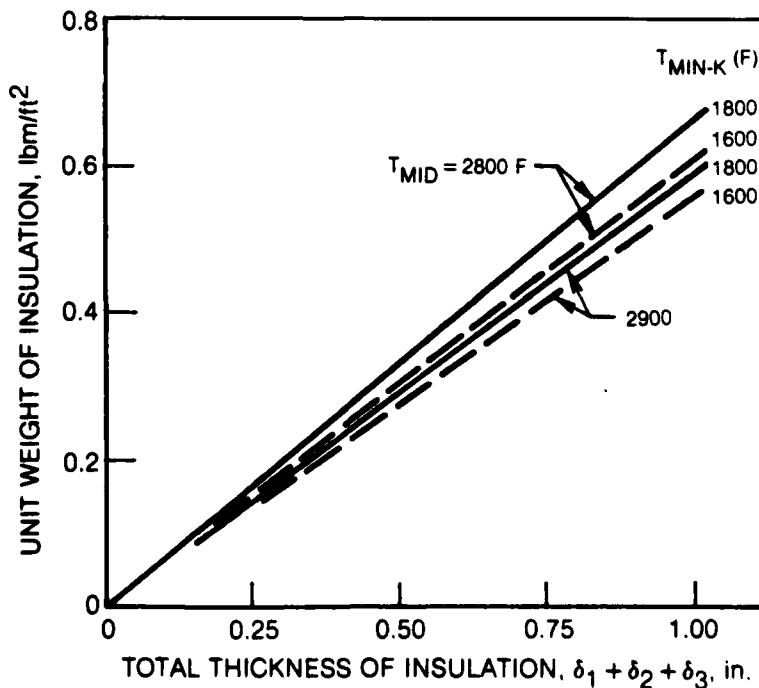
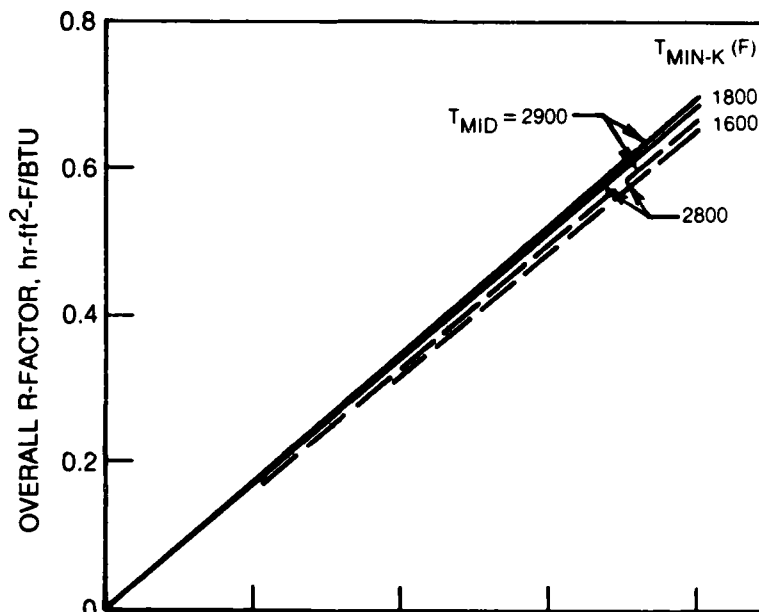
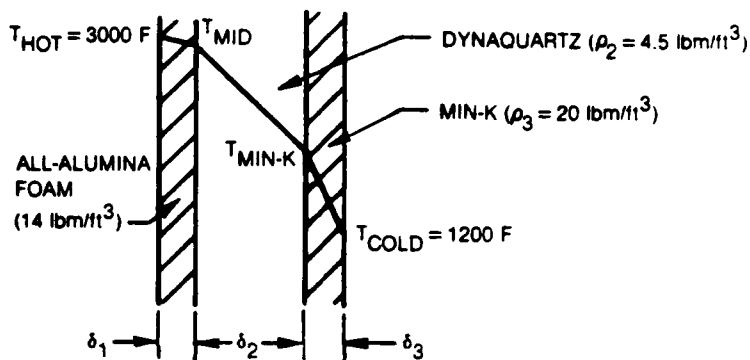
**OVERALL R-FACTOR AND UNIT WEIGHT OF TWO-LAYER RETARDATION DEVICE**



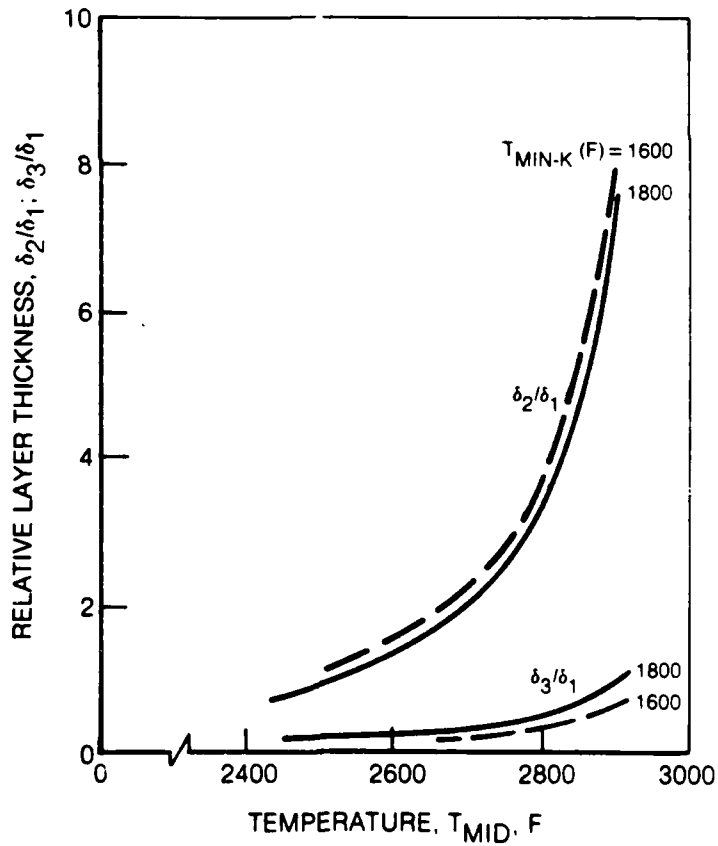
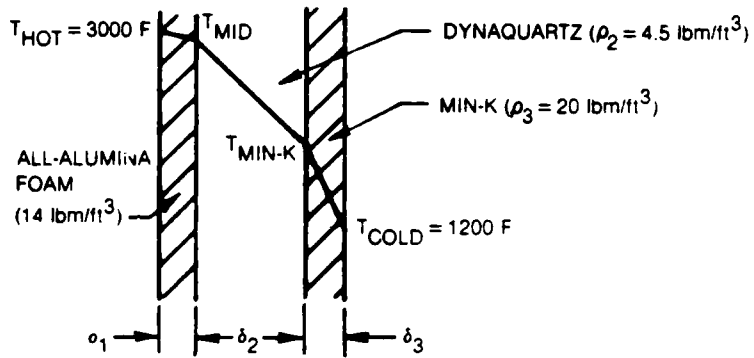
**RELATIVE LAYER THICKNESS OF TWO-LAYER RETARDATION DEVICE  
ALL-ALUMINA FOAM/CERABLANKET**



**OVERALL R-FACTOR AND UNIT WEIGHT OF THREE-LAYER RETARDATION DEVICE  
ALL-ALUMINA FOAM/DYNAQUARTZ/MIN-K**



**RELATIVE LAYER THICKNESS FOR THREE-LAYER RETARDATION DEVICE**  
**ALL-ALUMINA FOAM/DYNAQUARTZ/MIN-K**



AD-A133 509

HEAT TRANSFER RETARDATION AT ELEVATED TEMPERATURES  
PHASE I ANALYSIS OF HE. (U) UNITED TECHNOLOGIES  
RESEARCH CENTER EAST HARTFORD CT C W DEANE SEP 83

2/2

UNCLASSIFIED

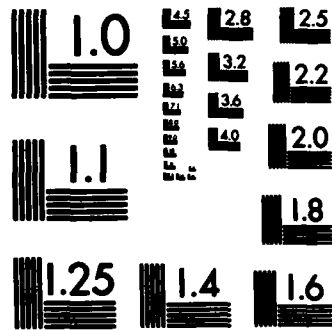
UTRC/R83-956216-1 N00014-82-C-0671

F/G 20/13

NL

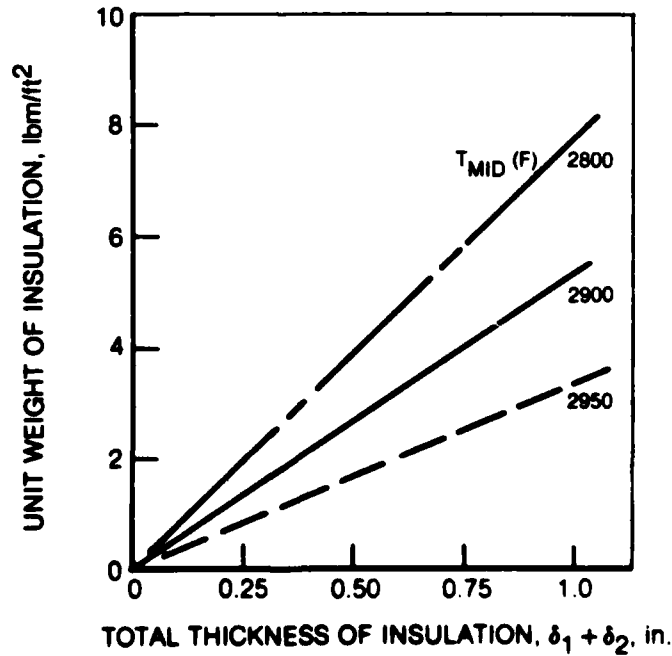
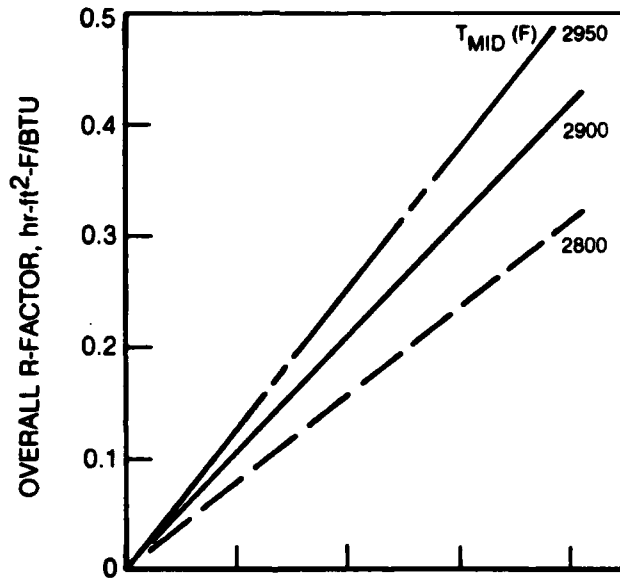
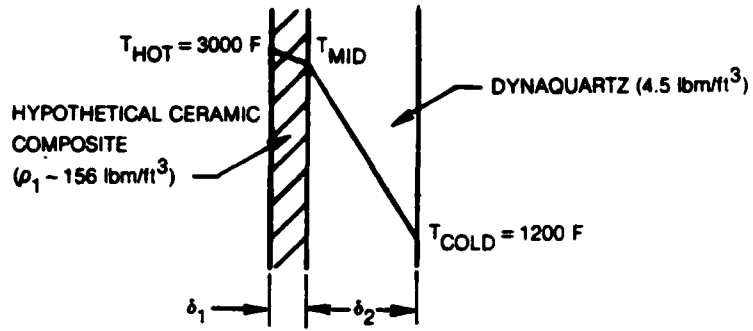


END  
-1-

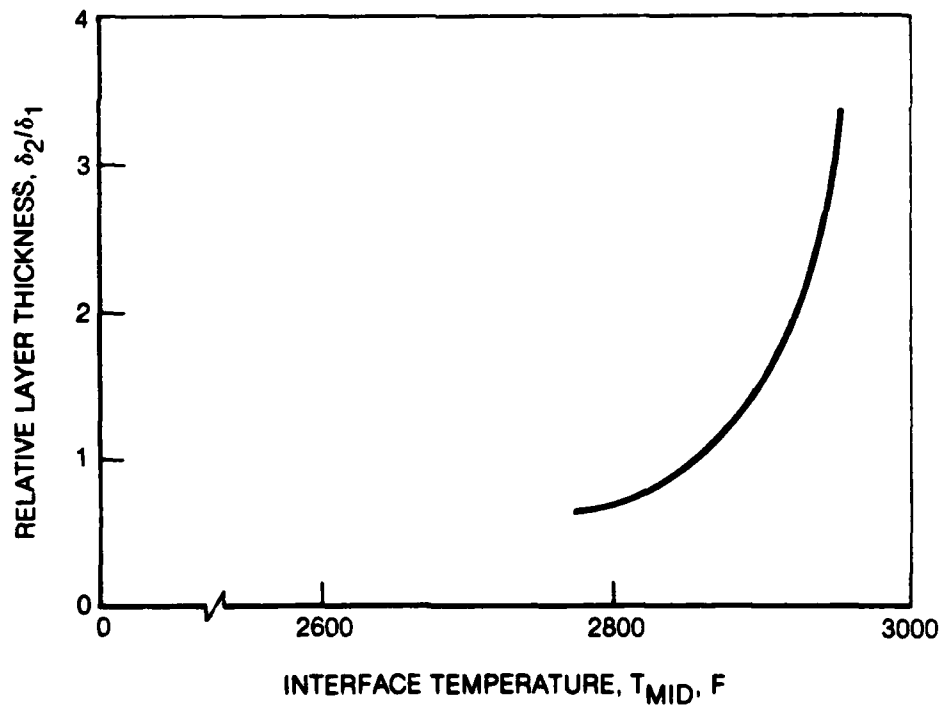
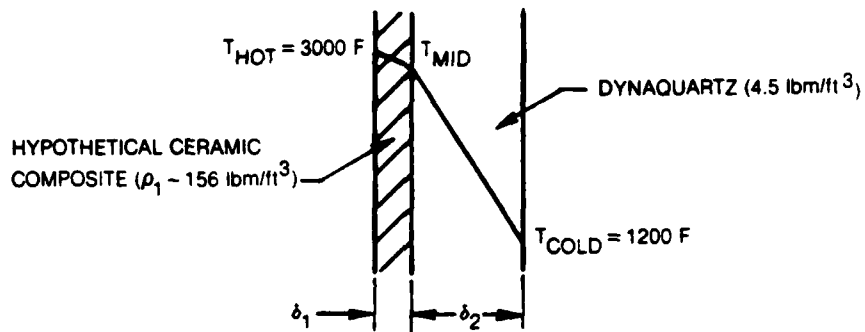


MICROCOPY RESOLUTION TEST CHART  
NATIONAL BUREAU OF STANDARDS-1963-A

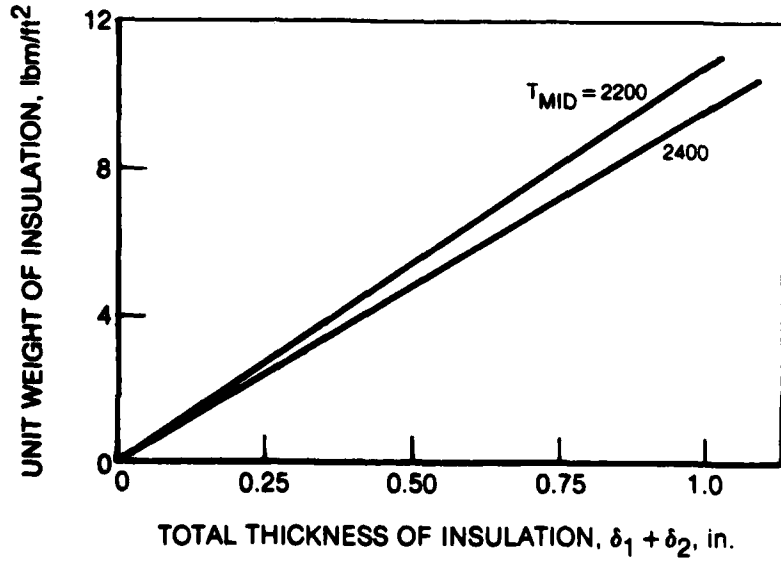
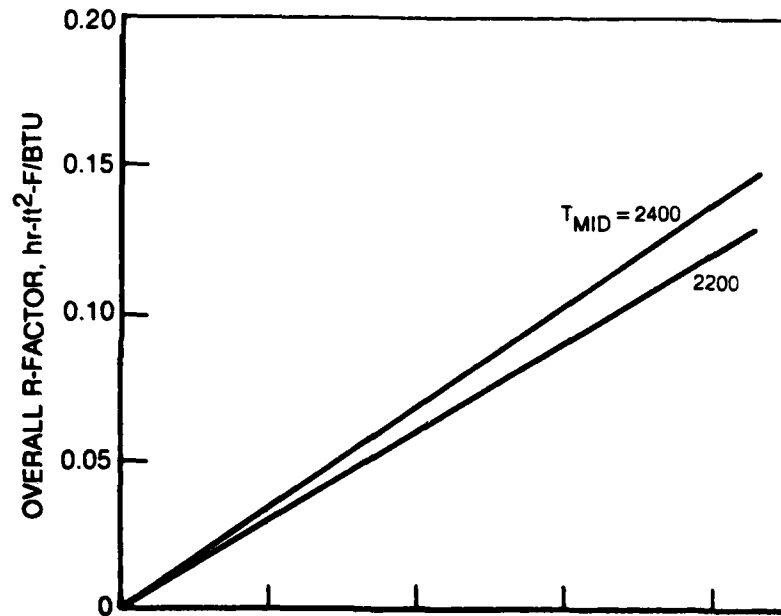
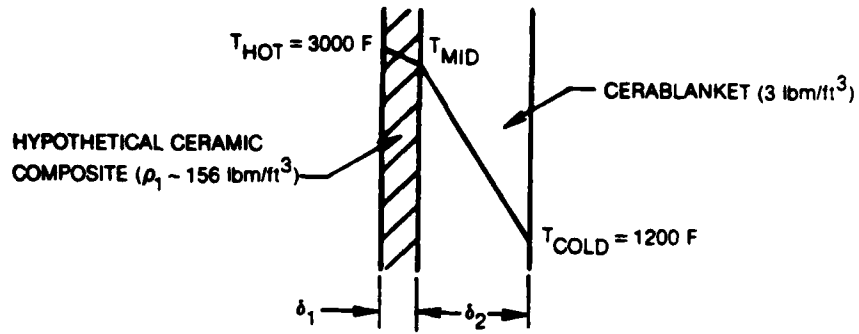
**OVERALL R-FACTOR AND UNIT WEIGHT OF TWO-LAYER RETARDATION DEVICE  
CERAMIC COMPOSITE/DYNAQUARTZ**



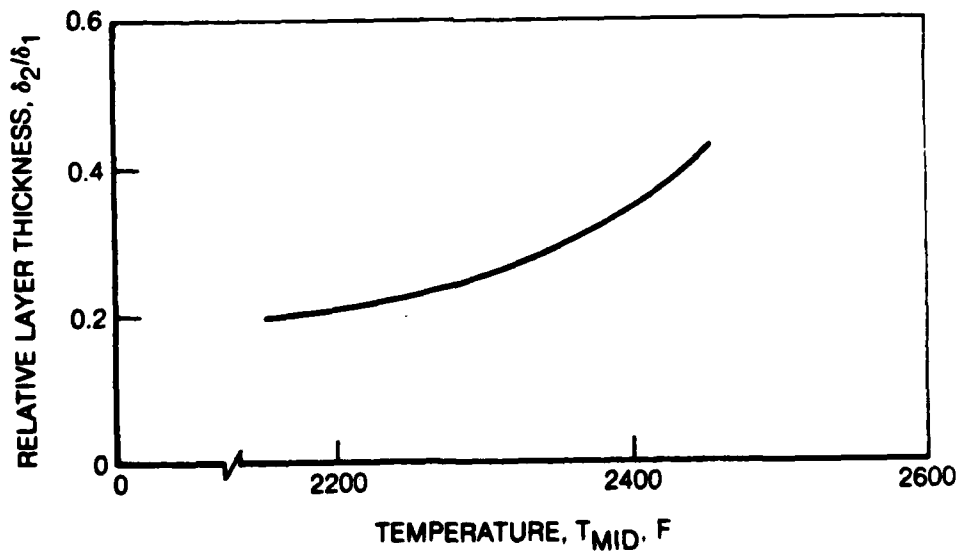
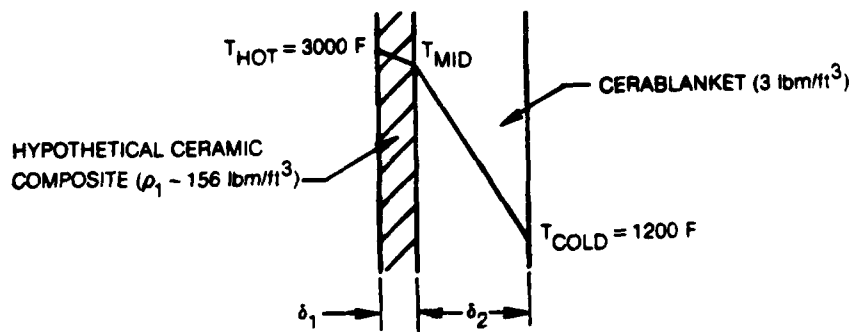
**RELATIVE LAYER THICKNESS FOR TWO-LAYER RETARDATION DEVICE  
CERAMIC COMPOSITE/DYNAQUARTZ**



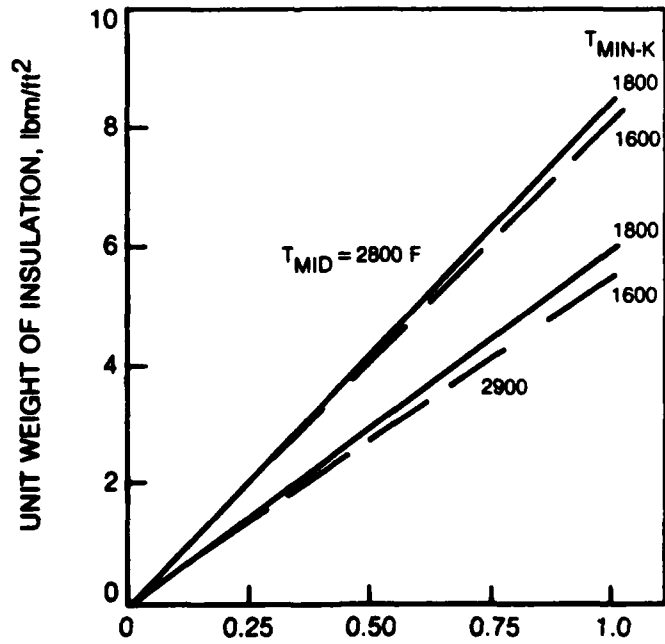
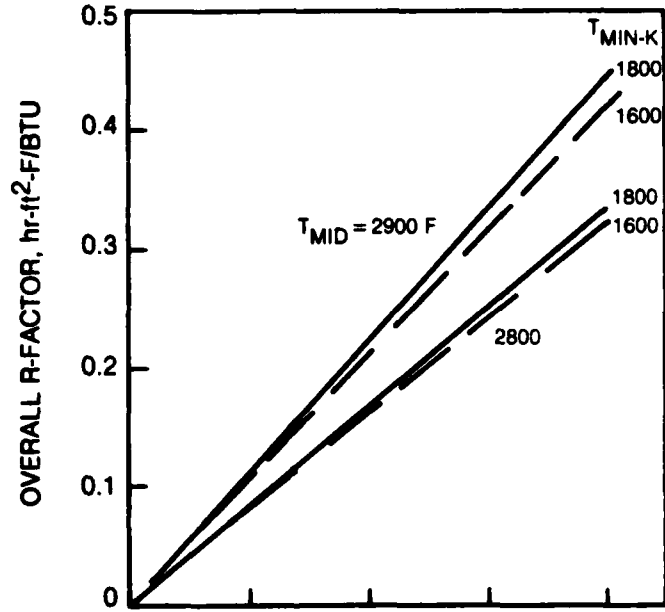
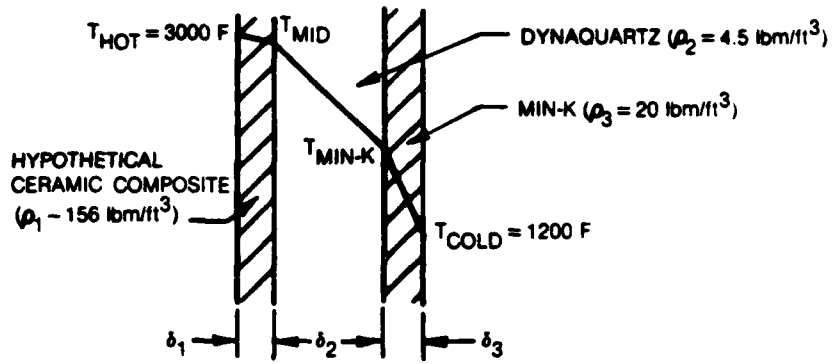
**OVERALL R-FACTOR AND UNIT WEIGHT OF TWO-LAYER RETARDATION DEVICE  
CERAMIC COMPOSITE/CERABLANKET**



**RELATIVE LAYER THICKNESS  
CERAMIC COMPOSITE/CERABLANKET**

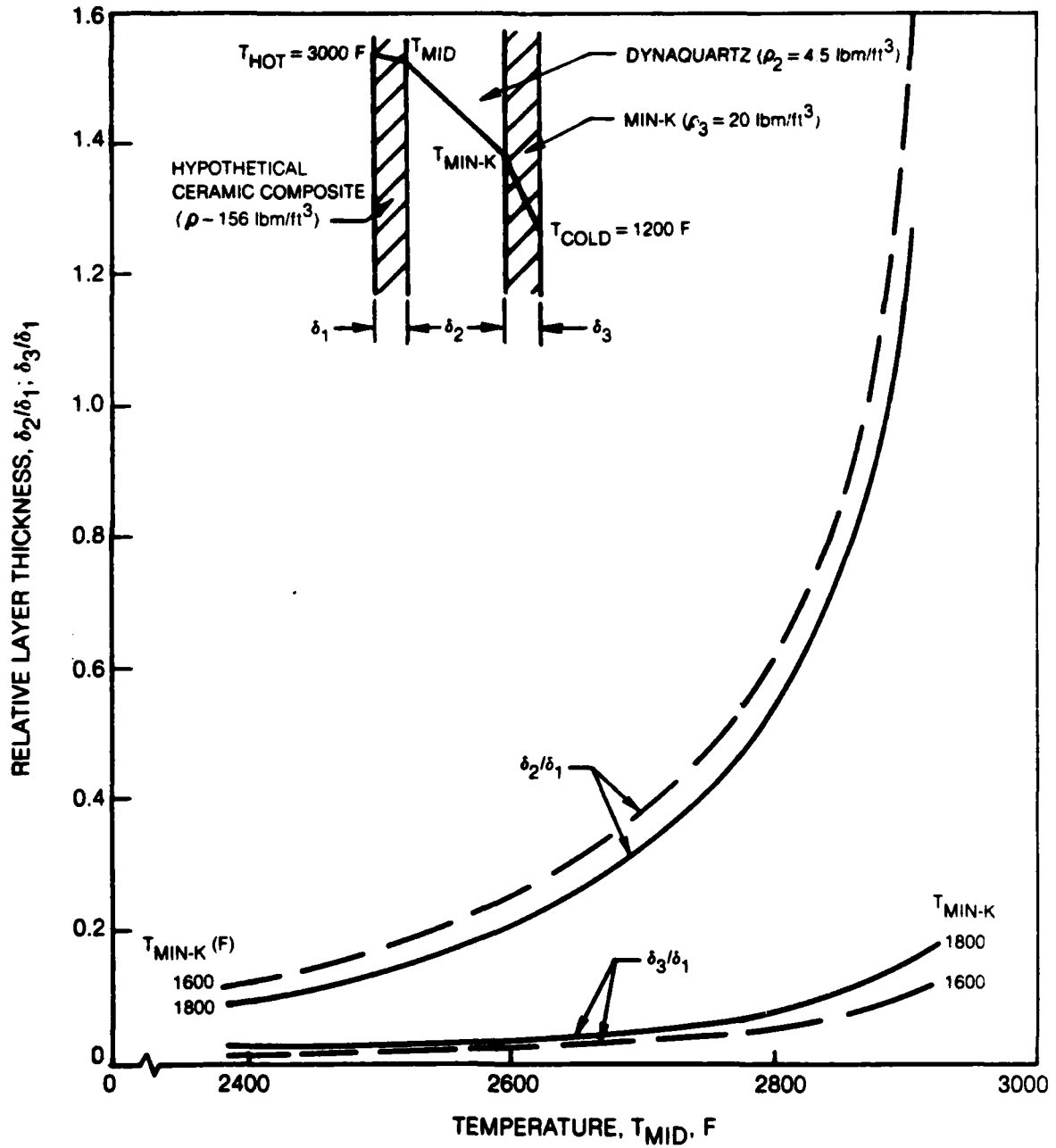


**OVERALL R-FACTOR AND UNIT WEIGHT OF THREE-LAYER RETARDATION DEVICE**

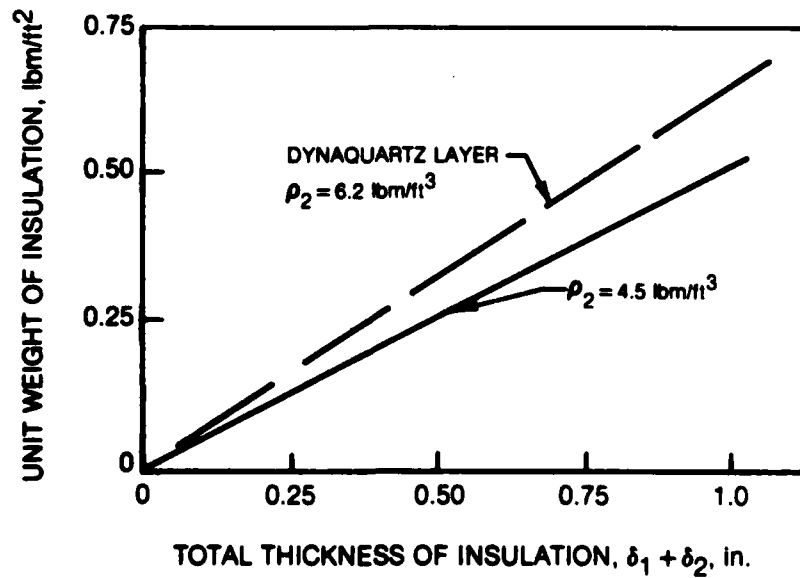
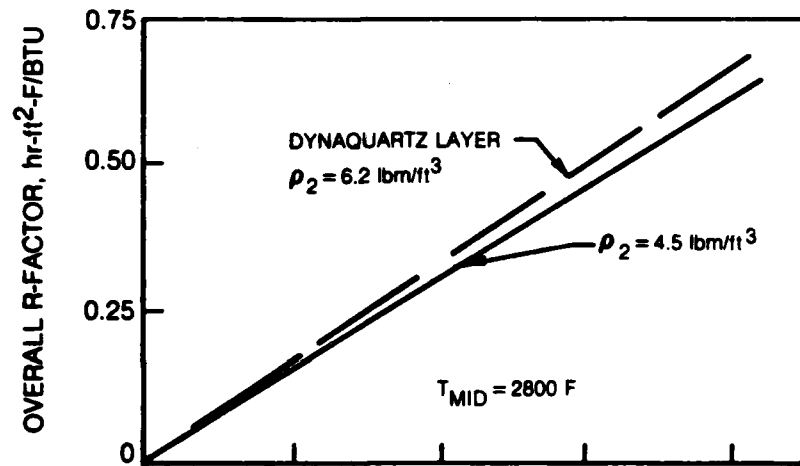
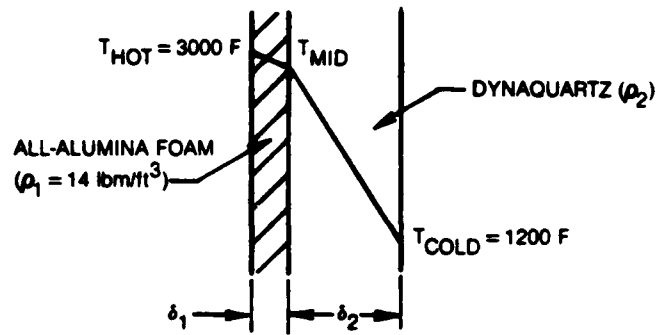


TOTAL THICKNESS OF INSULATION,  $\delta_1 + \delta_2 + \delta_3$ , in.

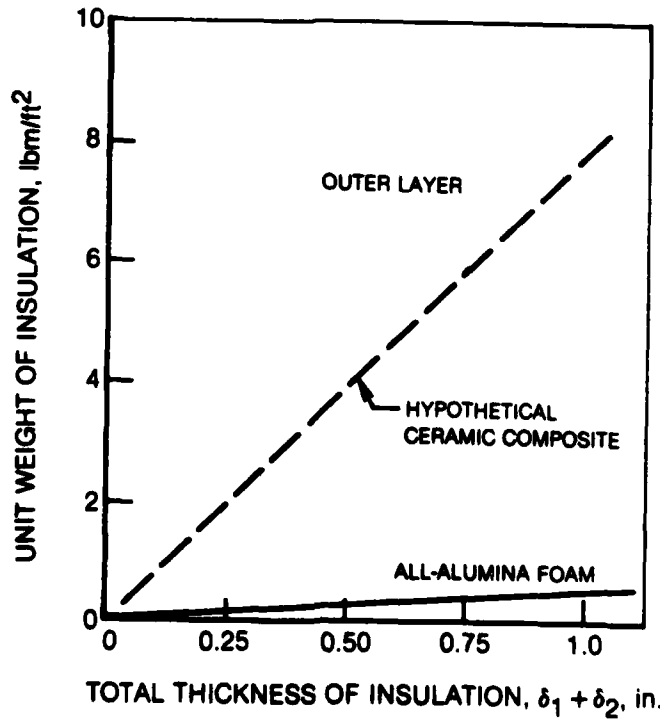
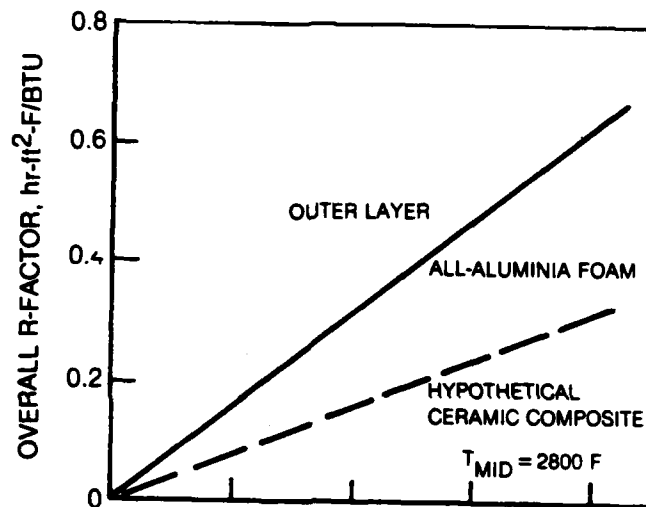
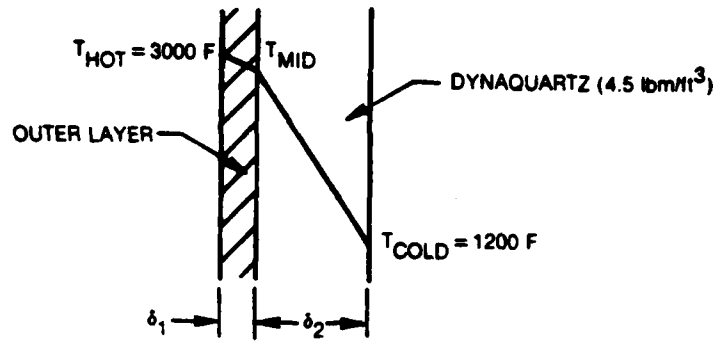
RELATIVE LAYER THICKNESS FOR THREE-LAYER RETARDATION DEVICE



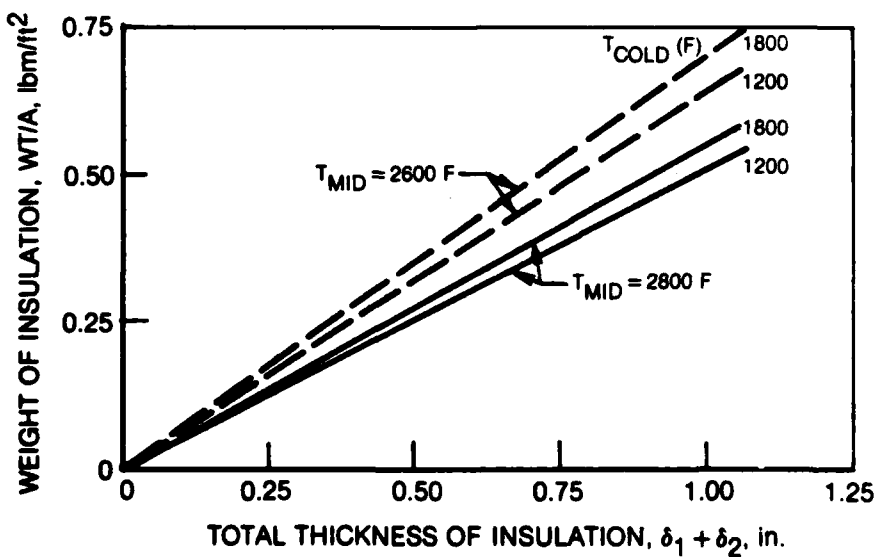
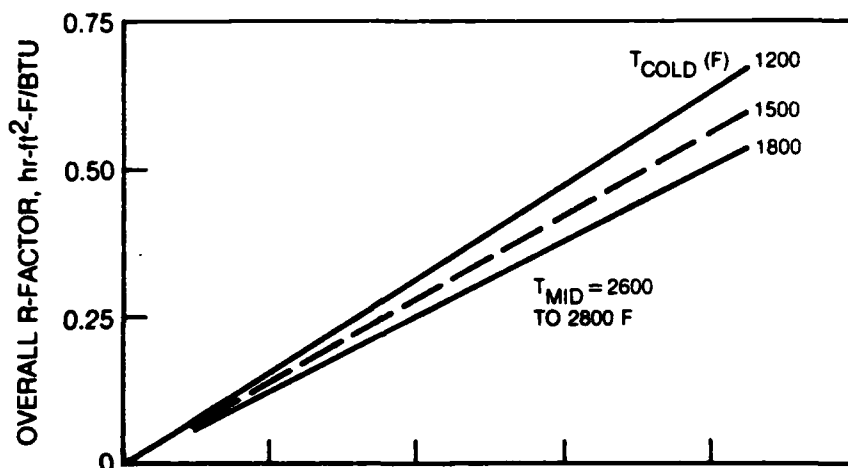
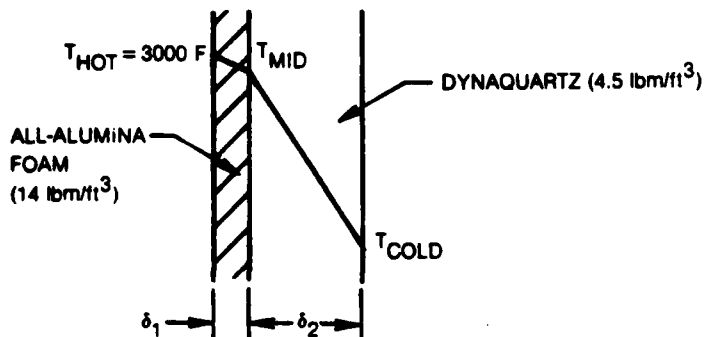
**EFFECT OF INNER MATERIAL ON OVERALL R-FACTOR AND UNIT WEIGHT**



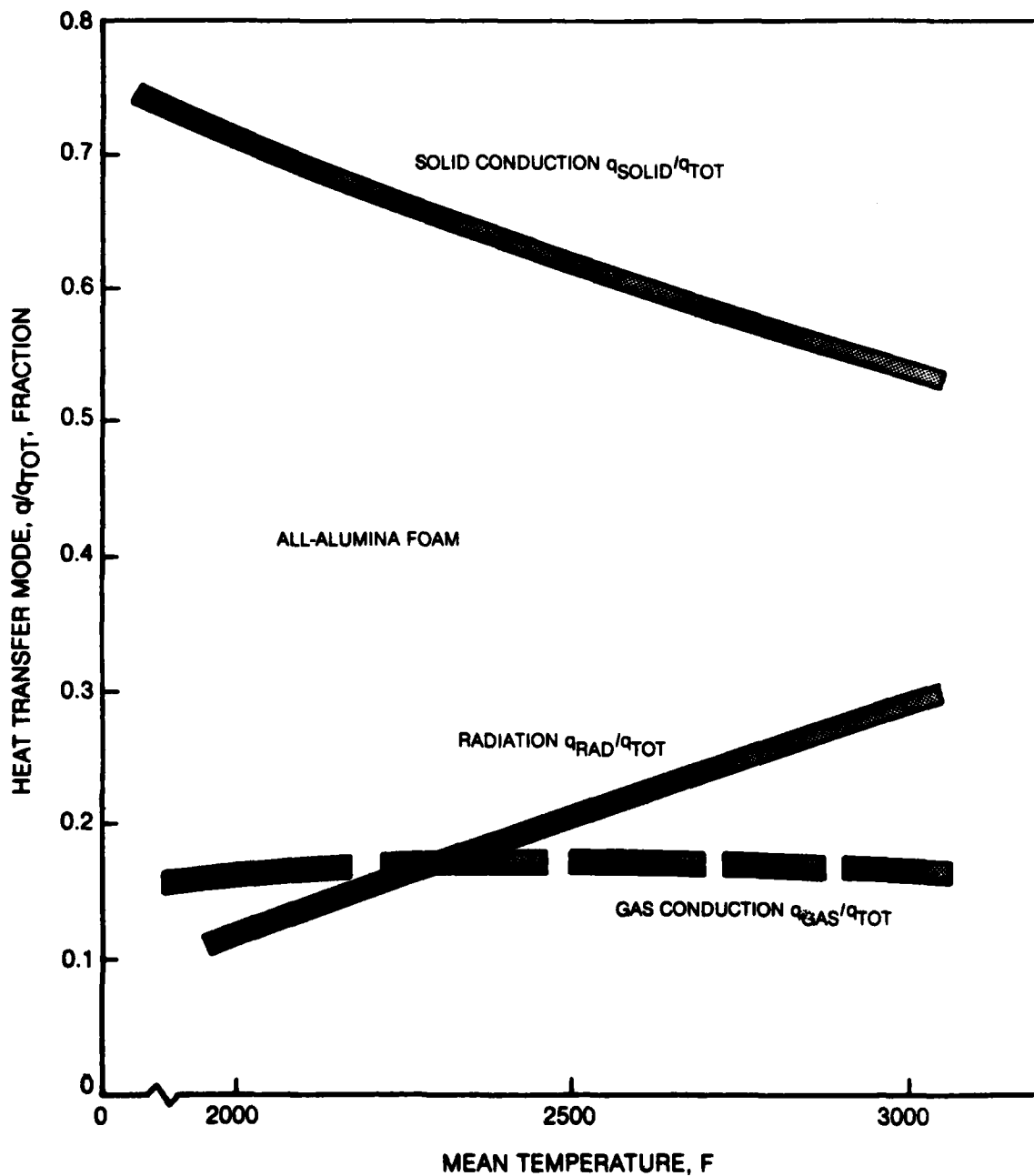
**EFFECT OF OUTER-LAYER MATERIAL ON OVERALL R-FACTOR AND UNIT WEIGHT**



**EFFECT OF TEMPERATURE ON RETARDATION AND WEIGHT CHARACTERISTICS**



### RELATIVE CONTRIBUTIONS OF HEAT TRANSFER MODES



DISTRIBUTION LIST

TWO PHASE FLOW

One copy except  
as noted

Mr. M. Keith Ellingsworth  
Power Program, Code 473  
Office of Naval Research  
800 N. Quincy Street  
Arlington, VA 22217

5

Defense Documentation Center  
Building 5, Cameron Station  
Alexandria, VA 22314

12

Technical Information Division  
Naval Research Laboratory  
4555 Overlook Avenue SW  
Washington, DC 20375

6

Professor Paul Marto  
Department of Mechanical Engineering  
US Naval Post Graduate School  
Monterey, CA 93940

Professor Bruce Rankin  
Naval Systems Engineering  
US Naval Academy  
Annapolis, MD 21402

Dr. Alan Wood  
Engineering Sciences, Room 619  
Office of Naval Research  
Ballston Centre Tower #1  
800 North Quincy Street  
Arlington, VA 22217

Mr. Mike Chaszeyka  
Office of Naval Research Branch Office  
536 South Clark Street  
Chicago, Ill. 60605

Mr. Charles Miller, Code 05R13  
Crystal Plaza #6  
Naval Sea Systems Command  
Washington, DC 20362

Steam Turbines Branch, Code 5221  
National Center #4  
Naval Sea Systems Command  
Washington, DC 20362

Mr. Ed Ruggiero, NAVSEA 08  
National Center #2  
Washington, DC 20362

Dr. Earl Quandt Jr., Code 272  
David Taylor Ship R&D Center  
Annapolis, MD 21402

Mr. Wayne Adamson, Code 2722  
David Taylor Ship R&D Center  
Annapolis, MD 21402

Dr. George Lea, Director  
Fluid Mechanics Program  
National Science Foundation  
Washington, DC 20550

Mr. Michael Perlsweig  
Department of Energy  
Mail Station E-178  
Washington, DC 20545

Professor J. A. C. Humphrey  
Department of Mechanical Engineering  
University of California, Berkeley  
Berkeley, CA 94720

Professor Brian Launder  
Thermodynamics and Fluid Mechanics Division  
University of Manchester  
Institute of Science & Technology  
POSS Sackville Street  
Manchester M601QD England

**Professor Shi-Chune Yao**  
Department of Mechanical Engineering  
Carnegie-Mellon University  
Pittsburgh, PA 15213

**Dr. Branko Leskovar**  
Electronics R&D Group  
Lawrence Berkeley Laboratory  
University of California  
Berkeley, CA 94720

**Dr. Ryszard Gajewski, Director**  
Division of Advanced Energy Projects  
Office of Basic Energy Sciences  
Department of Energy  
Washington, DC 20545

**Dr. David Elliot**  
NASA Jet Propulsion Laboratory  
4800 Oak Grove Drive  
Stop 67-201  
Pasadena, CA 91103

**Mr. Lance Hays, President**  
BiPhase Energy Systems  
2800 Airport Blvd.  
Santa Monica, CA 90405

**Professor Paul A. Libby**  
Department of Applied Mechanics and Engineering Sciences  
University of California San Diego  
P.O. Box 109  
La Jolla, CA 92037

**Professor C. Forbes Dewey Jr.**  
Fluid Mechanics Laboratory  
Massachusetts Institute of Technology  
Cambridge, Massachusetts 02139

**Professor Warren Rohsenow**  
Mechanical Engineering Department  
Massachusetts Institute of Technology  
77 Massachusetts Avenue  
Cambridge, Massachusetts 02139

**Professor A. Louis London**  
**Mechanical Engineering Department**  
**Bldg. 500, Room 501B**  
**Stanford University**  
**Stanford, CA 94305**

**Professor T. N. Veziroglu**  
**Clean Energy Research Institute**  
**University of Miami**  
**Coral Gables, Florida 33124**

**Professor Daryl Metzger**  
**Chairman, Mechanical and Energy**  
**Systems Engineering**  
**Arizona State University**  
**Tempe, Arizona 85281**

**Professor T. H. Gawain**  
**Department of Aeronautics**  
**Naval Postgraduate School**  
**Monterey, California 93940**

**Dr. J. E. Minardi**  
**University of Dayton**  
**Research Institute**  
**Dayton, Ohio 45469**

**Professor Frank E. Marble**  
**Mail Code 205-45**  
**California Institute of Technology**  
**Pasadena, California 91125**

**Dr. Oscar Manley**  
**Div. of Engineering, Math., & Geo-Sciences**  
**US Department of Energy**  
**Washington, DC 20545**

END

FILMED

11-83

DTIC